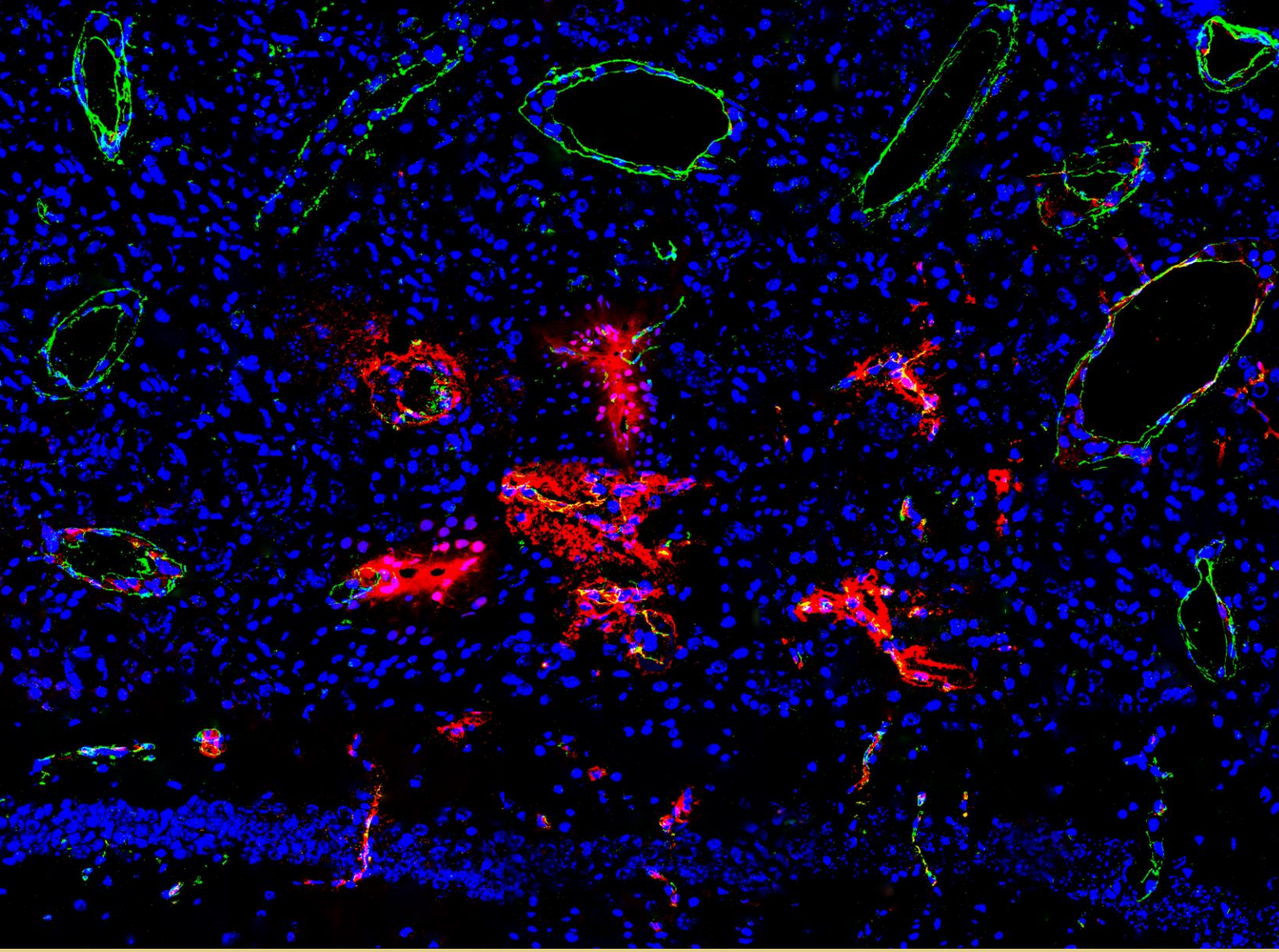

Ricardo Alexandre Gomes Leitão

ROLE OF AQUAPORIN-4 IN METHAMPHETAMINE-INDUCED BLOOD-BRAIN BARRIER DYSFUNCTION AND CEREBRAL EDEMA FORMATION

Doctoral Thesis in Biomedical Engineering, supervised by Doctor Ana Paula Pereira da Silva Martins, presented to the Faculty of Sciences and Technology of the University of Coimbra

Abril 2017

· U C ·

Universidade de Coimbra

Ricardo Alexandre Gomes Leitão

Papel da aquaporina 4 na disfunção da barreira hematoencefálica e na formação do edema cerebral induzidos pela metanfetamina

Role of aquaporin-4 in methamphetamine-induced blood-brain barrier dysfunction and cerebral edema formation

Doctoral Thesis in Biomedical Engineering, supervised by Doctor Ana Paula Pereira da Silva Martins, and presented to the Faculty of Sciences and Technology of the University of Coimbra

April 2017

Front cover:

Montagem de fotografias de microvasos de murganhos C57BL/6 marcados para colagénio IV (verde; proteína da membrana basal de reveste os microvasos cerebrais), e para os núcleos celulares (azul). A marcação para a albumina (a vermelho) é usada como um marcador de aumento da permeabilidade da barreira hematoencefálica.

Composite of images from C57BL/6 mice brain microvessels stained for collagen IV (green; basal membrane protein that surrounded brain microvessels), and for cell nuclei (blue). Albumin staining (in red) is used as a marker of blood-brain barrier disruption.

Support

O trabalho experimental apresentado nesta tese foi elaborado no Instituto de Farmacologia e Terapêutica Experimental e no Instituto de Imagem Biomédica e Ciências da Vida (IBILI), Faculdade de Medicina, Universidade de Coimbra, Portugal, sob a supervisão da Doutora Ana Paula Pereira da Silva Martins.

Este trabalho foi financiado com uma bolsa de doutoramento (SFRH/BD/84408/2012) através da Fundação para a Ciência e Tecnologia (FCT)/Ministério da Educação e Ciência (MEC), com fundos QREN e POPH/FSE. Este trabalho foi também suportado através do projeto PTDC/SAU-FCF/098685/2008 financiado pela FCT através de fundos COMPETE e FEDER, e ainda pelos projetos estratégicos Pest-C/SAU/UI3282/2013-2014 e CNC.IBILI UID/NEU/04539/2013, através de fundos nacionais, no âmbito do Acordo de Parceria PT2020/COMPETE 2020 e Programa Operacional Competitividade e Internacionalização (POCI) (referências: FCOMP-01-0124-FEDER-028417 e POCI-01-0145-FEDER-007440).

This work was conducted at the Institute of Pharmacology and Experimental Therapeutics and the Institute for Biomedical Imaging and Life Sciences (IBILI), Faculty of Medicine, University of Coimbra, Portugal, under the supervision of Doctor Ana Paula Pereira da Silva Martins.

This work was granted with a Ph.D. fellowship (SFRH/BD/84408/2012) from the Portuguese Foundation for Science and Technology (FCT)/Ministry of Education and Science (MEC), with funds through QREN and POPH/FSE. The present work was supported by FCT under the frame of the following project: PTDC/SAU-FCF/098685/2008 (COMPETE and FEDER funds); and the following strategic projects: Pest-C/SAU/UI3282/2013-2014, CNC.IBILI UID/NEU/04539/2013 with national funds PT2020/COMPETE 2020 and the Operational Program for Competitiveness and Internalization (POCI) (references: FCOMP-01-0124-FEDER-028417 and POCI-01-0145-FEDER-007440).

Agradecimentos

O primeiro obrigado tem que ir para os meus pais. Apesar de todo o apoio que recebi das restantes pessoas (já lá chegaremos), se não fossem estes dois pilares não tinha chegado aqui. Obrigado por sempre me incentivarem a seguir o que queria, mesmo sabendo que este mundo da ciência não é fácil. Obrigado pela ajuda a atravessar esta tormenta que são estes anos de Ph.D. Obrigado por estarem também nos momentos bons, e nos menos bons. Não havia obrigados suficientes para descrever tudo o que vos tenho a agradecer.

Batalha a batalha, resultado a resultado, tenho muito que agradecer à Doutora Ana Paula Silva. Por tão pronta e cegamente me ter acolhido no seu grupo de investigação, mesmo eu não tendo nenhuma experiência cientifica. Pela sua orientação, ensinamentos, e toda a confiança que depositou em mim nestes últimos anos. Pelas oportunidades que me deu e que me permitiram crescer como cientista, como crítico, e como pessoa. E porque apesar desta tese ser minha, muito devo à minha orientadora.

Retribuo um profundo agradecimento ao Professor Carlos Fontes Ribeiro por tão bem me ter recebido no Instituto de Farmacologia e Terapêutica Experimental, e me ter permitido fazer parte desta equipa espetacular. Tenho que agradecer ao doutor Francisco Ambrósio por me ter acolhido na sua linha de investigação Neuro8, onde pude desenvolver o meu sentido critico, e discutir ciência no seu âmbito mais transversal. Finalmente, gostaria de agradecer à Fundação para a Ciência e Tecnologia (FCT) pelo apoio financeiro, sem o qual não teria chegado até aqui.

Imperitivelmente, tenho que fazer um especial agradecimento à Vanessa, por tudo o que partilhámos na nossa segunda “casa”. Pela preciosa ajuda que me deu para a elaboração do segundo capitulo desta tese. Pelas aventuras, ou melhor, viagens de trabalho, por esse mundo fora. Pelas conversas de trabalho, e não só.

Gostaria ainda de fazer um agradecimento à Joana Gonçalves e à Sofia Baptista. Foi com estas duas pessoas espetaculares que dei os primeiros passos na ciência. Foi com elas que aprendi as regras básicas de laboratório. Foi com elas que tive as primeiras discussões cientificas. Por isso, devo a elas parte daquilo que hoje sou como cientista e apaixonado por ciência.

Agradeço também à Patricia e à Susana por termos partilhado a ímpar vida académica de Coimbra. Aos vários elementos do grupo Neuro8/IBILI, Andreia, Margarida, Filipa Baptista, Rita Gaspar, Daniela, Sara, Sofia. Por todos os convívios pós-laborais, os momentos de descontração, que tão necessários são para enfrentar as adversidades que vamos encontrando. Tenho também que agradecer a todos os “amigos de Coimbra”, Rosa, Inês, Sara, Marta, Carmo, Ludgero, etc. Por ouvirem os desabafos, e por me levantarem o ânimo nos piores momentos.

Depois queria também agradecer a toda a minha família. Pelo suporte que, mesmo que à distância, sempre me deram. Pelas mesas partilhadas, pelas histórias, e pelas novas adições à família.

Os que não estão mencionados aqui, prometo que não foi de propósito, mas são tantas as pessoas que passam pela nossa vida e que deixam a sua marca que, quando chega esta altura de resumi-las todas em poucas palavras, vai ser alguém ficar de fora. Para todas essas pessoas o meu agradecimento está representado na primeira letra de cada parágrafo desta secção.

TABLE OF CONTENTS

List of Abbreviations

ACM	Astrocyte-conditioned medium
ADC	Apparent diffusion coefficient
ADHD	Attention deficit hyperactivity disorder
AJs	Adherens junctions
AMs	Adhesion molecules
ANOVA	Analysis of variance
AP-1	Activator protein-1
AQP4	Aquaporin-4
BBB	Blood-brain barrier
BMVECs	Brain microvascular endothelial cells
CSF	Cerebrospinal fluid
CNS	Central nervous system
DAT	Dopamine transporter
DNA	Deoxyribonucleic acid
EB	Evans blue
ECF	Enhanced chemifluorescence
ECs	Endothelial cells
ELISA	Enzyme-linked immunosorbent assay
FDA	Food and Drug Administration
GAPDH	Glyceraldehyde 3-phosphate dehydrogenase
GFAP	Glial fibrillary acidic protein
GLUT-1	Glucose transporter-1
H_2O_2	Hydrogen peroxide
HBMECs	Human brain microvascular endothelial cells
HRP	Horseradish peroxidase
i.p.	Intraperitoneal

ICAM-1	Intercellular adhesion molecule-1
IgG	Immunoglobulin G
IL-1β	Interleukin-1beta
JAM	Junctional adhesion molecule
LPA	Lysophosphatidic acid
MDMA	3,4-Methylenedioxymethamphetamine
METH	Methamphetamine
MMPs	Matrix metalloproteinases
MRI	Magnetic resonance imaging
Na-F	Sodium fluorescein
NF-κB	Nuclear factor kappa-light-chain-enhancer of activated B cells
NOX	Nicotinamide adenine dinucleotide phosphate oxidase
OAPs	Orthogonal arrays of particles
PBS	Phosphate buffered saline
PFA	Paraformaldehyde
PTL	Parthenolide
RBMVECs	Rat brain microvascular endothelial cells
RNA	Ribonucleic acid
RNS	Reactive nitrogen species
ROS	Reactive oxygen species
RT	Room temperature
s.c.	Subcutaneous
S.E.M.	Standard error of the mean
siRNA	Small interference ribonucleic acid
TEER	Transendothelial electrical resistance
TGN	2-(Nicotinamide)-1,3,4-thiadiazole
TJs	Tight junctions
TNF-α	Tumor necrosis factor-alpha

TNFR1	Tumor necrosis factor receptor 1
TNFR2	Tumor necrosis factor receptor 2
VCAM-1	Vascular cell adhesion molecule-1
ZO	Zonula occludens

Published work

The results presented in this thesis have been published in the international peer-reviewed journals as follows:

Coelho-Santos V*, Leitão RA*, Cardoso FL, Palmela I, Rito M, Barbosa M, Brito MA, Fontes-Ribeiro CA, Silva AP. (2015) The TNF-α/NF-κB signaling pathway has a key role in methamphetamine-induced blood-brain barrier dysfunction. J Cereb Blood Flow Metab, 35: 1260-1271 (doi: 10.1038/jcbfm.2015.59) (*These authors contribute equally to work) – **Chapter 2**

Leitão RA, Sereno J, Castelhano JM, Gonçalves SI, Coelho-Santos V, Fontes-Ribeiro C, Castelo-Branco M, Silva AP. (2017) Aquaporin-4 as a new target against methamphetamine-induced brain alterations: focus on the neurogliovascular unit and motivational behavior. Mol Neurobiol: 1-14. doi: 10.1007/s12035-017-0439-0 – **Chapter 3**

The present thesis also contributed to the following book chapter:

Leitão RA, Coelho-Santos V, Silva AP (2016) Methamphetamine and the blood-brain barrier. In Victor R Preedy (ed) Neuropathology of Drug Addictions and Substance Misuse Volume 2: Part I Stimulants, 1st edn Academic Press-Elsevier, London, pp 155-168.

In this dissertation, the results presented in chapter 2 and 3 are formatted as requested by the journal where the work was published, with minor modifications and respective licenses for reproduction of the material.

Resumo

A metanfetamina (MET) é uma droga de abuso muito viciante com grande popularidade mundial, e que causa sérios problemas de saúde. Apesar da extensa caracterização da sua neurotoxicidade nos últimos anos, muitas questões continuam sem resposta. Alguns estudos têm mostrado que o stresse oxidativo, a disfunção mitocondrial e a neuroinflamação são alguns dos efeitos nefastos da MET. Mais recentemente demonstrou-se que a MET interfere com a função normal da barreira hematoencefálica (BHE), causando alterações na homeostase da água o que pode levar a uma situação de edema cerebral. Para além disso, sabe-se também que os astrócitos têm um papel muito importante na modulação da estrutura e função da BHE, bem como na regulação do conteúdo de água cerebral. No entanto, o efeito da MET na comunicação entre as células endoteliais (CEs) e os astrócitos nunca foi estudado anteriormente. Por outro lado, o movimento de moléculas de água entre os diferentes compartimentos do cérebro e entre o parênquima cerebral e a corrente sanguínea ocorre de forma controlada. Assim, distúrbios nesta homeostase irão causar uma situação de edema, o qual terá um impacto negativo na função cerebral. O transporte de água na BHE é regulado por canais de água, denominados aquaporinas (AQPs), sendo que a AQP4 é a mais importante no Sistema Nervoso Central, e encontra-se expressa nas terminações dos astrócitos que contactam com os vasos cerebrais. De facto, o edema cerebral ocorre em muitas neuropatologias, e o consumo de MET não é exceção. No entanto, o papel da AQP4 nos efeitos da MET é ainda desconhecido. Além disso, a AQP4 tem duas isoformas, a M1 e a M23, e é a sua proporção que regula a homeostase da água, uma vez que a presença da isoforma M23 estabiliza a função do canal de água enquanto a isoforma M1 causa alterações na função da AQP4. Deste modo, é importante esclarecer o papel da AQP 4 na disfunção da barreira hematoencefálica e na formação do edema cerebral induzidos por MET.

A presente tese está dividida em 5 capítulos. No **capítulo 1** é apresentada uma revisão da literatura sobre os diversos temas estudados no laboratório e detalhados nos capítulos seguintes.

No **capítulo 2** investigou-se o efeito da MET na comunicação entre astrócitos e CEs com particular interesse no papel do fator de necrose tumoral alfa (TNF-α). Depois de mostrar um aumento da libertação de TNF-α induzido por MET, quer pelos astrócitos quer pelas CEs, provou-se que esta citocina pró-inflamatória estava envolvida no aumento da permeabilidade das CEs através da ativação da via de sinalização do fator nuclear kappa B (NF-κB). Estes resultados foram corroborados por estudos em animais onde se observou um aumento da permeabilidade da BHE e dos níveis de TNF-α no estriado de murganho, efeitos estes que foram prevenidos pelo bloqueio da via do NF-κB. Deste modo, conclui-se que a via de sinalização do TNF-α/NF-κB está envolvida na disfunção da BHE induzida por MET.

De seguida, no **capítulo 3** avaliou-se o impacto direto da MET no sistema da AQP4 e foi possível demonstrar que esta droga de abuso, para além de induzir uma disfunção da BHE, também originou um edema cerebral citotóxico e comportamento do tipo depressivo. Curiosamente, a AQP4 teve um papel predominante nestas alterações já que o seu bloqueio preveniu todos os efeitos observados nos murganhos. *In vitro* foi também possível comprovar o papel importante da AQP4 via produção de espécies reactivas de oxigénio já que o silenciamento deste canal de água ou a sua inibição farmacológica, bem como a exposição a um antioxidante (vitamina C) preveniram as alterações morfológicas induzidas pela MET nos astrócitos. Em conclusão, a AQP4 foi identificada como um alvo importante para prevenir as alterações neurogliovasculares e comportamento depressivo induzidos por MET.

Na sequência dos efeitos negativos da MET observados nos capítulos 2 e 3, colocou-se a hipótese de uma nova abordagem com um produto natural de origem vegetal. Deste modo, no **capítulo 4** concluíu-se que o partenolídeo (PTL), um extrato obtido da artemísia dos prados (*Tanacetum parthenium*), tem um papel anti-inflamatório e preveniu o aumento

da permeabilidade da BHE e formação de edema cerebral induzidos por MET. Mais ainda, foi possível demonstrar que o TNF-α, através da ativação do seu recetor TNFR1, estava envolvido no aumento de volume dos astrócitos observado na presença de MET. Assim, este trabalho permitiu concluir que o PTL tem um feito benéfico em condições de neuroinflamação e disfunção neurogliovascular induzidos por MET.

Por último, o **capítulo 5** inclui uma discussão geral sobre os resultados obtidos nos capítulos anteriores.

Em conclusão, esta tese permitiu mostrar que a MET interfere não só com a homeostase da água no cérebro, mas também com a função da BHE, e que estes efeitos podem conduzir a alterações comportamentais. Para além disso, demonstrou-se ainda que a neuroinflamação e o stresse oxidativo estão subjacentes aos efeitos negativos causados pela MET e foram identificadas duas abordagens para prevenir estes efeitos, tais como o bloqueio da AQP4 e o uso do partenolídeo.

Palavras-chave: Aquaporina-4; Astrócitos; Barreira hematoencefálica; Comportamento animal; Edema cerebral; Fator de necrose tumoral alfa; Metanfetamina; Neuroinflamação; Partenolídeo.

Summary

Methamphetamine (METH) is a powerful psychostimulant drug of abuse that has gained worldwide popularity, and its use originates severe health problems. Despite extensive characterization of METH-induced neurotoxicity over the last years, many questions remain unanswered. Several reports have demonstrated that oxidative stress, mitochondrial dysfunction, and neuroinflammation are some of the neurotoxic features of METH. More recently, it was shown that METH compromises the blood-brain barrier (BBB) and causes a disturbance in the water homeostasis leading to brain edema. Additionally, it is well known that astrocytes play a crucial role in modulating BBB structure and function, as well as in regulating brain water content. However, the effect of METH on the crosstalk between brain endothelial cells (ECs) and astrocytes has never been addressed before. Also, water fluxes that take place between the different compartments of the brain, and between brain parenchyma and the blood are highly controlled. Thus, disturbances in this well-regulated homeostasis cause brain edema, which will have deleterious effects on brain function. Importantly, the water transport at BBB is regulated by water channels, aquaporins (AQPs), and AQP4 is the most important at the Central Nervous System, being express on astrocytic endfeet in contact with brain vessels. Brain edema is a hallmark of several neuropathologies, and METH consumption is not an exception. Yet, to date, nothing is known about the role of AQP4 under METH conditions. Furthermore, AQP4 has two isoforms, M1 and M23, and the ratio M1/M23 regulates water homeostasis since M23 stabilizes the channel function but M1 disrupts the AQP4 structure. Taking into consideration all the gaps in this field, it is urgent to clarify the role of AQP4 in METH-induced BBB dysfunction and brain edema formation.

The present thesis is divided into 5 chapters. In **chapter 1** is presented a review of the literature about the different themes that were explored in the laboratory and detailed in the following chapters.

In **chapter 2**, the impact of METH on astrocytes-ECs crosstalk was investigated with a particular interest in the role of tumor necrosis factor alpha (TNF-α). After observing that METH increased TNF-α released by both astrocytes and ECs, it was also proved that this proinflammatory cytokine was responsible for endothelial permeability through the activation of nuclear factor kappa-light-chain-enhancer of activated B cells (NF-κB) pathway. These *in vitro* results were corroborated by animal studies showing an increase of BBB permeability and TNF-α levels in the mice striatum, which was prevented by NF-κB pathway blockade. Overall, it was shown that TNF-α/NF-κB signaling pathway has a key role in METH-induced BBB dysfunction.

Next, in **chapter 3**, it was investigated the direct effect of METH on AQP4 system concluding that METH, besides BBB dysfunction, is also able to induce a cytotoxic brain edema and depressive-like behavior. Curiously, AQP4 was shown to have a predominant role of such alterations since its inhibition prevented all the effects observed in mice. Moreover, AQP4 via reactive oxygen species (ROS) production was involved in cell swelling and altered astrocyte morphology triggered by METH since AQP4 knockdown or its pharmacological blockade, as well as an antioxidant treatment (namely vitamin C) were able to prevent METH effects in astrocytes. In conclusion, AQP4 was identified as a new target against METH-induced neurogliovascular dysfunction and depressive-like behavior.

Following the results observed in chapter 2 and 3, a new strategy to counteract the negative effects of METH was applied by using a natural flower product. Thus, in **chapter 4**, it was proved that parthenolide (PTL), a feverfew plant extract, has an anti-inflammatory role and prevented METH-induced BBB permeability and brain edema. Additionally, TNF-α via activation of its receptor 1 (TNFR1) was involved in astrocytic swelling induced by METH. In sum, PTL plays a beneficial role against neuroinflammation and neurogliovascular dysfunction triggered by METH.

Finally, in **chapter 5**, a general discussion is presented.

Overall, the present work shows that METH interferes with brain water homeostasis and BBB function, culminating in behavioral abnormalities. Moreover, both neuroinflammation

and oxidative stress are involved in such negative effects of METH, and new strategies to counteract these deleterious consequences were identified, such as AQP4 blockade and the use of PTL.

Keywords: Animal behavior; Aquaporin-4; Astrocytes; Blood–brain barrier; Brain edema; Methamphetamine; Neuroinflammation; Parthenolide; Tumor necrosis factor-alpha

CHAPTER 1

Introduction

1.1. Methamphetamine

Methamphetamine (METH) is a highly addictive drug of abuse that belongs to the group of amphetamine-like stimulants, along with amphetamine and ecstasy (or 3,4-methylenedioxymethamphetamine, MDMA). METH was first synthesized in 1893 by the Japanese chemist Nagai Nagayoshi, however, its use has only become trivial during World War II mostly among German air force pilots.

METH can be consumed in various ways such as smoked, the most common, but can also be injected, snorted and taken orally (Winslow et al., 2007; Nakama et al., 2008). The worldwide amphetamines consumption annual prevalence is between 0.5% and 2.1%, in Europe and Australia, respectively, among people aged 15-64. These numbers make METH the second most widely used synthetic drug globally (UNODC, 2015; EMCDDA, 2016). Concerning the consumption in Portugal, the last report from "Serviço de Intervenção nos Comportamentos Aditivos e nas Dependências 2016" (SICAD, 2016) shows that in 2012, 0.5% of the total population and of young adults were amphetamine consumers. However, this report includes both amphetamine and methamphetamine, which means that there are no national statistics of detailed METH consumption.

In humans, after the rapid absorption of METH in the gastrointestinal tract, it is metabolized in the liver by aromatic hydroxylation, N-dealkylation, and deamination. Additionally, METH excretion takes place mainly in the urine and it is dependent on urine pH. In fact, alkaline urine increases METH half-life. The biological half-life of this drug ranges between 4 to 5h and within 24h more than 60% of an oral dose will be eliminated in the urine (de la Torre et al., 2012). Commonly abused doses are between 100-1000 mg/day, and up to 5000 mg/day in chronic binge use (NHTSA, 2015). In contrast, a therapeutic dose of METH (under the name of Desoxyn) does not exceed 60 mg/day.

METH negatively interferes with the normal function of peripheral organs (Darke et al., 2008) as well as with the central nervous system (CNS) (Silva et al., 2010; Gonçalves et al., 2014), leading to widespread organ failure. Indeed, METH can cause irreversible disturbance of brain cells creating neurological and psychiatric abnormalities. Immediately after consumption, METH leads to euphoria, alertness, wakefulness, increased activity (Quinton et al., 2006; Yamamoto et al., 2010), hyperthermia (Kiyatkin et al., 2007), and a decrease in appetite (Buchanan et al., 2010). At long-term, this drug originates anxiety, confusion, insomnias, mood disturbances and weight loss (Buchanan et al., 2010). Specifically, chronic METH abusers can experience psychotic and violent behavior, impaired verbal learning and memory, visual and auditory hallucinations, delusions, and even seizures (Quinton et al., 2006; Ramirez et al., 2009, Yamamoto et al., 2010; Buttner, 2011). The cognitive impairments observed in METH consumers seems to be correlated with severe gray matter deficits in the cingulate, limbic, and paralimbic human cortices, as well as with white matter hypertrophy (Thompson et al., 2004).

1.1.1. Mechanisms of Action: an Overview

METH has great similarity with the neurotransmitter dopamine (**Figure 1.1**), which explains the most well-known METH cellular effects. When this drug is present in the extracellular space it can enter to the cytoplasm by two ways: diffuse transport due to lipophilic characteristics and via membrane dopamine transporter (DAT).

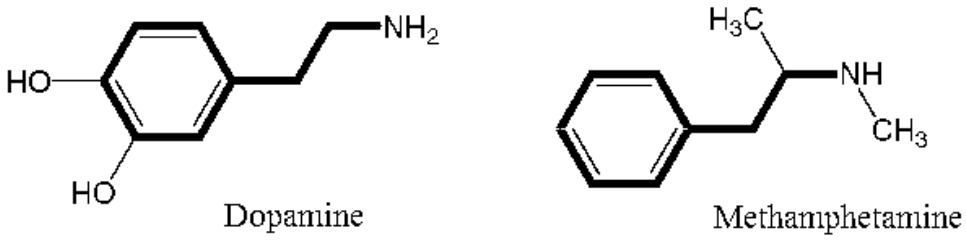

Figure 1.1. The chemical structure of dopamine and methamphetamine clearly shows the similarity between both (adapted from Fleckenstein et al., 2007).

Due to its chemical properties, METH can also enter the mitochondria or other cellular compartments. More specifically, it can inhibit vesicular monoamine transporter (VMAT) acting as a competitive antagonist (Yamamoto et al., 2010). This will increase the dopamine content in the cytoplasm (**Figure 1.2**), which consequently causes oxidative stress accompanied by reactive oxygen species (ROS) and reactive nitrogen species (RNS) accumulation. Moreover, the increase of dopamine in the cytoplasm can also reverse DAT transporters leading to a great release of dopamine into the synaptic cleft, causing an overstimulation of postsynaptic neurons via dopamine receptors (**Figure 1.2**; Kish, 2008). At the same time, METH is also capable of inhibiting the dopamine uptake (Rothman et al., 2001) contributing to the high levels of dopamine in the synaptic cleft. METH-induced oxidative stress and lipid peroxidation have been described in the rat striatum (Yamamoto and Zhu, 1998) and in human brain microvascular endothelial cells (Ramirez et al., 2009). Moreover, METH can inhibit glucose uptake in neurons and astrocytes (Muneer et al., 2011), as well as inhibit mitochondrial electron transport chain enzyme complexes causing mitochondrial dysfunction (Quinton et al., 2006; Yamamoto et al., 2010). Besides interfering with dopaminergic system, METH also acts as an uptake inhibitor of serotonin and norepinephrine increasing their levels in the extracellular space (Yamamoto and Raudensky, 2008).

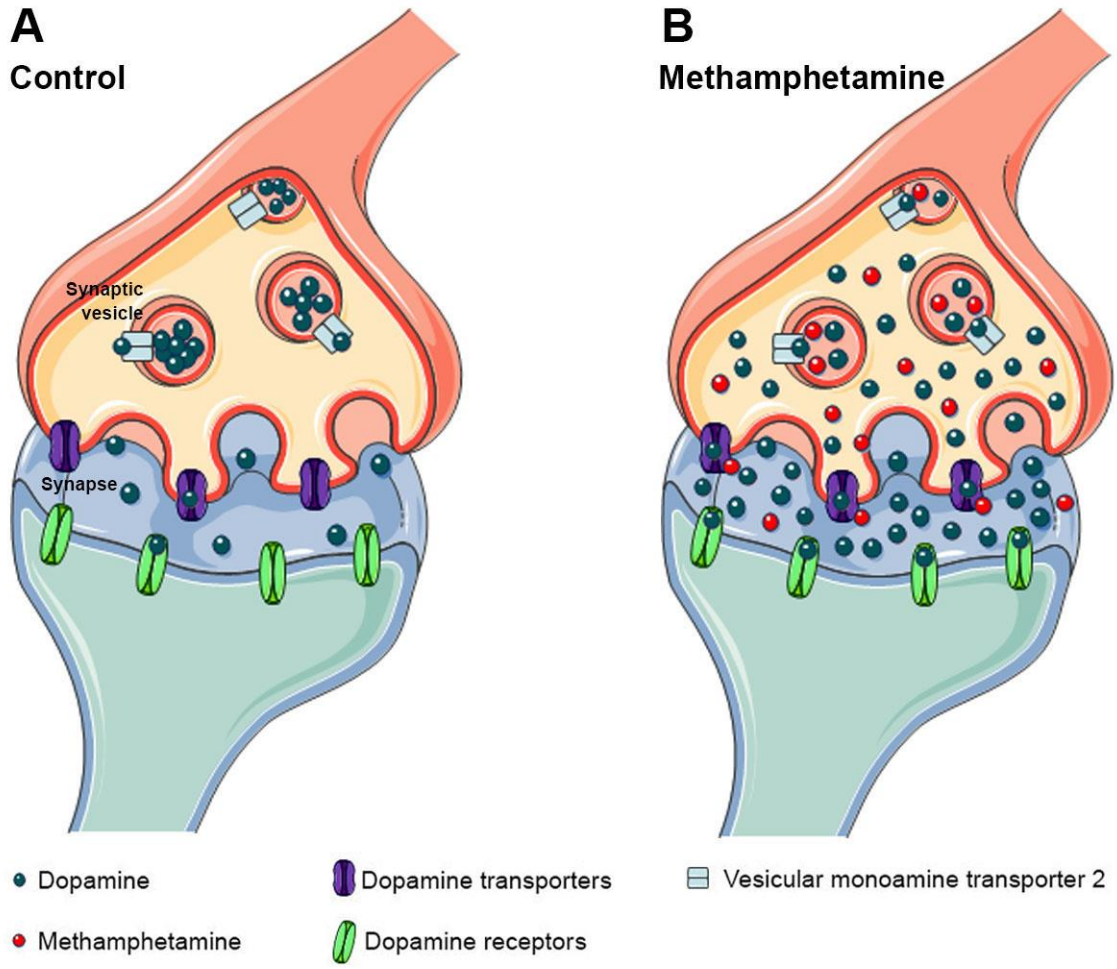

Figure 1.2. Effect of METH on dopaminergic neurons. METH passes through neuronal membranes leading to a release of dopamine from storage vesicles, which consequently reverse the membrane transporter and dopamine is released into the synapse. Moreover, METH is also capable of directly bind to dopamine transports, inhibiting dopamine influx into the cell and leading to the accumulation of this neurotransmitter in the synaptic cleft. **(A)** Control situation; **(B)** Methamphetamine exposure.

The glutamatergic system can also be affected by METH exposure (**Figure 1.3**). In fact, METH increases glutamate release (Mark et al., 2004) and intracellular calcium levels with activation of several kinases and proteases resulting in the disruption of cytoskeleton and formation of ROS (Cadet et al., 2007). Also, NMDA (N-methyl-D-aspartate) and AMPA (α-amino-3-hydroxy-5-methyl-4-isoxazolepropionic acid) glutamate receptors (NR and GluR, respectively) are altered since it has been observed an upregulation of NR2A and GluR2 subunits in the rat hippocampus (Simões et al., 2007) and frontal cortex (Simões et al.,

2008) after single high dose of METH (30 mg/kg), and in striatum (Simões et al., 2008) after an escalating dose METH paradigm (from 10 to 30 mg/kg/day, for 7 days). Nevertheless, METH caused a decrease in the NR1 protein levels in the hippocampus after single METH administration (Simões et al., 2007), and in frontal cortex after escalating METH protocol (Simões et al., 2008).

METH-induced neuronal dysfunction and death have already been demonstrated in several rodent brain regions such as the mice hippocampus (Gonçalves et al., 2010) and caudate-putamen (Bowyer et al., 2008), as well as in the rat neocortex and limbic system (Kuczenski et al., 2007). Despite the well-known impact of METH on neurons, it is now unquestionable that it also interferes with other brain cells. In fact, several authors have shown that METH triggers a neuroinflammatory response (Yamamoto and Raudensky, 2008; Gonçalves et al., 2010) characterized by astrogliosis in the rodent cortex, hippocampus and striatum (Pubill et al., 2003; Sharma and Kiyatkin, 2009; Gonçalves et al., 2010), as well as microglial activation in the striatum, caudate-putamen (Pubill et al., 2003; Bowyer et al., 2008) and hippocampus (Gonçalves et al., 2010).

More recently, some studies have suggested that METH-induced brain aberrations may also result from its capability to interfere with blood-brain barrier (BBB) function (**Figure 1.3**), which is a crucial structure for the unique features of brain environment (Bowyer et al., 2006; Ramirez et al., 2009; Martins et al., 2011; Gonçalves et al., 2014). Accordingly, brain infection is expected as a consequence of BBB disruption mediated by METH. In fact, there are some studies correlating the abuse of METH with cerebral infections, such as human immunodeficiency virus (HIV) that causes acquired immunodeficiency syndrome (AIDS). Though the direct effects of both METH and/or HIV on BBB properties are less understood. The available literature suggests that only the co-exposure of METH and HIV viral proteins causes an increase in BBB permeability (Mahajan et al., 2008;

Banerjee et al., 2010). On the contrary, METH alone seems to be capable of increase the brain fungi colonies after cryptococcal infection (Park et al., 2009; Patel et al., 2013).

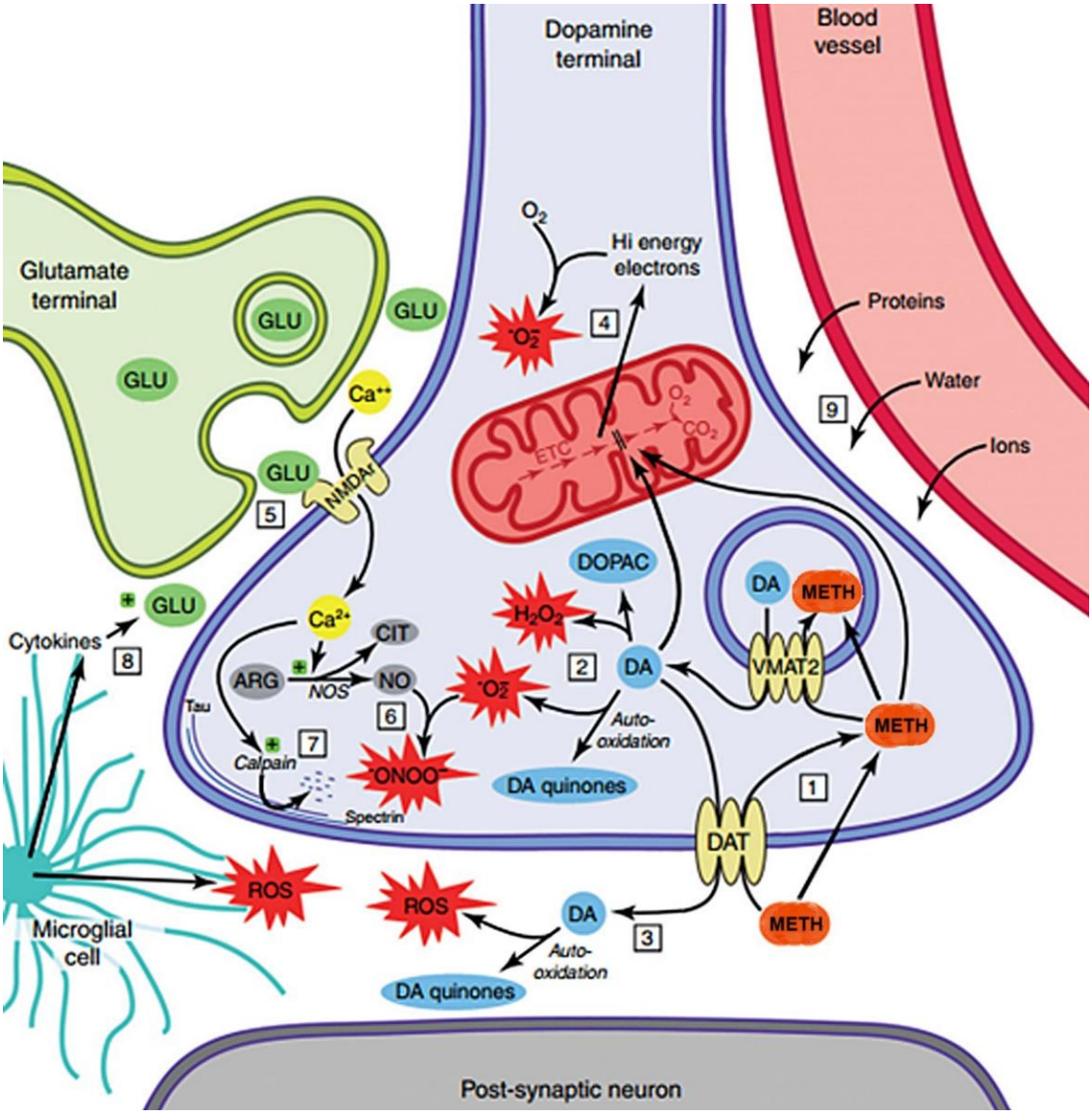

Figure 1.3. Scheme summarizing the cytotoxicity mechanisms triggered by METH. (1) METH can enter the cell by diffuse transport via plasma membrane or by transport through dopamine transporters (DAT). Once in the cytoplasm, METH enters in dopaminergic vesicles causing an intracellular accumulation of dopamine (DA). **(2)** The presence of DA in the cytoplasm increases reactive oxygen species (ROS). **(3)** The free DA can be transported by DAT from cytosol to extracellular space, where it can be oxidized leading to an augmentation of ROS in the synaptic cleft. **(4)** Another negative effect caused by the presence of METH is the mitochondrial stress, characterized by inhibition of the electron transport chain (ETC). **(5)** Furthermore, METH exposure also causes an increase in neuronal glutamate release**,** leading to an increase in intracellular Ca^{2+} levels**. (6)** By its turn, Ca^{2+} will stimulate nitric oxide synthase (NOS) activity, causing an increase in reactive nitrogen species (RNS). **(7)** This cellular stress induced by METH is followed by

activation of calpain and proteolysis of cytoskeleton proteins, such as tau and spectrin. **(8)** Regarding glial cells, METH triggers the release of ROS and cytokines, such as tumor necrosis factor-alpha (TNF-α) and interleukin 1-beta (IL-1β). **(9)** Finally, METH is also responsible for blood-brain barrier (BBB) dysfunction, which allows plasma proteins and water to cross the barrier into the brain parenchyma (adapted from Marshall and O'Dell, 2012).

1.1.2. Medical Use

The first medical use of METH was under the brand name of Pervitin, which was given to German air force pilots during World War II until 1940. After that, it was only in the 1950s that Obetrol Pharmaceuticals launched the first pharmaceutical METH product, Obetrol, to treat obesity, turning it into a popular diet pill in 1960s in the United States of America (USA). In fact, until today METH is prescribed for obese patients but it is mainly used to treat attention deficit hyperactivity disorder (ADHD), under the name of Desoxyn (manufactured by Ovation Pharma) approved by the Food and Drug Administration (FDA) from USA (US-FDA, 2013). Besides the USA, the medical use of METH is only recognized by a few countries, such as Hong Kong and Australia. In most European countries, as well as in Canada and Japan, the possession/consumption and production of METH are illegal (INCD, 2005).

Desoxyn is sold in 5 mg tablets for oral administration for treatment of 6-year-old children or older diagnosed with ADHD, or for exogenous obesity as a short-treatment option. Regarding ADHD, the administration is recommended to be once or twice a day with a usual effective dose of 20-25 mg daily. For obesity, one tablet (5 mg) is taken 30 min before each meal, and the treatment schedule should include only a few weeks in duration and is not recommended for children under 12 years of age (US-FDA, 2013).

Finally, METH can also be ultimately recommended as a last effort in the treatment of narcolepsy, at a maximum dose of 40-60 mg daily, and of idiopathic hypersomnia (US-FDA, 2013).

1.2. Blood-Brain Barrier

The blood-brain barrier (BBB), one of the blood-neural barriers, is present in almost all brain regions and has a role in the regulation of autonomic nervous system and endocrine glands (Ballabh et al., 2004; Cardoso et al., 2010). At the cellular level, this dynamic and specialized structure is composed of endothelial cells (ECs), connected with each other by tight (TJs) and adherens (AJs) junctions, and associated with pericytes, basement membrane, astrocyte endfeet, microglia, and neurons comprise the neurovascular unit (NVU) (**Figure 1.4**). The brain endothelium, with the lack of fenestrations and low fluid-phase endocytosis (pinocytosis), is the first "physical barrier" where intercellular complexes confer low paracellular permeability and high electrical resistance to the BBB (Choi and Kim, 2008; Cardoso et al., 2010). The core importance of the BBB is demonstrated by its role in the maintenance of brain homeostasis and protection against toxic compounds and blood fluctuations, but simultaneously provides nutrients essential for the normal brain function (Abbott et al., 2006; Dietrich, 2009; Cardoso et al., 2010). The transports across the BBB are limited, highly selective and generally divided into paracellular and transcellular routes

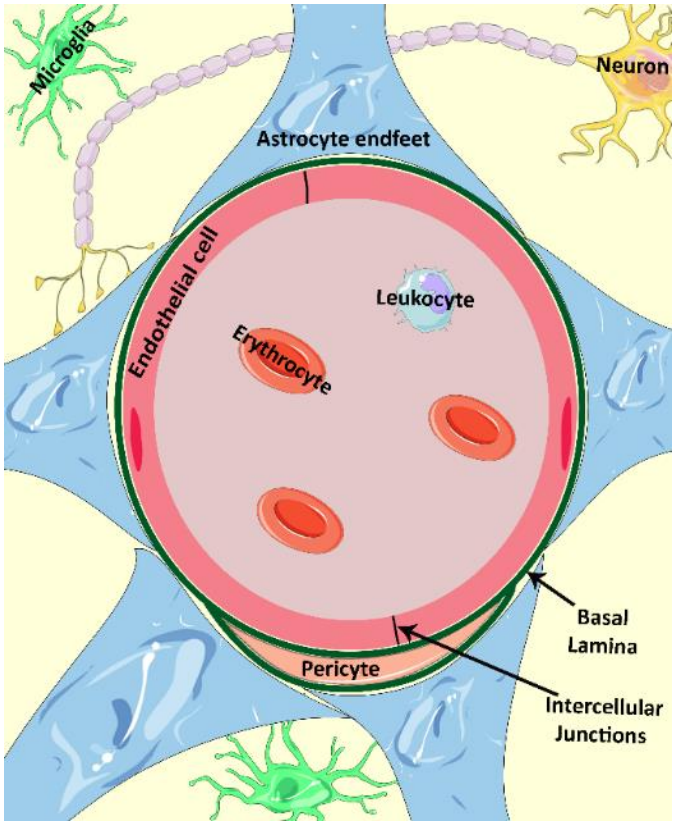

Figure 1.4. Schematic representation of the neurovascular unit. The neurovascular unit is formed by endothelial cells delimitating the brain microvessels, which are surrounded by basal lamina, pericytes, astrocytes endfeet, microglia and neurons (from Leitão et al., 2016 with permission).

Besides the BBB, there is also the blood-cerebrospinal fluid barrier, blood-retinal barrier and blood-spinal cord barrier (**Figure 1.5**). The blood-cerebrospinal fluid barrier (BCSF) is present in choroid plexus at the ventricular system and it is important for the production of cerebrospinal fluid (CSF) that will protect the brain and spinal cord. The capillaries of this barrier are more permeable and have more fenestrations than BBB, but they also express TJs proteins. Interestingly, these proteins are not all the same since the types of claudins differ from one barrier to another (Ballabh et al., 2004; Choi and Kim, 2008).

The blood-retinal barrier (BRB) is important to deliver oxygen and nutrients to the retina, and it is divided in two barriers: the outer and the inner BRB. The outer BRB is formed by retinal pigment epithelium with fenestrations, unlike the BBB. The inner BRB is formed by

two beds of capillary endothelia, pericytes, supporting glial cells (Müller cells and astrocytes) and neural cells (Choi and Kim, 2008). Finally, the blood-spinal cord barrier (BSCB) is very similar to BBB, since it is also formed by microvessels surrounded by pericytes and astrocytes endfeet. The only differences between these two barriers are that BSCB has glycogen deposits and a higher permeability when compared to BBB (Choi and Kim, 2008).

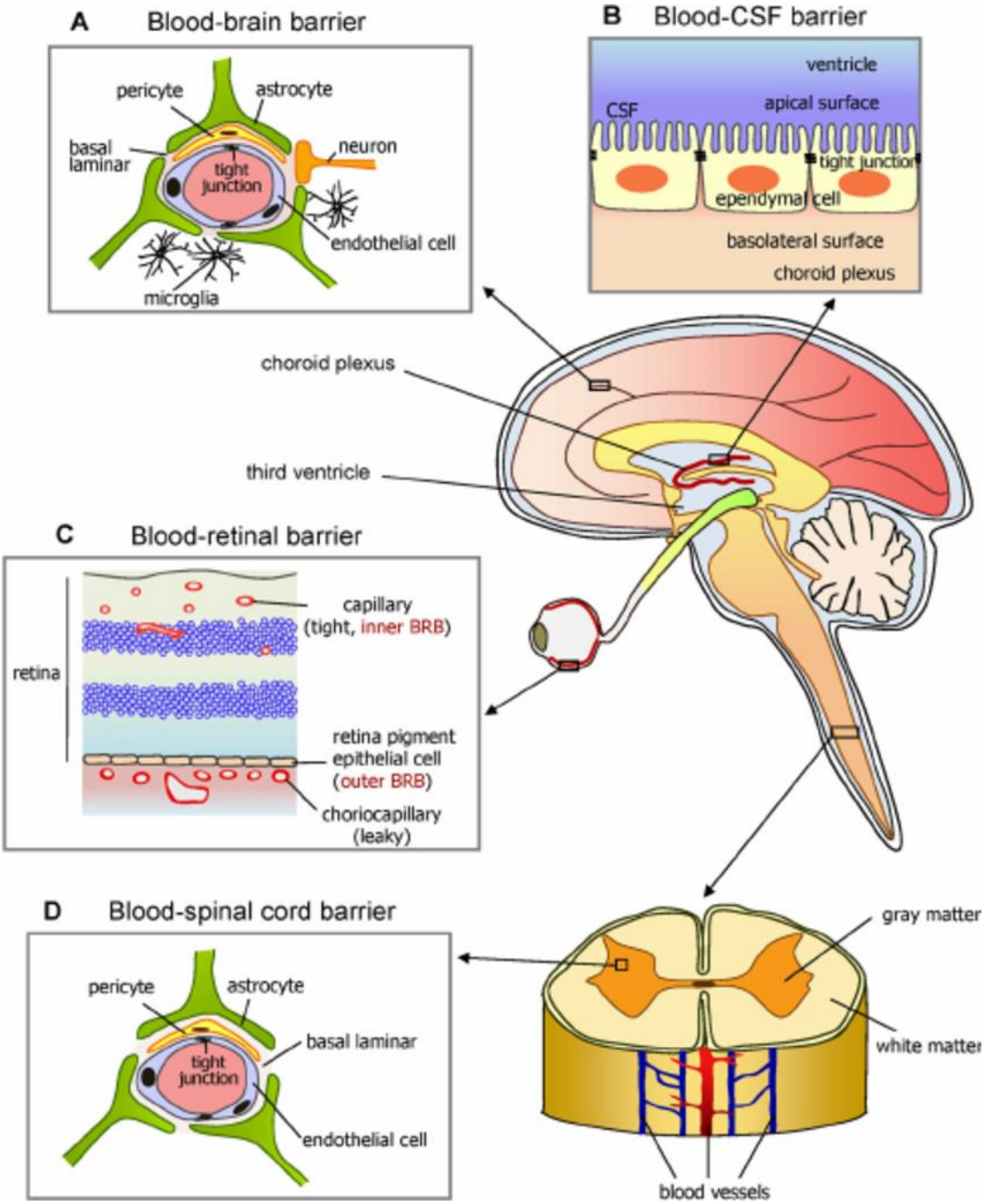

Figure 1.5. Blood-neural barriers present in the CNS. There are four different types of barriers. **(A)** The blood-brain barrier (BBB) separates the blood from de cerebral parenchyma. **(B)** The ependymal cells present in the blood-cerebrospinal fluid barrier (BCSF) are responsible for the production of the cerebral spinal fluid. In this barrier, the brain vessels are more fenestrated making the BCSF less restrictive than BBB. **(C)** The blood-retinal barrier (BRB) is composed of both inner and outer barriers. The inner BRB has a structure and properties similar to BBB and is formed by microvessels surrounded by pericytes and astrocytes endfeet; the outer BRB present fenestrated blood vessels and is its retinal pigment epithelium layer that forms the barrier. **(D)** The blood-spinal cord barrier protects the spinal cord microenvironment (adapted from Choi and Kim, 2008).

1.2.1. Cellular Composition of the Neurogliovascular Unit

The term of neurovascular unit emerged from the necessity to include the neurons surrounding brain microvessels in the BBB structure. This improvement in the designation of such structure enlightens the importance of neuronal cells in vascular tonus maintenance and control of vasoconstriction or vasodilatation under the specific stimulus. Nevertheless, the interface between blood flow and brain parenchyma is not composed only of endothelial cells, but also by the direct contact (by adhesion molecules and GAP junctions) and the indirect contact (by soluble molecules) with the basal membrane, pericytes (muscle cells), astrocytes, microglia and neurons that altogether are responsible for the transport/passage of molecules and cells between the two compartments (brain and blood). Thus, the term neurogliovascular unit appeared in 2007 reinforcing the importance of glial cells on the BBB (Bastide et al., 2007), and since then it is a widely used terminology.

1.2.1.1. Endothelial Cells

Brain ECs are the major cellular component of the NVU and have unique characteristics, such as high active metabolism with large number of mitochondria, presence of several transporters, low pinocytosis activity and absence of fenestrations (Ballabh et al., 2004; Kim et al., 2006; Cardoso et al., 2010). These features provide to ECs the capacity to

import and export different types of molecules, such as nutrients and toxic compounds, respectively (Cardoso et al., 2010). ECs are the main responsible for the barrier function, mainly due to the presence of intercellular junctions between adjacent ECs that seal the brain microvasculature maintaining the barrier structure and properties. Such intercellular complex is formed by TJs that are localized closer to the luminal side of the ECs, whereas the AJs are below the TJs, more close to the abluminal side (**Figure 1.6**; Mahajan et al., 2008). TJs act as a physical barrier by limiting the paracellular transport and as membrane domain barrier dividing both luminal and abluminal sides (Abbott et al., 2006; Kim et al., 2006; Cardoso et al., 2010). This polarity is also due to the distribution of several transporters.

1.2.1.1.1. Tight Junctions

The TJs are formed by transmembrane proteins, such as claudins, occludin and junctional adhesion molecules (JAMs), and cytoplasmic proteins, like zonula occludens (ZO), cingulin, AF-6, and 7H6. The cytoplasmic proteins are important to mediate interactions between transmembrane proteins and actin cytoskeleton (Mahajan et al., 2008; Cardoso et al., 2010). In detail, the claudin protein family comprises, until now, 27 members. Claudin-1, -3 and -5 are the most important in brain microvascular cells, and these phosphoproteins (20-22 kDa) have four transmembrane domains (Gonçalves et al., 2013). The cytoplasmic domain is the responsible for the connection with actin cytoskeleton mediated by ZO proteins, which act as a scaffold protein by linking the COOH-terminal of claudins with the actin COOH-terminal through its PDZ domain (Ballabh et al., 2004). Occludin and claudins show strong structural homology but with no amino acid sequence homology (Ballabh et al., 2004). Claudin-3 and -5 are important for BBB integrity, contributing to lower permeability and high transendothelial electrical resistance (Abbott et al., 2006; Mahajan et al., 2008; Cardoso et al., 2010). Several studies have shown that claudins form the primary seal of TJs by homotypic connection with claudins in the adjacent ECs (reviewed in Gonçalves et al., 2013). Also, Nitta et al. (2003) demonstrated

that homozygous mutant mice (*Cld5*−/− mice) were born in the expected Mendelian ratios, and looked normal macroscopically. However, their movements gradually ceased, and they all died within 10h of birth. On the other hand, the overexpression of claudin-5 was shown to improve the barrier function in cultured brain ECs (Ohtsuki et al., 2007).

Regarding occludin, it is also a phosphoprotein with four transmembrane domains and two extracellular loops (Ballabh et al., 2004; Abbott et al., 2006). The first extracellular loop mediates Ca^{2+}-independent adhesion, although ZO-1 presence is required (Cardoso et al., 2010). The cytoplasmic domain is responsible for the association between this protein and the cytoskeleton, mediated by accessory proteins, like ZO-1 through its guanyl kinase-like (GUK) domain which stabilizes the linkage with actin COOH-terminal (Ballabh et al., 2004; Abbott et al., 2006). Moreover, occludin is responsible for the high electrical resistance of the brain ECs contributing also to BBB stabilization. Although this protein plays an important role in barrier function (Huber et al., 2002; Brown and Davis, 2005), it is not essential for proper TJs formation, and normal expression and localization of other junctional proteins can compensate for occludin absence. Specifically, Saitou et al. (2000) demonstrated that occludin knockout mice did not show any morphologic changes in TJs but presented impairments in general development and breeding.

Another group of transmembrane proteins is the JAM family that includes three members as follows: JAM-1, -2, and -3. JAM-1 (or JAM-A) and JAM-3 are expressed almost exclusively in the brain (Ballabh et al., 2004; Cardoso et al., 2010). These proteins are part of the TJs formation as integral membrane proteins together with occludin and claudins (Vorbrodt and Dobrogowska, 2003). Moreover, the JAMs proteins have an important role in cell–cell adhesion and regulation of leukocytes migration through BBB (Persidsky et al., 2006). Importantly, altered expression of JAM-1, in addition to affecting the junctional tightness, may also disturb leukocyte trafficking with implications for the immune status of the brain (Abbott and Friedman, 2012). Although JAM-1 and -3 do not need accessory proteins to bind with the cytoskeleton, they can be linked to the ZO-1 protein (Mahajan et al., 2008).

Additionally, cytoplasmic proteins make the connection between the transmembrane proteins and the actin cytoskeleton. Besides their important structural/support function, cytoplasmic proteins are also involved in the regulation of gene transcription and cell proliferation (González-Mariscal et al., 2009; Cardoso et al., 2010). Among these, ZO proteins are found in the submembranous region and mediate the connection between claudin or occludin with the actin cytoskeleton (Kim et al., 2006). ZO-1 is a phosphoprotein that seems to be one of the most important ZO family member (Kim et al., 2006; Cardoso et al., 2010), since its loss leads to an increase in permeability and decrease in BBB tightness (Choi and Kim, 2008; Cardoso et al., 2010). ZO-2 is also a phosphoprotein that shows a great homology in amino acid sequence and structure with ZO-1 (Ballabh et al., 2004; Cardoso et al., 2010). The ZO-2 protein is mainly related to gene expression and cell cycle progression (González-Mariscal et al., 2009; Wolburg et al., 2009). Finally, ZO-3 shows protein homology with ZO-1 and -2, and some studies have suggested that ZO-3 is capable to directly bind to both occludin and ZO-1, stabilizing the link between these proteins (Cardoso et al., 2010). Additionally, cingulin, AF-6, and 7H6 play a role as a scaffold between transmembrane proteins and the cytoskeleton, being involved in TJs permeability to ions and large molecules (Sandoval and Witt, 2008).

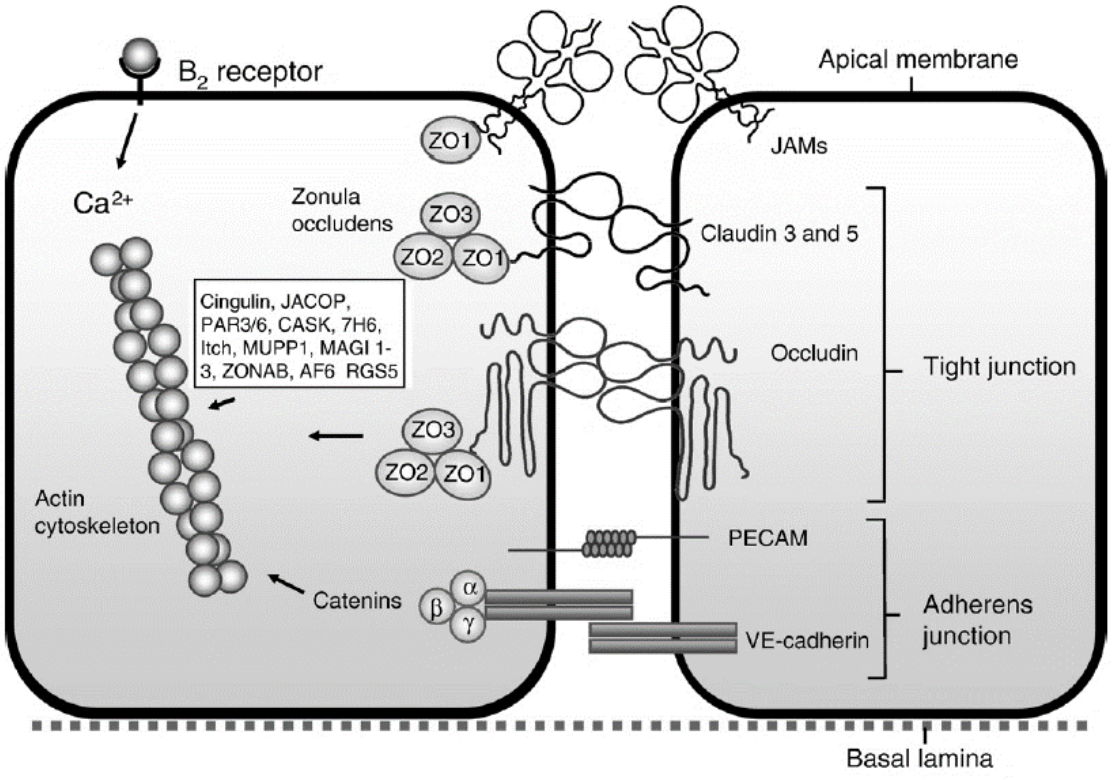

Figure 1.6. Distribution of tight and adherens junctions in the brain endothelial cells. The intercellular complex between two adjacent endothelial cells is composed by tight and adherens junctions. Tight junctions (TJs) are formed by transmembrane proteins, such as occludin, claudins (from a total of 24 different claudins, the type 1 and 5 are the most expressed in the BBB) and JAMs, 1, 2 and 3. The accessory proteins of TJs are zonula occludens (ZO-1, -2 and -3) and cingulin, among others. Adherens junctions (AJs) are formed by transmembrane proteins cadherins, being VE-cadherin the most expressed in brain microvessels, and by accessory proteins such as catenins. Cytoplasmic proteins of both tight and adherens junctions make the connection between the transmembrane proteins and the actin cytoskeleton (adapted from Abbott et al., 2010).

1.2.1.1.2. Adherens Junctions

The AJs are localized closer to the abluminal side of ECs and are responsible for cell–cell adhesion and for cell polarity, acting as a gate between luminal and abluminal sides (Hawkins and Davis, 2005). These junctions include the protein family cadherins, composed by more than 80 different subtypes, with vascular endothelial (VE)-cadherin (Navarro et al., 1998) and neural(N)-cadherin (Vorbrodt and Dobrogowska, 2003) the most express cadherins in brain microvessels and in the brain tissue, respectively. These transmembrane glycoproteins mediate cell adhesion in a Ca^{2+}-dependent manner, inhibit

cell proliferation, and decrease cell permeability and migration. Additionally, the catenins are responsible for the connection between cadherins and the actin cytoskeleton. This protein family is constituted by four different isoforms (α-, β-, δ- and γ-catenin), in which β-catenin is the most expressed in brain endothelial cells. Besides the role of β-catenin in the anchorage of cadherins to the cellular cytoskeleton, this protein plays also an important role as transcription factor regulating several genes (Vorbrodt et al., 2008).

1.2.1.1.3. Transport Across Endothelial Cells

The presence of intercellular junctions is responsible for the control of paracellular pathway, which includes the passage of small and water-soluble molecules between adjacent ECs. In fact, this pathway is used by small water soluble agents and ions that cross the BBB accordingly to their concentration gradient (**Figure 1.7**; Petty and Lo, 2002). Since this type of transport is regulated by TJs and AJs, alterations of endothelial intercellular junctions will interfere with this route. Further, molecular features of compounds can also interfere with their entry into the brain since a polar surface area higher than 80 Å and/or a molecular weight greater than 450 Da will restrict BBB permeability.

Regarding the transcellular transport, it can occur by passive diffusion of lipophilic compounds, or mediated by vesicles or selective transporters (**Figure 1.7**; Abbott et al., 2006), such as the glucose transporter-1 (GLUT-1) and adenosine triphosphate(ATP)-binding cassette transporters (ABC transporters). Small lipophilic molecules and gasses (like oxygen and carbon dioxide) pass through endothelium by diffuse transport (Ballabh et al., 2004; Cardoso et al., 2010). On the other hand, most polar molecules cannot enter the brain by diffuse transport and for that ECs express a large number of transporters in the cell membrane. This type of transport includes GLUT-1 that is expressed in higher concentration in the abluminal membrane when compared with the luminal side (Cardoso et al., 2010). The importance of this asymmetrical expression is to prevent the accumulation of glucose in the brain in concentrations higher than those present in the

blood stream (Cardoso et al., 2010). The other group of transporters present in ECs is the ABC transporters, that includes the P-glycoprotein 1 (P-gp) and the multidrug resistance-associated proteins (MDR). The main role of ABC transporters is to act as efflux pumps of a diversified range of lipid-soluble compounds (Abbott et al., 2010). The presence of P-gp transporter in the luminal membrane is three times greater than in the abluminal cell membrane, and so prevents the passage of blood-borne molecules into the brain and facilitates their transport out of the brain tissue. Further, P-gp can also be found on the cell membrane of astrocytes and pericytes (Bendayan et al., 2006). MDR transporters are expressed mainly in the luminal membrane of ECs and are responsible for the efflux transport of anionic compounds (Cardoso et al., 2010).

Transcytosis of macromolecules in BBB can be divided as follows: receptor-mediated (RMT) or the adsorptive-mediated (AMT) transcytosis (**Figure 1.7**). The RMT involves the binding of a ligand to its specific receptor which will trigger the internalization of the newly formed complex and ultimately leads to its exocytosis on the opposite side of the cell (Abbott et al., 2010). Alternatively, in AMT an excessively charged molecule interacts with cell surface binding sites inducing the endocytic process (Abbott et al., 2010). Noteworthy, brain ECs present a low pinocytic activity (Claudio et al., 1989) that can highly increase under pathological conditions. Indeed, endocytic vesicles play an important role in the transport into the brain, and the most studied are the caveolae-derived vesicles. Importantly, caveolin-1 is the primary coat protein of caveolae and regulates cell proliferation, as well as both nitric oxide and calcium signaling (Minshall et al., 2003). Moreover, this vesicular protein seems to have a role in the downregulation of TJs proteins after exposure to HIV-1 Tat protein (Zhong et al., 2008). Interestingly, authors observed that caveolin-1 silencing protected the human brain microvascular endothelial cells from Tat protein-induced damage, and this effect seems to be mediated by small GTPase Ras pathway (Zhong et al., 2008).

In addition to the abovementioned routes of transport, migration of cells through the BBB is a tightly regulated and complex process. However, peripheral immune cells are recruited

into the brain parenchyma under some pathological conditions. This phenomenon, known as diapedesis, is rare under physiological conditions and can occur through the transcellular or paracellular pathways with the involvement of several adhesion molecules (Engelhardt, 2006). A complex sequence of events ensures that leukocytes only enter into the brain tissue at the specific inflammatory site. The sequence of leukocytes diapedesis can be divided into four main steps. The first is the attachment of leukocytes to the vessel wall which involves L-selectin, very late antigen 4 (VLA-4), E-selectin and P-selectin ligand expression in leukocytes, whereas in endothelial cells the sialyl-Lewis x antigen, vascular cell adhesion molecule 1 (VCAM-1), E-selectin and P-selectin are the players involved in this migration step (Muller, 2013). Afterward, leukocytes will locomote on ECs toward the cell borders by an on-off interaction between leukocytes macrophage-1 antigen (Mac-1, also known as CD11b) and the intercellular adhesion molecule-1 (ICAM-1) expressed in ECs (Muller, 2013). The third step corresponds to the leukocytes transmigration through the endothelium and the basement membrane, and involves the interaction of platelet/endothelial cell adhesion molecule 1 (PECAM-1 or CD31) and CD99, both expressed in leukocytes and ECs (Muller, 2013). Importantly, this is a no-return step, meaning that once the diapedesis start there is no cellular mechanism to stop such process. The passage of leukocytes between adjacent ECs can occur by a rearrangement of TJs proteins or by a previous downregulation of intercellular proteins induced by a BBB injury (Engelhardt, 2006; Abbott et al., 2010). Finally, the last step of transmigration is the passage through the interstitial tissue where the interaction between leukocytes Mac-1/CD11b proteins with ICAM-1 from ECs or pericytes will guide the immune cells from the bloodstream into the brain parenchyma (Muller, 2013). Nevertheless, the peripheral immune cells can penetrate brain tissue with an intact BBB using the transcellular pathway. Despite the poorly understanding about this diapedesis pathway, some of the paracellular players are also involved in the transcellular migration of immune cells, such as ICAM-1, PECAM, and CD99 (Muller, 2013).

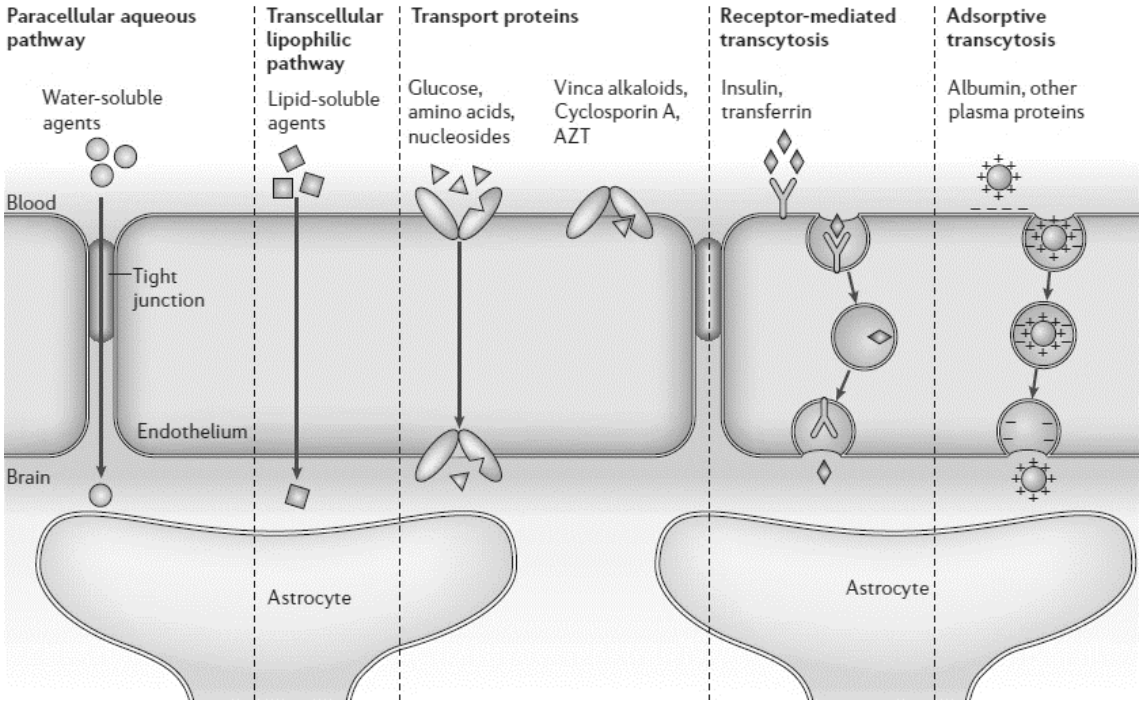

Figure 1.7. Routes across brain endothelial cells. The paracellular transport is relevant for ionic homeostasis. The selective transporters of proteins are important to suppress the nutritional needs of the brain. Both receptor-mediated and adsorptive transcytosis may also occur under physiological conditions, but at a low level (adapted from Abbott et al., 2006).

1.2.1.2. Pericytes

Pericytes, also known as vascular smooth muscle cells, cover approximately 30% of the brain capillaries. They have contractile proteins that give them the capacity to regulate blood flow and provide structural stability to brain microvasculature (Sweeney et al., 2016). Importantly, pericytes can communicate with ECs by gap junctions, adhesion plaques and soluble factors (Cardoso et al., 2010). Additionally, these cells are responsible for producing and releasing components of the basal lamina, including several types of proteoglycans (Cardoso et al., 2010), and also have an important role in the control of transcytosis (Bell et al., 2010) and BBB properties via upregulation of both TJs and AJs proteins (Armulik et al., 2010; Bell et al., 2010) In fact, more recently a triple primary cultures model of BBB (endothelial cells, pericytes and astrocytes) was developed with higher values of transendothelial electrical resistance (TEER) and lower levels of

permeability when compared to both co-cultures (endothelial cells and astrocytes) or monocultures (only endothelial cells) (Helms et al., 2016). Degeneration of pericytes causes BBB hyperpermeability (Bell et al., 2010) and an increase of proinflammatory molecules (Kovac et al., 2011; Jansson et al., 2014).

1.2.1.3. Basal Lamina

The basal lamina is the acellular component of the NVU and is composed predominantly of collagen type IV, laminin, fibronectin and proteoglycans (Kim et al., 2006; Cardoso et al., 2010). This structure is important for anchoring endothelial cells and pericytes, and for connecting these cells with other neighbor cells (Cardoso et al., 2010). Disruption of basal lamina, by downregulation of its components or by degradation, will negatively interfere with BBB properties (Cardoso et al., 2010). In fact, the major contributor to basal lamina degradation is matrix metalloproteinases (MMP), which are zinc-dependent endopeptidases capable of both extracellular matrix and TJs proteolytic cleavage (Rosenberg, 2002). Specifically, a cause-effect relation between augmentation of MMP expression/activity and BBB disruption with TJs protein degradation was demonstrated in mice exposed to a single dose of METH (Martins et al., 2011) and in a rat cerebral ischemia model (Yang and Rosenberg, 2011).

1.2.1.4. Astrocytes

Astrocytes, or more specifically the astrocytic endfeet, play an important role in the formation and maintenance of the NVU (Ballabh et al., 2004; Abbott et al., 2006; Kim et al., 2006; Kou and Lu, 2011). In fact, one of their functions is to connect ECs with close neurons by its processes (**Figure 1.8**; Kim et al., 2006), and to control brain water homeostasis due to the expression of water channels denominated aquaporins (Abbott et al., 2006; Nag et al., 2009).

It is important to highlight that astrocytes can have a dual role. They can release trophic and soluble factors important for neuronal survival, as well as for BBB formation and maintenance (Ballabh et al., 2004). Additionally, astrocytes are responsible for the reuptake and metabolism of some neurotransmitters, specifically glutamate and gamma-aminobutyric acid (GABA; Abbott et al., 2006; Allaman et al., 2011). On the other hand, astrocytes can release MMPs (Rosenberg, 2002), proinflammatory cytokines, such as interleukin-1 beta (IL-1β) and tumor necrosis factor-alpha (TNF-α; Abbott, 2002; Abbott et al., 2006), and high concentrations of calcium to the extracellular space leading to excitotoxicity (Rossi and Volterra, 2009).

1.2.1.5. Microglia

Microglia is the major component of the brain immune system, and can present itself in two main phenotypes: resting microglia, highly ramified with long cytoplasmic protrusions constantly surveying the surrounding microenvironment; and activated microglia, with short processes, high proliferation rate, migration and phagocytic activity (Du et al., 2016). The most recognize activation states is also known as M1 and M2 phenotypes. The M1 microglia is the classical activation state characterized by a robust release of inflammatory mediators, including ROS and proinflammatory cytokines (Choi and Kim, 2008, Coelho-Santos et al., 2012), recruitment of peripheral immune cells and phagocytosis (Barata-Antunes et al., 2017). In contrast, the M2 phenotype is associated with an anti-inflammatory role of microglia (Barata-Antunes et al., 2017). Despite the classical classification of resting and activated microglia, this is not straightforward since microglia can present several phenotypes and switch between them in response to microenvironments changes.

Activation of microglia can be triggered by several stimuli, such as inflammatory molecules released by astrocytes, increase in extracellular glutamate and blood serum molecules that pass through an impaired BBB (Ransohoff and Perry, 2009). In fact, these cells can be found in the surroundings of BBB suggesting their participation in the barrier function (Choi and Kim, 2008). Moreover, growing evidence has suggested that microglial cells have a crucial role in neuronal development and in synaptic fine-tune (Kettenmann et al., 2013)

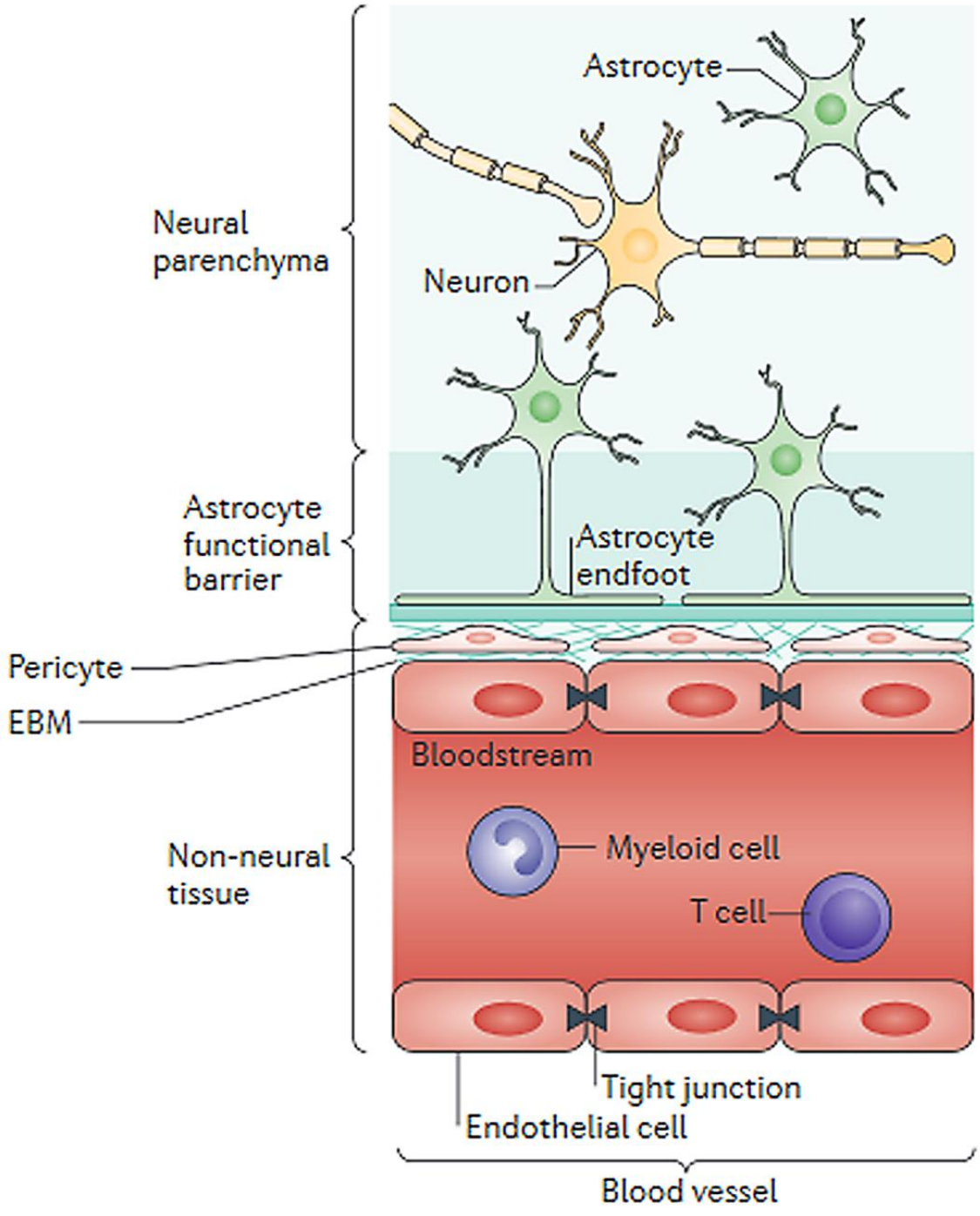

Figure 1.8. Schematic representation of astrocytes localization in the neurovascular unit. Astrocytes indirectly contact with brain vessels by their endfeet, forming the astrocyte functional barrier. Moreover, the intercellular junctions (tight and adherens junctions) are the molecular players that form the barrier seal between adjacent endothelial cells. Surrounding the brain vessels there are also pericytes and extracellular basal membrane (EBM). Importantly, astrocytes have also a role in communication between neurons and endothelial cells, acting as an intermediary player (adapted from Sofroniew, 2015).

1.2.1.6. Neurons

Neurons are considered the major and more important cells in the brain. Regarding BBB, neurons are not directly connected to brain ECs and require astrocytes to mediate this link (Kim et al., 2006). Nevertheless, noradrenergic, serotonergic, cholinergic, and GABAergic neurons (Hawkins and Davis, 2005) can influence ECs function by controlling blood flow (Kim et al., 2006; Cardoso et al., 2010)

1.3. Brain Edema

The water content in a normal brain corresponds approximately to 78% of total tissue weight (McIlwain and Bachelard, 1985). An alteration in this tightly controlled content leads to a pathophysiological condition, known as brain edema, and defined by an excessive water accumulation in the intracellular or extracellular spaces. Since skull free space is scarce, the abnormal water accumulation in the brain, even if small, will lead to an increase in intracranial pressure, which in turn causes brain microvasculature squeezing resulting in severe oxygen and nutrients supply depletion followed by cell death (Adeva et al., 2012; Papadopoulos and Verkman, 2013).

Brain edema can be divided into four main categories as follows: vasogenic, cytotoxic, osmotic and hydrostatic, being the main differences between them the pathological conditions that induce the edema formation. Nevertheless, this classification cannot be done in a straightforward manner. In fact, in situations such as hypoxia/ischemia (Ho et al., 2012), traumatic brain injury (Barzó et al., 1997, Dalle Lucca et al., 2012), neuroinflammation (Lazovic et al., 2005), and schizophrenia (Koch et al., 2001) both cytotoxic and vasogenic edema can occur (Hackett, 1999).

1.3.1. Types of Cerebral Edema

Vasogenic edema is more frequent in the white matter than in the gray matter (Adeva et al., 2012) and is associated with microvasculature disruption leading to an accumulation of water in the extracellular space (**Figure 1.11**). This type of edema is found after trauma, tumors, focal inflammation, ischemia and hypertensive encephalopathy (Adeva et al., 2012; Benga and Huber, 2012). Concerning cytotoxic edema, it is characterized by an intracellular water accumulation (**Figure 1.11**), due to an impairment in sodium and potassium pumps or in water channels present in cell membranes. Cytotoxic edema occurs in several intoxications, such as with dinitrophenol (Ennis and Keep, 2006), isoniazid (Hawkes et al., 2008) and hexachlorophene (Kinoshita et al., 2000), as well as

in ischemia, stroke or hypoxia (Strbian et al., 2012). In this type of brain edema, the BBB is usually found intact. Interestingly, both vasogenic and cytotoxic edemas can co-exist in conditions like infarct, being the cytotoxic the first to appear followed by the vasogenic type.

In osmotic edema, an osmolality imbalance between cerebral-spinal fluid and plasma is observed. The water flow occurs from plasma into the brain due to the pressure gradient that is caused mainly by salts and nutrients imbalance. This type of edema is frequently found in hyponatremia (Ayus et al., 2008) and hemodialysis (Bagshaw et al., 2004) pathological conditions. Finally, in the hydrostatic type of edema the water flow into the brain tissue by an augmentation of cerebral capillary pressure, as observed in hypertension (Adeva et al., 2012).

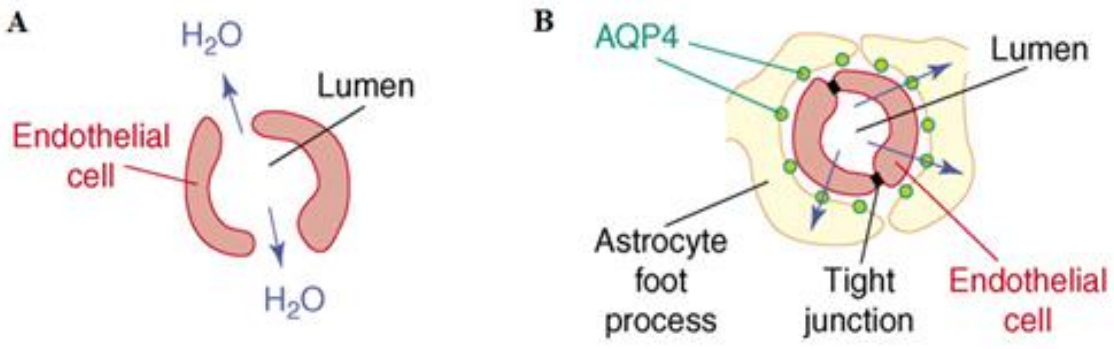

Figure 1.11. Vasogenic and Cytotoxic Edema. (A) Scheme representing a vasogenic edema, where brain water accumulation is independent of aquaporins (AQPs), but AQP4 has a key role in the clearance of the excessive water volume. **(B)** Cytotoxic edema, in which the increase in water brain content is due to an increase in water transport through astrocytic AQP4 (adapted from Tait et al., 2008).

1.3.2. Some Causes of Brain Edema

Considering the several types of brain edema it is also expected that each one present different etiologies. Firstly, vasogenic edema is always linked to BBB disruption, so alterations in the expression levels or organization of intercellular junctions' proteins can explain, at least in part, the appearance of such type of edema. One of the important

players in BBB disruption is the MMPs because of their proteolysis ability to degrade basal membrane and TJs proteins (Rempe et al., 2016). Indeed, in a mouse model of acute liver failure, MMP-9 activity was shown to be involved in brain edema and BBB disruption and its inhibition prevented both water accumulation and microvasculature breakdown (Chen et al. 2009). On the other hand, cytotoxic edema is not usually accompanied by such TJs/AJs alterations, since BBB appears intact. Thus, water accumulation can be caused by ionic or water imbalance that forces water accumulation in brain parenchyma, or by the dysfunction of a system that somehow regulates the brain water homeostasis. The most prominent key player in this type of edema is the water channel aquaporin 4 (AQP4). AQP4 is highly expressed by astrocytes endfeet that surround brain microvasculature (**Figure 1.12**), and in ependymal cells (Tait et al., 2008). Despite the important role of this water channel in brain water homeostasis, it has also a role in formation and resolution of brain edema. Notwithstanding, the molecular mechanisms beyond its regulation, function, and involvement in BBB dysfunction are still unknown.

Several mediators have been shown to have an active role in cytotoxic brain edema, such as ROS, vascular endothelial growth factor (VEGF), and proinflammatory cytokines (Walcott et al., 2012). Nevertheless, some of these molecules, such as ROS, can also be involved in vasogenic edema since they can lead to BBB disruption (Panahpour et al., 2014; Abdul Muneer et al., 2015). In fact, in pathological conditions as hypoxia and diabetic ketoacidosis, where brain edema is a key feature, high levels of free radicals can be detected (Fraser, 2011). Moreover, VEGF was shown to be involved in the increase of brain water content and BBB hyperpermeability via hypoxia-inducible factor (HIF) upregulation (Argaw et al., 2009; Adeva et al., 2012). Brain tumor cells are also able to produce and release VEGF to increase blood and nutrients supply that are needed to grow and develop metastases (Trevisan et al., 2014). Additionally, proinflammatory cytokines, like TNF-α, interleukins, and CCL2 (chemokine (C-C motif) ligand 2), are also capable of causing BBB disruption (Candelario-Jalil et al., 2007) and brain edema (Collins and Neafsey, 2012; Kim et al., 2013). In fact, it was already demonstrated that both IL-1β and

TNF-α lead to an upregulation of AQP4 in cultured astrocytes (Asai et al., 2013). Moreover, a very recent work by Liu and collaborators (2015) showed that IL-1β knockdown diminished astrocyte swelling, a marker of cytotoxic edema, in an animal model of hypoxia-ischemia. Also, a mixed solution of IL-1β, TNF-α, and interferon-gamma (IFN-γ) caused an upregulation of AQP4 in cultured astrocytes (Asai et al., 2013).

1.3.3. Therapeutic Approaches

Even though brain edema is a serious health condition, the available treatments are scarce and ineffective. The current treatments consist mainly of osmotherapy, control of arterial blood pressure, and surgical decompression, as the last effort to relieve the increase in intracranial pressure.

The most used drug in osmotherapy is mannitol, a powerful compound that exerts its beneficial effects by promoting a gradient that ultimately will force water molecules to move out the brain tissue into the blood flow. However, mannitol can also lead to a general hypotension, heart failure, electrolyte abnormalities and acute renal failure (Grände and Romner, 2012). Another drug widely used in osmotherapy is a hypertonic saline solution, which shows the same effectiveness as mannitol in reducing the brain water content but without the diuretic effect of mannitol. Nevertheless, it can cause an imbalance in blood sodium levels (Walcott et al., 2012). When osmotherapy fails, barbiturates are the second option. One example is pentobarbital that act by reducing both intracranial blood volume and the metabolic demand within brain parenchyma (Walcott et al., 2012). Another approach to treating brain edema specifically related with brain tumors is the administration of corticosteroids (Heiss et al., 1996).

Despite the abovementioned treatments, most of the times they are not sufficient to avoid severe sequels or even death. Therefore, it is important to improve our knowledge about the underlying mechanisms involved in brain edema formation to allow a more effective approach. Several transporters and receptors have been implicated as meaningful

mediators in the treatment of brain edema. One of those transporters is the Na-K-Cl cotransporter, responsible for the active transport of sodium, potassium, and chloride in and out of the cells. In fact, exposure to MDMA causes alterations in sodium homeostasis, leading to a reduction in sodium blood levels, known as hyponatremia (Ghatol and Kazory, 2012), whereas METH consumption causes hypernatremia, a rise in sodium levels (Sharma and Kiyatkin, 2009). Concerning the receptors involved in edema, the vasopressin receptor is one of the most promising therapeutic targets. Conivaptan, an antagonist of vasopressin receptor, has been used in the treatment of brain edema due to its inhibitory effect on the development of hyponatremia, which is associated with the formation of brain edema (Walcott et al., 2012).

1.3.4. Aquaporins

The specific mechanisms underlying edema formation are still unclear, which highlights the urgency of dissecting such pathways to identify new targets and approaches to control brain water movements and homeostasis. In fact, alterations in water channel AQP4 have been associated with the increase of brain water content in several neuropathologies, such as trauma, ischemia, epilepsy, and in tumors of astrocytic origin (Nag et al., 2009).

Aquaporins (AQPs) are small proteins with approximately 30 kDa. Despite different permeability coefficients, all the water channels form a tetramer and each monomer has its own functional channel (Smith and Agre, 1991). Aquaporin protein family comprises 13 different proteins (0 to 12; Itoh et al., 2005) and can be divided into 4 groups regarding its permeability as follows: type 0, 1, 2, 4 and 5 are water permeable; type 3, 7, 9 and 10 are also known as aquaglyceroporins due to their permeability to water and other small non-polar solutes, like glycerol and urea; type 6 and 8 are also permeable to ions; and type 11 and 12 although having amino acids sequence homology with other AQPs they lack structural characteristics similarities, nevertheless they are both permeable to water but at a low rate than the others water permeable AQPs (Rojek et al., 2008). Regarding the

cerebral tissue, the most expressed types are 1, 4 and 9 (Venero et al., 2001; Tait et al., 2008; Francesca and Rezzani, 2010). AQP1 has a role in CSF formation and is present in choroid plexus epithelium (Zelenina, 2010). AQP9 is important to energetic metabolism, and is present in neurons (Amiry-Moghaddam et al., 2005), in tanycytes from the wall of the third ventricle, and in endothelial cells of subpial blood vessels (Tait et al., 2008). Finally, AQP4 has a role in both formation and resolution of cerebral edema, in K^+ clearance during neuronal activity and can be found in astrocytes and ependymal cells (Zelenina, 2002).

Each AQP4 monomer has six transmembrane domains with both terminals, carboxyl and amino, in the intracellular space (**Figure 1.12**; Preston et al., 1994; Nag et al., 2009). This water channel has two main isoforms originated by alternative splice, known as M1 and M23 (**Figure 1.12**; Jung et al., 1994). An additional isoform has been recently identified in rats as Mz with 364 amino acids (**Figure 1.12**) that presents a Nh2-terminal 41 amino acids longer than the isoform M1 (323 amino acids) (Moe et al., 2008). Isoform M23 is the smallest isoform with 301 amino acids but it is the most expressed in the brain. M1 and M23 isoforms are organized in supramolecular structures composed of aggregates of both isoforms in a tightly regulated ratio (Sorbo et al., 2008), forming orthogonal arrays of particles (OAPs; Furman et al., 2003; Silberstein et al., 2004; Nicchia et al., 2010). Moreover, OAPs composition and function depend on the relative amounts of both isoforms since an increase in M1 isoform in the OAPs leads to a disruption of this structure causing a dysregulation in water homeostasis, whereas an increase of M23 stabilizes the supramolecular structure (Furman et al., 2003). In fact, in Chinese hamster ovary cells transfect with both AQP4 isoforms the presence of M23 alone creates large OAPs, while the presence of M1 alone creates singlets of AQP4 tetramers. Thus, when the two isoforms are expressed, the OAPs formed are more comparable to the structures found in astrocytes *in situ* (Furman et al., 2003).

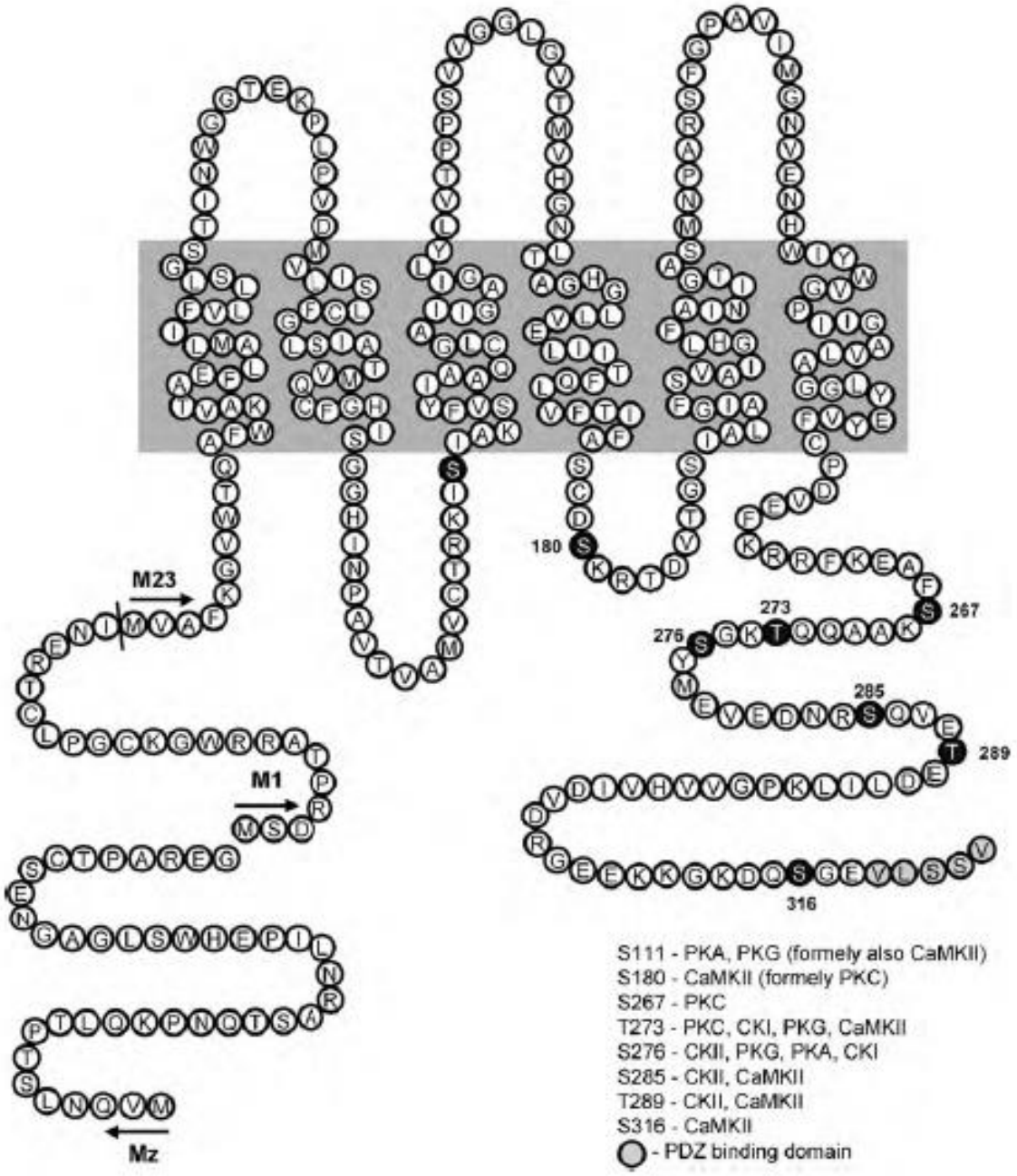

Figure 1.12. Schematic representation of aquaporin-4. AQP4 has three isoforms: Mz, M1, and M23. The Mz isoform is the longest with 364 amino acids and is express only in rat brain tissue. The M1 isoform has 323 amino acids and the M23 isoform is the smallest with 301 amino acids. Several residues of AQP4 can be phosphorylated by different kinases, such as protein kinase C and calcium-calmodulin-dependent protein kinase II (adapted from Zelenina, 2010).

Like other channels and membrane proteins, the regulation of AQPs is crucial for normal cellular function. AQP4 has two well-documented regulatory sites by phosphorylation of serine residues (Ser111 and Ser180, **Figure 1.12**). The serine residue present in position 111 (Ser111) can be indirectly phosphorylated by protein kinase C (PKC) or by calcium/calmodulin-dependent protein kinase II (CaMKII) through the recruitment of cGMP-dependent protein kinase (PKG). Interestingly, the inhibition of nitric oxide synthase (NOS) prevented the phosphorylation of Ser111 (Yukutake and Yasui, 2010; Zelenina, 2010), however, the specific mechanism behind this effect is still poorly understood. Several studies suggest that phosphorylation of Ser111 causes an increase in AQP4 water permeability (Gunnarson et al., 2005; Gunnarson et al., 2008). In turn, serine residue present in position 180 (Ser180) is directly phosphorylated PKC (Zelenina et al., 2002; McCoy et al., 2010), rapidly reducing the AQP4 water permeability (Zelenina et al., 2002; Nagelhus and Ottersen, 2013). Moreover, longstanding PKC activation causes AQP4 internalization and even a decrease in its *de novo* expression (Zelenina, 2010). Kadohira and collaborators (2008) also showed that phosphorylation of other COOH-terminal residues (Ser276, Ser285, and Thr289) by casein kinase II (CKII; **Figure 1.12**) are responsible for AQP4 transport from Golgi complex to the plasma membrane. Moreover, phosphorylation of Ser276 has been correlated with internalization and degradation of AQP4 in renal epithelial cells (Madrid et al., 2001). Importantly, AQPs are also regulated by metals ions like mercury (Hg) and lead (Pb). Most types of AQPs are inhibited by Hg (Amiry-Moghaddam and Ottersen, 2003) except for AQP6 that is activated by this metal (Hazama et al., 2002). Concerning AQP4, an older study classified it as mercurial-insensitive (Shi and Verkman, 1996; Nicchia et al., 2000), but afterward, Yukutake and collaborators (2008) demonstrated that isoform M23 can be inhibited by Hg. This inhibitory mechanism involves two cysteine residues in position 178 and 253 (**Figure 1.13**; Yukutake et al., 2008). The isoform M1 of AQP4 is probably regulated by mercury through NH_2-terminal residues (Yukutake and Yasui, 2010). Additionally, AQP4 can be regulated by

other metal ions such as zinc (Zn) and copper (Cu), causing an inhibition of AQP4 M23 isoform (**Figure 1.13**; Yukutake and Yasui, 2010).

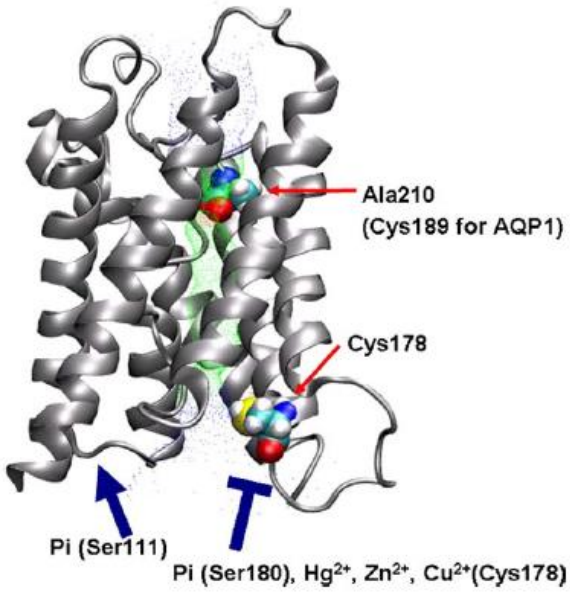

Figure 1.13. Structural 3D representation of aquaporin-4. Model of the AQP4 structure showing the residues involved in AQP4 inhibition by phosphorylation (Ser180) and metal binding (Cys178). The phosphorylation residue (Ser111) described as an inductor of water permeability is also indicated. The Ala210 residue, which corresponds to Cys189 on aquaporin 1 (AQP1), has been described as the residue responsible for channel selectivity to water molecules (adapted from Yukutake and Yasui, 2010).

Regarding AQP4 localization, it is mainly found in perivascular astrocytes endfeet that surround the ECs (**Figure 1.14**; Amiry-Maghaddam and Ottersen, 2003), where it plays an important role in BBB function. The AQP4 presence in perisynaptic astrocyte processes is involved in neurotransmitter uptake. Moreover, its expression in astrocyte processes close to nodes of Ranvier and to nonmyelinated axons is involved in the K^+ clearance (Zelenina, 2010). There is ample support for the claim that AQP4 has a crucial role in the control of water flux in and out the brain, and so on brain edema formation and resolution, respectively. Indeed, in several neuropathologies, like ischemia, traumatic brain injury, and brain tumors, alterations in AQP4 expression and activity are observed (Tait et al., 2008; Nag et al., 2009; Zelenina, 2010).

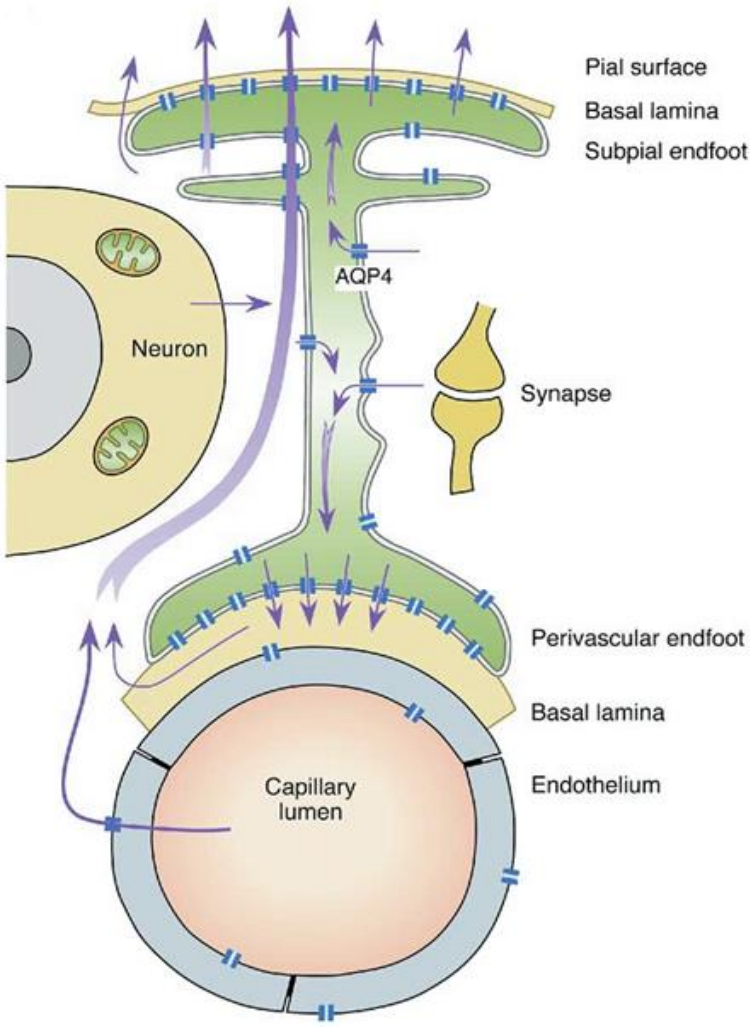

Figure 1.8. Aquaporin-4 in astrocytes and water movement between the capillary lumen and brain parenchyma. This image shows water uptake and release by astrocytic endfeet. The arrows indicate the direction of water movement (adapted from Amiry-Moghaddam et al., 2004).

In the brain, AQP4 anchorage to cellular membrane and consequently to extracellular matrix is mediated by dystrophin-glycoprotein complex, that comprises dystrophin (being the Dp-71 the most expressed in the brain), syntrophins (with α-syntrophin the most important in AQP4 anchorage), and both α- and β-dystroglycan (**Figure 1.15**; Amiry-Maghaddam et al., 2004; Connors et al., 2004). Interestingly, Neely and collaborators (2001) showed that in mice lacking α-syntrophin, the AQP4 became mislocalized and lose the characteristic distribution in astrocyte endfeet surrounding brain microvasculature.

Furthermore, an analogous effect was observed in null mice for dystrophin (Vajda et al., 2002). Nevertheless, many questions remain unanswered particularly related to the molecular mechanisms that regulate AQP4 function and its possible involvement on BBB dysfunction.

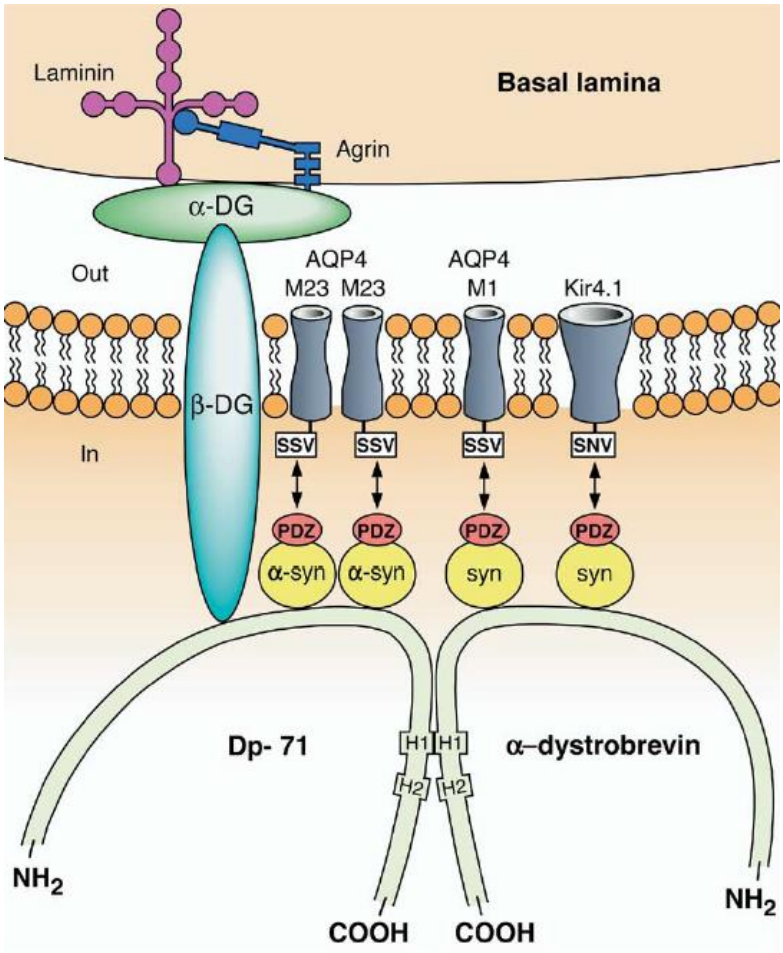

Figure 1.15. Anchoring of aquaporin-4 and interaction with dystrophin complex. AQP4 is anchored to the cytoplasm and basal lamina through connection with α- and β-dystroglycan (α-DG and β-DG, respectively) and α-syntrophin (α-syn). The association between AQP4 and α-syn occurs via PDZ domains. The α-syn links AQP4 to dystrophin-family proteins, such as dystrophin Dp-71 and α-dystrobrevin. Anchorage of AQP4 to basal lamina is mediated by α-DG and β-DG that is associated with laminin and agrin (adapted from Amiry-Moghaddam et al., 2004).

As abovementioned, in vasogenic edema (**Figure 1.11A**) there is an accumulation of water in brain extracellular space, and AQP4 has a role in the clearance of water excess. Thus, the water influx is AQPs-independent and seems to be due to BBB opening, whereas water efflux is AQP4-dependent (Venero et al., 2001; Tait et al., 2008; Nag et al., 2009;

Francesca and Rezzani, 2010). On the other hand, the cytotoxic edema (**Figure 1.11B**) involves the swelling of astrocytes probably due to an increase of AQP4 activity (Tait et al., 2008; Nag et al., 2009; Francesca and Rezzani, 2010). Therefore, depending on the type of brain edema, different therapeutic strategies must be adopted. The control of vasogenic edema can be performed via the increase of AQP4 activity, but cytotoxic edema treatment necessarily involves the reduction of the activity of this water channel (Nag et al., 2009; Francesca and Rezzani, 2010).

Despite some advances in the field, the role of AQP4 in cerebral edema is still unclear. In fact, several studies with knockout (KO) animals showed contradictory results. In models of cytotoxic brain edema, like hyponatremia (Papadopoulos and Verkman, 2007), bacterial meningitis (Manley et al., 2000) and in early focal cerebral ischemia (Papadopoulos and Verkman, 2005), the AQP4 knockdown showed a protection against brain edema formation. On the contrary, AQP4 KO animals present a higher vulnerability to vasogenic edema, such as under brain tumor conditions (Papadopoulos et al., 2004). These observations suggest that in cytotoxic edema AQP4 is responsible for the increase of brain water content, whereas in vasogenic edema AQP4 is responsible for removing the water excess out of the brain. Also, some studies have shown the involvement of AQP4 in K^+ clearance under epileptic conditions, and its deletion led to an increase in seizure threshold and duration (Amiry-Moghaddam and Ottersen, 2003; Binder et al., 2006). More recently, it was demonstrated that the inhibition of AQP4 with a novel specific inhibitor, TGN-020, has a protective effect against the increase of brain water content after water intoxication (which consists of an injection of water in a volume equal to 20% of body weight) and vasopressin administration (a protocol that causes brain edema without BBB disruption), thereby mimicking cytotoxic edema (Igarashi et al., 2011).

1.4. Neuroinflammation

Neuroinflammation is a complex and heterogeneous process that occurs in the CNS. The tissue response can occur after bacterial or viral infections, toxins exposure, autoimmune reactions, or mechanical damage. Additionally, neuroinflammation has been implicated in several chronic neurodegenerative disorders, such as Alzheimer's and Parkinson's disease, amyotrophic lateral sclerosis, Huntington's disease, HIV-induced dementia, among others (Sochocka et al., 2016).

After the injury, the innate immune response is turned on by the expression and release of cellular mediators, like cytokines and chemokines, ultimately leading to proliferation and activation of glial cells (microglia and astrocytes). The reactive glia produces a broad spectrum of inflammatory factors, such as IL-1β, IL-6, TNF-α, chemokines and nitric oxide, promoting the buildup of the inflammatory environment (Sochocka, et al., 2016). An acute neuroinflammatory process has usually a beneficial effect for infectious agents or toxic compounds cleansing, neurogenesis, synaptic modulation and brain repair (Sochocka, et al., 2016; Gualtierotti et al., 2017). However, if the resolution mechanisms fail or the insult persists over time, a situation of chronic neuroinflammation appears with the characteristic glial cells overactivation (Sochocka, et al., 2016). Under this condition, the death of brain cells will be caused by the accumulation of neurotoxic compounds and extensive peripheral immune cells infiltration (Gualtierotti et al., 2017), leading to tissue degeneration and development of autoimmune diseases (Sochocka, et al., 2016).

The main cellular players of neuroinflammation processes are microglia and astrocytes. Despite that, ECs have a crucial role in interpreting and propagate the inflammatory signals to the brain parenchyma (Sochocka, et al., 2016). Regarding microglia, these cells were the first described brain-resident immune cells. In fact, microglia cells, with a crucial active role in brain surveillance, can trigger neuroinflammatory processes leading to neurodegeneration or neuroprotection, depending on the type and duration of stimulus (Gualtierotti et al., 2017). On the other hand, astrocytes are the most abundant glial cell

type in the CNS, and despite the well-known roles of astrocytes on BBB maintenance, neuronal modulation, and water and ionic homeostasis, these stellate glial cells are also immune-competent cells capable of responding to insults by secrete cytokines, chemokines and by increasing the proliferation rate (Sochocka, et al., 2016).

Importantly, the neuroinflammatory players are not only cells but also chemical compounds, such as chemokines, ROS, and both anti- and proinflammatory cytokines. Chemokines are small heparin-binding proteins responsible for recruitment of peripheral and CNS immune cells to the damaged local (Gualtierotti et al., 2017). Moreover, both ROS and RNS cause oxidative stress leading to lipid peroxidation and NF-κB pathway activation (Sochocka, et al., 2016). ROS are also a well-known inducer of deoxyribonucleic acid (DNA) mutations (Sochocka et al., 2013), in both nucleus and mitochondria, and causes Ca^{2+} homeostasis dysfunction (Correale, 2014). Regarding anti-inflammatory cytokines, IL-10 has a role in neuronal homeostasis and cell survival, being also an important inhibitor of proinflammatory cytokines, such as IL-1β and TNF-α. In addition, IL-4 and IL-13 exert the anti-inflammatory effect by inducing microglial neuroprotective phenotype and by suppressing the expression of IL-1α/β and TNF-α. Among the proinflammatory molecules, TNF-α and IL-1β are the most relevant, but the IL-15 and IL-18 have also a role in microglial and inflammatory status activation. Regarding IL-1β, it has been shown a link between its overexpression and neurodegeneration, glial cells apoptosis and Alzheimer's disease progression (Sochocka, et al., 2016). Finally, TNF-α is expressed and release mainly by microglia and astrocytes. Importantly, this cytokine has a dual role in brain tissue being involved in neuroprotection and neurodegeneration depending on its levels and the receptor activated (Sriram and O'Callaghan, 2007).

1.4.1. Tumor Necrosis Factor-Alpha

TNF-α is a pleiotropic cytokine produced as a 26 kDa membrane-associated precursor (tmTNF) that is cleaved by TNF-α converting enzyme (TACE; a matrix metalloproteinase family member) releasing the soluble form (sTNF) with 17 kDa as a homotrimer (Montgomery and Bowers, 2012). TNF-α can be produced by immune (lymphocytes and macrophages) and non-immune (endothelial cells, muscle cells, fibroblasts, among others) cells, and within CNS it is produced mainly by microglia and astrocytes, and also by neurons (Montgomery and Bowers, 2012).

Regulation of TNF-α can occur in three different stages. First, at the transcriptional level TNF-α is controlled in its 5' gene flanking region by κB-like enhancers and a Y-box similar to that present on Major Histocompatibility Complex (MHC) class II gene (Montgomery and Bowers, 2012). Among the several transcription factors that have an affinity to TNF-α promoter are included the NF-κB, the CCAAT/enhancer-binding protein β (C/EBPβ), Sp1 transcription factor and c-Jun (Montgomery and Bowers, 2012). Secondly, the presence of adenine-uracil rich elements in 3' untranslated region of TNF-α gene post-translationally targets the messenger ribonucleic acid (mRNA) for degradation (Kontoyiannis et al., 1999). Finally, some inflammatory mediators can induce a downregulation of transcription and translation of this cytokine (Montgomery and Bowers, 2012).

There are two different TNF-α receptors: TNF-receptor 1 (TNFR1) and TNF-receptor 2 (TNFR2). Both receptors can be activated by sTNF and tmTNF forms but ligand-receptor combinations preference can be found. Specifically, sTNF has high affinity to both receptors, whereas tmTNF has a greater affinity to TNFR2 than to TNFR1 (**Figure 1.16**; Pozniak et al., 2014). Like TNF-α, also both receptors can be found in membrane-bound or in proteolytic cleaved form, whereas the soluble fragments have a role as a neutralizing molecule against TNF-α, protecting the tissue from its deleterious effects (Montgomery and Bowers, 2012). Importantly, both receptors lack enzymatic activity, therefore activation of signaling pathways is dependent of intracellular adaptor molecules binding through

death domains present in the receptors (**Figure 1.16**; Sriram and O'Callaghan, 2007). Thus, despite the well described neurotoxic effects of TNF-α, this cytokine has indeed a dual role dependent on to the receptor involved.

TNF-α is found overexpressed in amyloid β plaques in human post-mortem brain tissue and in transgenic rodent models of Alzheimer's disease (Montgomery and Bowers, 2012). Moreover, it has been already described that some polymorphisms on TNF-α gene are linked to late-onset of Alzheimer's disease (Collins et al., 2000). Further, the selective inhibition of sTNF, the administration of a monoclonal antibody against TNF-α (infliximab) or TNFR1 knockouts mice showed a protection against the accumulation of amyloid β peptide, an improvement in learning and memory scores, as well as a reduction in inflammatory status (Montgomery and Bowers, 2012). Regarding Parkinson's disease, TNF-α overexpression is found in the substantia nigra, within the striatum, and is correlated with the severity of the disease (Sriram and O'Callaghan, 2007). Moreover, cytokine neutralization protects dopaminergic neurons in a mouse model of Parkinson's disease (McCoy et al., 2006). However, data gathered by inhibition or knockdown of both TNF-α receptors are not consensual regarding the protective effect (Montgomery and Bowers, 2012). Concerning multiple sclerosis, it was expected that inhibition of TNF-α would result in patient improvements, however, in two clinical trials the administration of monoclonal antibodies caused an exacerbation of the disease (Montgomery and Bowers, 2012). Interestingly, in mouse models, the TNFR1 blockade repressed the development of the disease, but the inhibition of TNFR2 caused an exacerbation of disease severity (Kassiotis and Kollias, 2001). Finally, TNF-α upregulation is also associated with disease development and brain deterioration on HIV-dementia, ischemia and traumatic brain injury. Once again, antibodies against TNF-α had a protective role improving the neurological outcome (Sriram and O'Callaghan, 2007).

Although the abovementioned deleterious effects of TNF-α in the CNS, this cytokine has also a crucial role in several neuroprotective mechanisms. In particular, it was demonstrated that TNF-α mediated apoptosis during embryonic brain development

(Montgomery and Bowers, 2012) and acts as a neurogenic cytokine at low concentrations via activation of TNFR1 (Bernardino et al., 2008). Moreover, this cytokine has also a role in synaptic transmission by inducing expression of both glutamate receptors, AMPA and NMDA (Montgomery and Bowers, 2012). Moreover, pretreatment of mice with TNF-α before middle cerebral artery occlusion was able to protect from cerebral ischemia negative effects, such as microgliosis and infarct size (Nawashiro et al., 1997).

Besides TNF-α and its receptors, the specific intracellular pathway that is activated under a certain condition will influence the final result. TNF-α can activate several signaling cascades (**Figure 1.16**), such as NF-κB pathway (Sriram and O'Callaghan, 2007), mitogen-activated protein kinase (MAPK; Pozniak et al., 2014), AP-1 (Pozniak et al., 2014), c-jun N-terminal kinase (JNK; Montgomery and Bowers, 2012), and sphingosine-base ceramide (Montgomery and Bowers, 2012).

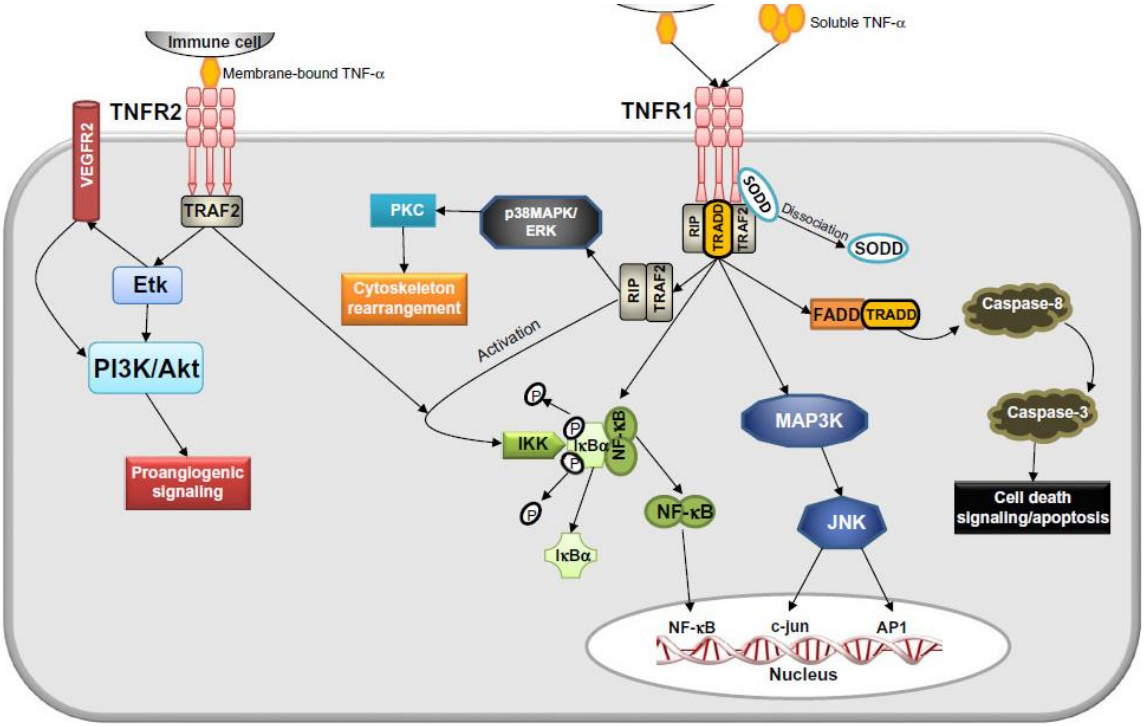

Figure 1.16. Schematic representation of tumor necrosis factor receptors 1 (TNFR1) and 2 (TNFR2) downstream signaling pathways after activation by TNF-α. Membrane-bound TNF-α (tmTNF) can activate TNFR2, and through Etk (endothelial/epithelial tyrosine kinase) leads to PI3K/Akt (phosphatidylinositol 3-kinase/protein kinase B) activation and subsequently proangiogenic pathways [for example vascular endothelial growth factor (VEGF) and its receptor 2 (VEGFR2)]. Also, activation of TNFR2 is sufficient to initiate NF-κB (nuclear factor kappa-light-chain-enhancer of activated B cells) pathway signaling. Additionally, both soluble and membrane-bound TNF-α can activate the TNFR1. The activation of this receptor requires the association of TRAF2 (TNFR-associated factor 2) and TRADD (TNFR1-associated death domain protein) with the intracellular death domain of the receptor. The activation of the TNFR1 can trigger three major signaling pathways, such as NF-κB, MAPK (mitogen-activated protein kinase), and caspases/apoptotic pathways. Importantly, MAPK pathway can activate the downstream pathways like JNK (c-Jun N-terminal kinase), ERK (extracellular signal-regulated kinase), PKC (protein kinase C), and AP-1 (activator protein-1). The activation of caspase-8 and -3 is mediated through the FADD (Fas-associated protein with death domain)/TRADD complex. Importantly, in order to convert NF-κB pathway to its activated form, the IKK (IκB kinase) complex is recruited to phosphorylate the IκBα (inhibitor of κB). This phosphorylation causes the unbinding of IκBα from NF-κB dimer, which in turn become available to nuclear translocation. Further, TNFR1 can also be negatively modulated by the interaction of SODD (silencer of death domains) with intracellular domains of the receptor (adapted from Urschel and Cicha, 2015).

1.4.2. NF-κB Signaling Pathway

NF-κB is a ubiquitously expressed transcription factor that ultimately controls DNA transcription of genes from cytokine production to cell survival, and is formed by several subunits as follow: p50, p52, p65 (also known as RelA), c-Rel, and RelB (Tak and Firestein, 2001). NF-κB pathway can be activated by growth factors, chemokines, oxidative stress and cytokines (Pozniak et al., 2014), and regulates several different types of genes encoding from cytokines (such as TNF-α and IL-1β), chemokines, inducible nitric oxide synthase (iNOS), GFAP protein, as well as, cell adhesion molecules, antiapoptotic proteins and neurotrophic factors (Kaltschmidt et al., 2005). Therefore, the outcome of NF-κB activation, either protective or neurodegenerative will depend on the duration of such activation and the differential involvement of regulatory proteins (Colombo and Farina, 2016).

After NF-κB activation, two different downstream pathways can be triggered, the canonic or the non-canonical, also known as classical or alternative pathway, respectively (**Figure 1.17**). The canonic starts with the activation of IκB kinase (IKK) complex, that contains two catalytic kinase subunits (IKKα, IKKβ) and the regulatory non-enzymatic scaffold protein NEMO (NF-κB essential modulator of IKKγ), causing the phosphorylation of IκB. After that, dissociation of IκB from p50 and p65 subunits allow them to translocate into the nucleus and initiate gene transcription (**Figure 1.17**; Srivastava and Ramana, 2009). In the non-canonical pathway, activation of IKK complex (which is composed of two subunits of IKKα) is dependent on the NF-κB-inducing kinase (NIK) activity, resulting in phosphorylation of the inactive form of NF-κB p100/RelB dimer. After that, the dimer is processed by selective degradation of its C-terminal region originating the active form of p52/RelB dimer that will be translocated into the nucleus and induce gene transcription (**Figure 1.17**; Srivastava and Ramana, 2009).

The biological significance of both NF-κB downstream pathways is still poorly understood, however, there is sufficient literature demonstrating a dual role of NF-κB activity in the

CNS. In fact, this pathway has a crucial role in glutamatergic transmission, dendritic arborization, and axonal growth (Pozniak et al., 2014). Likewise, NF-κB signaling is involved in proliferation and migration of neural progenitor cells, as well as in myelination processes (Pozniak et al., 2014). Additionally, a deleterious effect of NF-κB pathway activation in several cell types has been demonstrated as the responsible for leukocyte infiltration (Colombo and Farina, 2016), HIV-1 genes transcription (Pozniak et al., 2014), and the deleterious effects observed in animal models of stroke/ischemia (Tak and Firestein, 2001). Interestingly, in the particular case of multiple sclerosis, neuronal NF-κB inhibition aggravated the disease development in a mouse model (Emmanouil et al., 2009), but the inhibition of this pathway in all CNS cells protected the brain tissue (van Loo et al., 2006).

Taking into consideration the importance of NF-κB pathway, its modulation can have a high impact on clinical outcomes of several neurodegenerative disorders. For example, the inhibition of IκBα degradation is the target of non-steroidal anti-inflammatory drugs and disease-modifying antirheumatic class of drugs (Tak and Firestein, 2001). Moreover, the anti-inflammatory effect of Aspirin appears to be due to a competitive inhibition of IKK-β, preventing NF-κB nuclear translocation (Tak and Firestein, 2001). More recently, cutting-edge methodologies allowed the application of NF-κB decoy oligonucleotides, by *in situ* direct injection or by viral gene transfer, to decrease the expression of several subunits of the NF-κB complex (De Stefano, 2011). Similar results were obtained with the administration of p65 antisense oligonucleotides (Neurath et al., 1996). Equally important, IL-1β and TNF-α expression can be upregulated by the NF-κB pathway. On the other hand, the blockade of both cytokines can prevent the activation of NF-κB signaling pathway and so inhibit the inflammatory process. In addition, administration of antioxidants, as well as proteasome inhibitors have emerged as novel therapeutic targets for reducing the NF-κB activity and thereby diminishing the inflammatory status (Tak and Firestein, 2001).

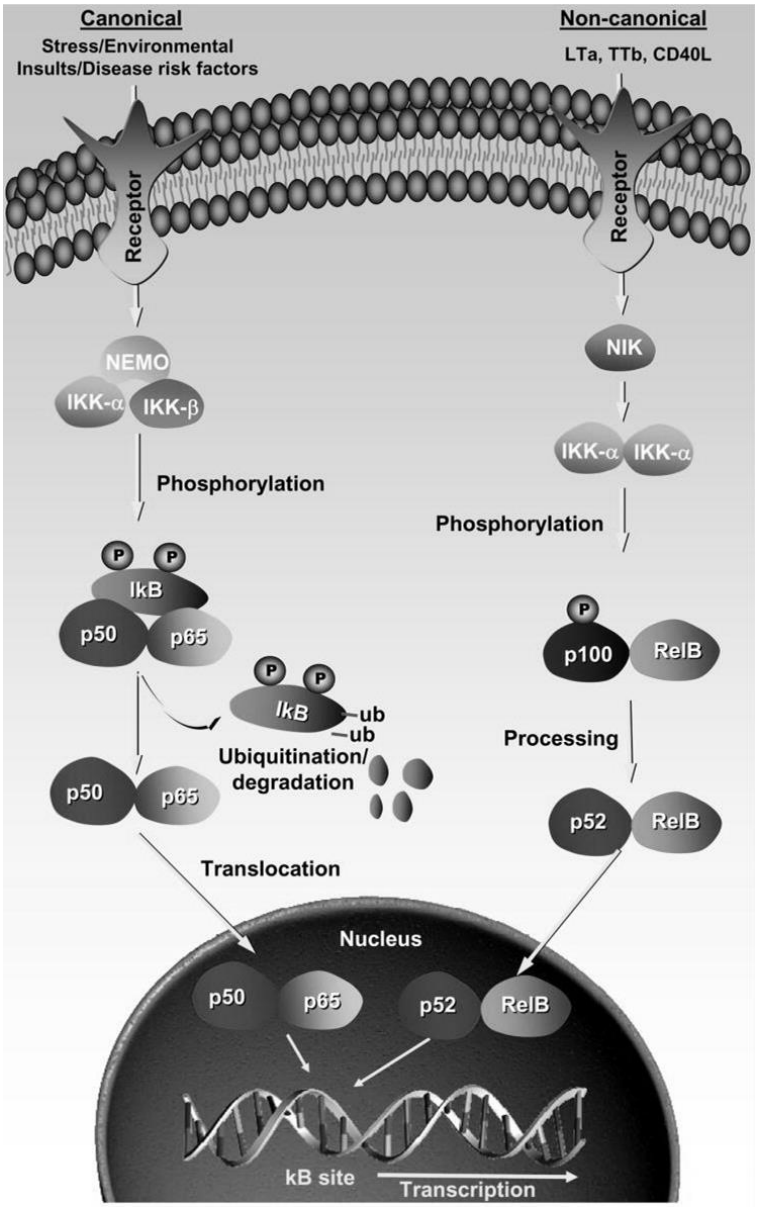

Figure 1.17. Nuclear factor kappa-light-chain-enhancer of activated B cells (NF-κB) signaling pathways. In canonical, or classical pathway (in left), the activation of a specific receptor will cause the phosphorylation of IκB by IκB kinase (IKK) complex, which comprises IKK-α, IKK-β and NF-κB essential modulator of IKKγ (NEMO). This phosphorylation allows the release of the active form of NF-κB dimer and its translocations into the nucleus where it will activate transcription of target genes. The non-canonical, or alternative pathway (right side of diagram) depends on processing the p100/RelB dimer, which occurs after the phosphorylation of p100 subunit by IKK complex (formed by two IKK-α subunits) activated by NF-κB-inducing kinase (NIK). The new formed p52/RelB dimer is now capable of nuclear translocation leading to transcription of the associated genes (adapted from Srivastava and Ramana, 2009).

1.5. Objectives

On average, 3.8% of all European adults report having used amphetamines at least once in their lives. Moreover, in Portugal, METH consumption has also increased during the last few years. Despite the seriousness of this drug problem, there are still many gaps regarding the mechanisms underlying METH-induced brain dysfunction, particularly related with neurogliovascular alterations.

Thus, our major goal was to uncover the impact of METH on the BBB and to identify new targets to ameliorate the negative effects of drug abuse/misuse.

CHAPTER 2

Rationale: Brain endothelial cells (ECs) together with the basal lamina, pericytes, astrocytes, surrounding microglia and neurons form the neurogliovascular unit. Barrier function is mainly provided by ECs but astrocytes have also a crucial role in formation and maintenance of BBB properties.

Aim 1: Clarify the direct impact of METH on brain ECs and the role of these cells as active players in neuroinflammatory processes.

Aim 2: Investigate how METH interferes with the astrocyte-endothelial crosstalk and unravel key mediators involved in such communication.

CHAPTER 3

Rationale: One consequence of METH abuse is the formation of brain edema, a phenomenon that can be linked to BBB disruption. Moreover, water homeostasis is controlled by specific water channels and AQP4 is the most abundant within the brain, in part due to its high concentration on astrocytic endfeet close to brain ECs.

Aim 1: Study the direct effect of METH on the AQP4 system and brain water homeostasis.

Aim 2: Evaluate the impact of METH-induced brain edema on BBB properties and animal behavior.

Aim 3: Investigate whether vitamin C, a well-described antioxidant, could have a protective role in astrocytic swelling and AQP4 system dysfunction induced by METH.

CHAPTER 4

Rationale: Neuroinflammation is recognized as one of the most deleterious effects of METH abuse/misuse. Yet, an effective pharmacological therapy for METH abuse is still missing. Importantly, the therapeutics based on natural products are seen as a promising strategy, and parthenolide (PTL) is one of the most used herbal extracts on the traditional Asian medical practice.

Aim 1: Unravel the protective role of PTL on METH-induced brain edema and BBB disruption.

Aim 2: Clarify the role of TNF-α signaling in such effects triggered by METH.

MAJOR GOAL:

Dissect the neurogliovascular alterations triggered by METH in order to uncover new targets, and so identify new therapeutic approaches to better treat the negative effects of METH consumption. Ultimately, we expect to give a contribution for health improvement of drug users.

CHAPTER 2

The TNF-α/NF-κB signaling pathway has a key role in methamphetamine-induced blood-brain barrier dysfunction

2.1. Abstract

Methamphetamine (METH) is a psychostimulant that causes neurologic and psychiatric abnormalities. Recent studies have suggested that its neurotoxicity may also result from its ability to compromise the blood-brain barrier (BBB). Herein, we show that METH rapidly increased the vesicular transport across endothelial cells (ECs), followed by an increase of paracellular transport. Moreover, METH triggered the release of TNF-α, and the blockade of this cytokine or the inhibition of NF-κB pathway prevented endothelial dysfunction. Since astrocytes have a crucial role in modulating BBB function, we further showed that conditioned medium obtained from astrocytes previously exposed to METH had a negative impact on barrier properties also via TNF-α/NF-κB pathway. Animal studies corroborated the in vitro results. Overall, we show that METH directly interferes with EC properties or indirectly via astrocytes through the release of TNF-α and subsequent activation of NF-κB pathway culminating in barrier dysfunction.

2.2. Introduction

METH abuse is a serious public health problem affecting over 35 million users worldwide (UNODC, 2007). The overall negative effects of this drug are well known, including irreversible brain damage that may cause neurologic and psychiatric anomalies (Thompson et al., 2004; Loftis and Janowsky, 2014). Indeed, studies with human subjects have shown that METH users present brain structural abnormalities, which can explain behavioral problems, recall capacity, as well as memory and performance deficits observed in verbal memory tests and executive functions (Thompson et al., 2004). Additionally, the long-term neuronal damage is well described in humans, nonhuman primates, and rodents (Krasnova and Cadet, 2009). However, despite extensive characterization of METH toxicity over the last years, many questions remain unanswered. Most hypotheses have focused on intraneuronal events such as dopamine oxidation, oxidative stress, and excitotoxicity (Krasnova and Cadet, 2009), but it has been recently suggested that METH-induced neurotoxicity may also result from its ability to compromise the BBB function (Martins et al., 2011).

The BBB is a dynamic and complex interface between the blood and the CNS, having a key role in brain homeostasis and protection (Cardoso et al., 2010). Although cerebral endothelium disturbance is commonly observed in the CNS pathologies (de Vries et al., 2012), neither its cause nor the effective participation of BBB in such diseases is well established. Thus, given that BBB damage is an early event in many neurologic conditions, it is not surprising the growing interest in this barrier as a therapeutic target. At the cellular level, this dynamic and specialized structure is composed of endothelial cells (ECs) associated with pericytes, basement membrane, astrocyte endfeet, microglia, and neurons, comprising the neurovascular unit (Cardoso et al., 2010). The brain endothelium remains the first ‘physical barrier’, with lack of fenestrations, low fluid-phase endocytosis (pinocytosis), and intercellular complexes that confer low paracellular permeability and high transendothelial electrical resistance (TEER) to the BBB (Cardoso et al., 2010).

Nevertheless, all BBB components have a unique role in its function and, among them, astrocytes are involved in the formation of the TJs complex, microvascular support, and in the control of water flux into the brain (Kuo and Lu 2011).

As aforementioned, alterations in BBB function are likely involved in many neurodegenerative diseases, and drug abuse is not an exception. In fact, it was previously shown that METH compromises BBB function and its capacity to protect the brain against infection by the human immunodeficiency virus (Loftis and Janowsky, 2014). However, the cellular mechanisms underlying these effects are still poorly understood. Most studies suggest that BBB alterations induced by METH result from alterations on TJs complex (Martins et al., 2011), involving oxidative stress (Ramirez et al., 2009), and activation of matrix metalloproteinases (MMPs) (Martins et al., 2011, Urrutia et al., 2013). Importantly, we have also shown that METH may trigger a neuroinflammatory response with increased production of proinflammatory cytokines, such as TNF-α (Gonçalves et al., 2010, Coelho-Santos et al., 2012). Accordingly, Lee et al (2001) showed that METH upregulates TNF-α gene and activates nuclear factor kappa-light-chain-enhancer of activated B cells (NF-κB) in human brain ECs. Moreover, astrocytes modulate endothelial responses under pathologic conditions by secreting factors that cause BBB leakage (Kuo and Lu 2011, Landoni et al., 2012). It is noteworthy the involvement of TNF-α in BBB dysfunction (Deli et al., 1995; Miller et al., 2005; Candelario-Jalil et al., 2007), as well as in promoting the passage of circulating leukocytes into the brain (Tang et al., 2011). Despite knowing that METH may induce BBB impairment and neuroinflammation, the possible involvement of proinflammatory cytokines in METH-induced BBB alterations has never been investigated. Herein, we show that METH increases BBB permeability by interfering with both paracellular and vesicular transport across ECs. Additionally, the crosstalk between astrocytes and ECs clearly shows the important role played by glial cells on barrier properties. Overall, we unravel the key role of TNF-α, via activation of NF-κB signaling, in METH-induced BBB dysfunction.

2.3. Materials and Methods

2.3.1. Animal Studies

Animal manipulation was performed by certified researchers (Portuguese National Authority for Animal Health) and in accordance with both the European Community Council Directives (2010/63/EU) and the Portuguese law for the care and use of experimental animals (DL nº 113/2013). The present study was approved by the Foundation for Science and Technology (PTDC/SAU-FCF/098685/2008). The experiments were performed in accordance with the ARRIVE guidelines. All efforts were made to minimize animal suffering and to reduce the number of animals used.

2.3.2. Primary Cultures of Rat Brain Microvascular Endothelial Cells

Primary cultures of rat brain microvascular ECs (RBMVECs) were prepared from 2-week-old Wistar rats, as previously described (Cardoso et al., 2012) with minor modifications. Specifically, forebrains were freed of meninges, dissociated into small pieces, and digested in Dulbecco's modified Eagle's medium/ Ham's F12 (DMEM/F12; Biochrom AG, Berlin, Germany), containing 1 mg/ml collagenase CLS2 (Sigma-Aldrich, St. Louis, MO, USA) and 14 µg/ml DNase (Sigma-Aldrich) for 90 min at 37°C. The suspension was centrifuged (1,000×*g*, 8 min) followed by a second centrifugation of the pellet (1,000×*g*, 20 min). Microvessels were further digested with 1 mg/ml collagenase-dispase (Roche Applied Sciences, Basel, Switzerland) and 7 µg/ml DNase (Sigma-Aldrich) in DMEM/F12 for 1h at 37°C, centrifuged (700×*g*, 5 min) and seeded at high density (1.5×10^5 cells/cm^2) onto tissue culture multiplates, coverslips or 12-mm Costar Transwells (Corning Life Sciences, Tewksbury, MA, USA) coated with collagen type IV/fibronectin (Sigma-Aldrich). Cultures were maintained in DMEM/F12 supplemented with 15% fetal bovine serum (GIBCO, Rockville, MD, USA), 1 ng/ml basic fibroblast growth factor (Roche Applied

Sciences), 100 µg/ml heparin (Biochrom AG), 5 µg/ml gentamicin (GIBCO) and 4 µg/ml puromycin (Sigma-Aldrich) at 37°C with a humidified atmosphere of 5% CO_2, for 2 days. On day 3, cells were incubated with a new medium that contained all components aforementioned, except puromycin. When RBMVECs were 90% confluent, hydrocortisone (550 nM; Sigma-Aldrich) was added for 1 day. Hydrocortisone was used to improve barrier proprieties of ECs, namely by the induction of TJs expression and enhancement of TEER (Cardoso et al., 2012).

2.3.3. Primary Cultures of Human Brain Microvascular Endothelial Cells

Primary cultures of human brain microvascular ECs (HBMVECs) were obtained from microvessels isolated from the lateral temporal cortex of adult patients undergoing surgery for the treatment of intractable epilepsy at the Neurosurgery Service, Coimbra Hospital and University Centre, as previously described (Bernas et al., 2010). The present study was approved by the Hospital Ethics Committee.

2.3.4. Terminal Deoxynucleotidyl Transferase dUTP Nick End Labeling (TUNEL) Assay

After the appropriate treatments, the whole population of cells was collected by trypsinization. Then, cells were fixed with 4% paraformaldehyde (PFA) and adhered to superfrost microscope slides (Thermo Scientific, Menzel GmbH & Co KG, Braunschweig, Germany) by centrifugation (113×*g*, 5 min; Cellspin I, Tharmac GmbH, Waldsolms, Germany). Apoptotic cell death was further evaluated by the TUNEL assay (Roche Diagnostics GmbH, Mannheim, Germany). Briefly, cells were permeabilized in 0.25% Triton X-100 for 30 min at room temperature (RT), and incubated with terminal deoxynucleotidyl transferase buffer for 1h at 37ºC in a humidified chamber. Incubation with

fluorescein Avidin D (1:100) was performed for 1h, followed by nuclei counterstaining with 5 µg/ml Hoechst 33342 for 5 min. Cell images were recorded using an Axiovert 200 M fluorescence microscope.

2.3.5. MTT Assay

After METH treatments (24h), MTT (3-(4,5-dimethylthiazol-2-yl)-2,5-diphenyltetrazolium bromide) was added to a final concentration of 0.5 mg/ml to each well of the cell plate and left at 37ºC for 1h. The reaction was stopped by 0.04 M HCl in isopropanol, and the optical density was measured at 570 nm, with the reference filter at 620 nm. The results are expressed as mean % of control.

2.3.6. Primary Cultures of Mouse Cortical Astrocytes

Astrocytes were isolated from C57BL/6J mouse pups aged P4-5. Brain cortices were isolated and incubated with digestion solution (Hank's Balanced Salt Solution (HBSS; GIBCO), 0.25% Trypsin (SAFC Biosciences Inc, Lenexa, KS, USA), 0.001% DNase (Sigma-Aldrich), 1% gentamicin (GIBCO) for 20 min at 37°C. After brief centrifugation (70×*g*, 3 min), the pellet was incubated with the inhibitory digestion solution (HBSS with 10% fetal bovine serum), cells were dissociated and centrifuged (143×*g*, 5 min), followed by pellet resuspension in astrocyte medium (DMEM high glucose supplemented with 10% fetal bovine serum and 1% gentamicin). Cells were plated in T-75 flasks at a density of 1.2 × 10^5 cells/cm^2, and the medium was changed after 6h and then every 2 days until reach confluence. Afterward, flasks were shaken (4h at 37°C) to detach nonastrocytic cells, and astrocytes (adherent cells) were washed with dissociation medium [HBSS with 1 mM ethylenediamine tetraacetic acid (EDTA, Sigma-Aldrich)] followed by trypsinization with 0.1% Trypsin (SAFC) in HBSS. This process was stopped by incubation with astrocyte medium followed by centrifugation (143×*g*, 5 min). Cells were plated at different densities depending on the experiments.

2.3.7. Evaluation of Endothelial Cell Monolayer Integrity

Rat and human ECs were left untreated (control) or treated with different drugs as follows: METH (1 or 50 μM), BAY 11-7085 (5 μM BAY), lysophosphatidic acid (10 μM; all from Sigma), TNF-α (0.01 μg/ml; R&D Systems, Abingdon, UK), and both anti-rat (0.01 μg/ml Ab TNF-α; PeproTech, Inc., Princeton, NJ, USA), and anti-mouse TNF-α antibodies (100 μg/ml Ab TNF-α; Upstate Biotechnology, Inc., Lake Placid, NY, USA). The flux of sodium fluorescein (Na-F, 376 Da; Sigma-Aldrich) across cell monolayer was determined as previously described (Martins et al., 2013). Moreover, TEER of monocultures was measured using a STX-2 electrode coupled to an EVOM resistance meter (World Precision Instruments, Hertfordshire, UK). Transendothelial electrical resistance readings of cell-free inserts were subtracted from the values obtained with cells, and results were expressed as % of control.

2.3.8. Horseradish Peroxidase Transport

Endothelial cells were left untreated (control) or exposed to METH (1 μM) either alone or in the presence of BAY (5 μM) for 1h at 37°C. Afterward, horseradish peroxidase (HRP, 10 mg/ml; Sigma-Aldrich) transport by confluent RBMVECs was quantified during 2h, as previously described (Martins et al., 2013).

2.3.9. Enzyme-Linked Immunosorbent Assay

Endothelial cells and astrocytes were left untreated (control) or exposed to METH (1 or 50 μM) for different time periods as indicated in the respective graphs. For blood analysis, blood samples were collected directly from cardiac left ventricle from mice of the three experimental groups (CTR, METH, and LPS as a positive control). The released levels of TNF-α from both cell types, and also from animal blood, were quantified by ELISA Ready-SET-Go kit (eBioscience, San Diego, CA, USA), as specified in the datasheet.

2.3.10. Immunocytochemistry

Endothelial cells were left untreated (control) or incubated with different drugs as specified in the respective figure legends. For p65 and intracellular adhesion molecule (ICAM)-1 identification, cells were fixed with 4% PFA (Sigma-Aldrich) for 20 min at room temperature (RT). Regarding claudin-5, cells were fixed with ethanol (95%)-acetic acid (5%) (v/v) for 10 min at −20°C, whereas for occludin identification, cells were pretreated with an extraction buffer (0.2% Triton X-100 in 100 mM KCl, 3 mM MgCl2, 1 mM CaCl2, 200 mM Sucrose, and 10 mM HEPES, pH 7.1) before fixation with PFA. Afterwards, cells were permeabilized with 0.25% Triton X-100 (Sigma-Aldrich) and blocked with 3% bovine serum albumin (Sigma-Aldrich) during 1h at RT, followed by incubation with primary antibodies (rabbit anti-p65, 1:100, 2h at RT, Cell Signaling Technology, Inc., Danvers, MA, USA; mouse anti-claudin-5, 1:100, Invitrogen, Inchinnan Business Park, UK; rabbit anti-occludin, 1:100, Invitrogen; and rabbit anti-ICAM-1, 1:100, Santa Cruz Biotechnology Inc., Dallas, TX, USA, all during 1h at 37°C). Then, cells were incubated with secondary antibodies (Alexa Fluor 488 or Alexa Fluor 594, 1:200, Invitrogen) for 1h at RT in the dark and nuclei were stained with 4 µg/ml Hoechst 33342 (Sigma-Aldrich) for 5 min at RT. Finally, cells were mounted in Dako fluorescence medium (Dako North America, Carpinteria, CA, USA) and images were recorded using a LSM 710 Meta Confocal microscope (Carl Zeiss, Oberkochen, Germany). To express these results, we counted the nuclear p65-positive ECs within a total of 1,000 cells obtained from 37 to 42 visual fields acquired from 3 different slides.

2.3.11. Western Blot Analysis

The protocol was performed as previously described (Coelho-Santos et al., 2012). Primary antibodies used were as follows: mouse anti-claudin-5 (1:200, Invitrogen), rabbit anti-occludin (1:150, Invitrogen) and rabbit anti-ICAM-1 (1:200, Santa Cruz). Secondary antibodies were as follows: alkaline phosphatase-conjugated secondary antibody anti-

mouse (1:10,000) and anti-rabbit (1:20,000; GE Healthcare Bio-Sciences, Pittsburgh, PA, USA). Immunoblots were reprobed with an antibody against glyceraldehyde 3-phosphate dehydrogenase (1:500; Abcam, Cambridge, UK) to ensure equal sample loading. Bands were visualized using the enhanced chemifluorescence reagent assay on the Typhoon FLA 9000 (both from GE Healthcare), and quantification was performed using the ImageJ 1.47 software (NIH, Bethesda, MD, USA).

2.3.12. Astrocyte-Conditioned Medium Experiments

Astrocytes were seeded in 6-well plates at a density of 5×10^4 cells/cm^2, and after 3 days cells were left untreated (control) or incubated with 50 μM METH for 4h. Afterwards, media from untreated [CTR astrocyte-conditioned medium (ACM)] and METH-treated astrocytes (METH ACM) were centrifuged (172×*g*, 5 min at 4°C), the supernatant was collected, and confluent RBMVECs were incubated with CTR ACM, METH ACM alone, or simultaneously with Ab TNF-α or BAY during different time periods, as indicated in the respective graphs.

2.3.13. METH Quantification in Astrocyte-Conditioned Medium

After 4h of exposure to METH, astrocytes culture media was collected and the samples were quantified by Methamphetamine ELISA (BIOTREND Chemicals, LLC), as specified in the datasheet.

2.3.14. Animal Treatments

Male wild-type C57BL/6J mice (3 months old; 24 to 26 g body weight; Charles River Laboratories, Barcelona, Spain) were housed under controlled environmental conditions (12h light:dark cycle, 24±1°C) with food and water ad libitum. Mice were divided into three different groups as follows: control group (4× 0.9% NaCl, 2h apart, intraperitoneal (i.p.) injections); METH binge group (4× 10 mg/kg METH, 2h apart, i.p.); METH+BAY group

(mice received 20 mg/kg BAY i.p., 30 min before each METH administration, as previously described; Lee et al., 2006). Animals were killed 1, 2, or 24h after the last drug injection.

2.3.15. Immunohistochemistry

Mice were anesthetized with sodium pentobarbital (80 mg/kg, i.p., Sigma- Aldrich) and transcardially perfused with 10 ml of 0.05 M sodium citrate in 1% PFA (pH 4.2, 37°C), followed by 20 ml of 4% PFA in 0.01 M PBS, pH 7.4. Brains were removed, postfixed in 4% PFA for 24h at RT and transferred to 30% sucrose in 0.01 M PBS, pH 7.4, for at least 24h at 4°C. Coronal sections (12 µm) were cut on a cryostat (Leica CM3050S, Nussloch, Germany), mounted directly onto superfrost microscope slides (Thermo Scientific, Menzel GmbH & Co KG, Braunschweig, Germany) and stored at −80°C until further use. Then, slices were rinsed in 0.01 M PBS, blocked with 5% bovine serum albumin in 0.01 M PBS for 1h at RT and incubated overnight at 4°C with rabbit anti-collagen IV (1:200; Abcam), goat anti-albumin (1:2,000; Bethyl Laboratories, Inc, Montgomery, TX, USA), and rabbit anti-TNF-α (1:100; Santa Cruz) antibodies. Afterward, slices were incubated with Alexa Fluor 488 and Alexa Fluor 594 secondary antibodies (1:200; Invitrogen) for 1h at RT, followed by nuclei staining with 5 µg/ml Hoechst 33342 (Sigma-Aldrich) for 5 min at RT in the dark. For glial fibrillary acidic protein (GFAP) staining, slices were incubated with anti-GFAP-Cy3 conjugated antibody (1:2,000; Sigma-Aldrich). Finally, slices were mounted with Dako fluorescence medium (Dako North America) and images were recorded using a LSM 710 Meta Confocal microscope (Carl Zeiss). Quantification of collagen IV, albumin, TNF-α, and GFAP immunoreactivity was performed using the NIH ImageJ 1.47 analysis software. Specifically, a region was drawn around each striatum vessel, as well as in a close area without staining (black) to be used for background subtraction. To determine the corrected total vessel fluorescence, we used the following formula: correct total fluorescence of each vessel = (integrated intensity) − (area for the selected vessel × mean

background). The results are expressed as mean of fluorescence intensity (arbitrary units) of six brain slices obtained from three different animals for each experimental group.

2.3.16. Statistical Analysis

Evaluation of EC monolayer integrity and western blot analysis were performed by a person blinded to treatments. Results are expressed as mean + standard error of the mean (S.E.M.). Data were analyzed using the one-way ANOVA followed by Dunnett's or Bonferroni's post hoc test, as indicated in figure legends. All statistics were calculated using GraphPad Prism 5.0 (GraphPad Software, San Diego, CA, USA). The level of significance was $P<0.05$ and the 'n' represents the total number of experiments obtained from at least three independent cell cultures or animals.

2.4. Results

2.4.1. Methamphetamine Impairs the Barrier Function of Endothelial Cells

To study barrier alterations induced by METH, we used freshly prepared primary RBMVECs since this in vitro model preserves many characteristics of the intact BBB, such as expression of continuous adherens and TJs, as well as low permeability to macromolecules (Cardoso et al., 2010). Regarding METH concentrations used in the present study, it is important to highlight that abusers with lower dose-METH exposure present blood levels of this drug within a range of 0.1 and 11.1 μM (Melega et al., 2007). However, they tend to self-administer METH in binge manner leading to higher levels. It is estimated that binge doses in a 260 mg to 1 g range may lead to 17 to 80 μM of METH circulating in the blood. Thus, we decided to use concentrations that are closer to the human condition. Our results show that METH (1 and 50 μM) increased the permeability to Na-F at 2, 3, and 4h of drug exposure (**Figure 2.1A**). Thus, we further aimed to reproduce these results in HBMVECs. Indeed, METH (1 μM) increased Na-F flux (**Figure 2.1B**) across human cells. Moreover, to clarify whether BMVEC-increased permeability was due to alterations in the paracellular pathway, we further measured TEER values on both cultures. In RBMVECs, both METH concentrations led to a significant decrease in TEER at 3h after drug exposure (**Figure 2.1C**), which was maintained until 24h (**Figure 2.1C**). We used lysophosphatidic acid (10 μM) as a positive control since it produces a strong and transient opening of the ionic barrier (Bernas et al., 2010). Accordingly, TEER values of HBMVECs were decreased at 2h after drug exposure up until 24h (**Figure 2.1D**). Noteworthy, the concentrations of METH used in the present study neither caused EC death nor decreased cell viability (**Figure 2.2**). These results show that METH at a low concentration does not interfere with cell viability but impairs barrier properties, proven by the increased permeability to Na-F and decreased TEER values in both rat and human BMVECs.

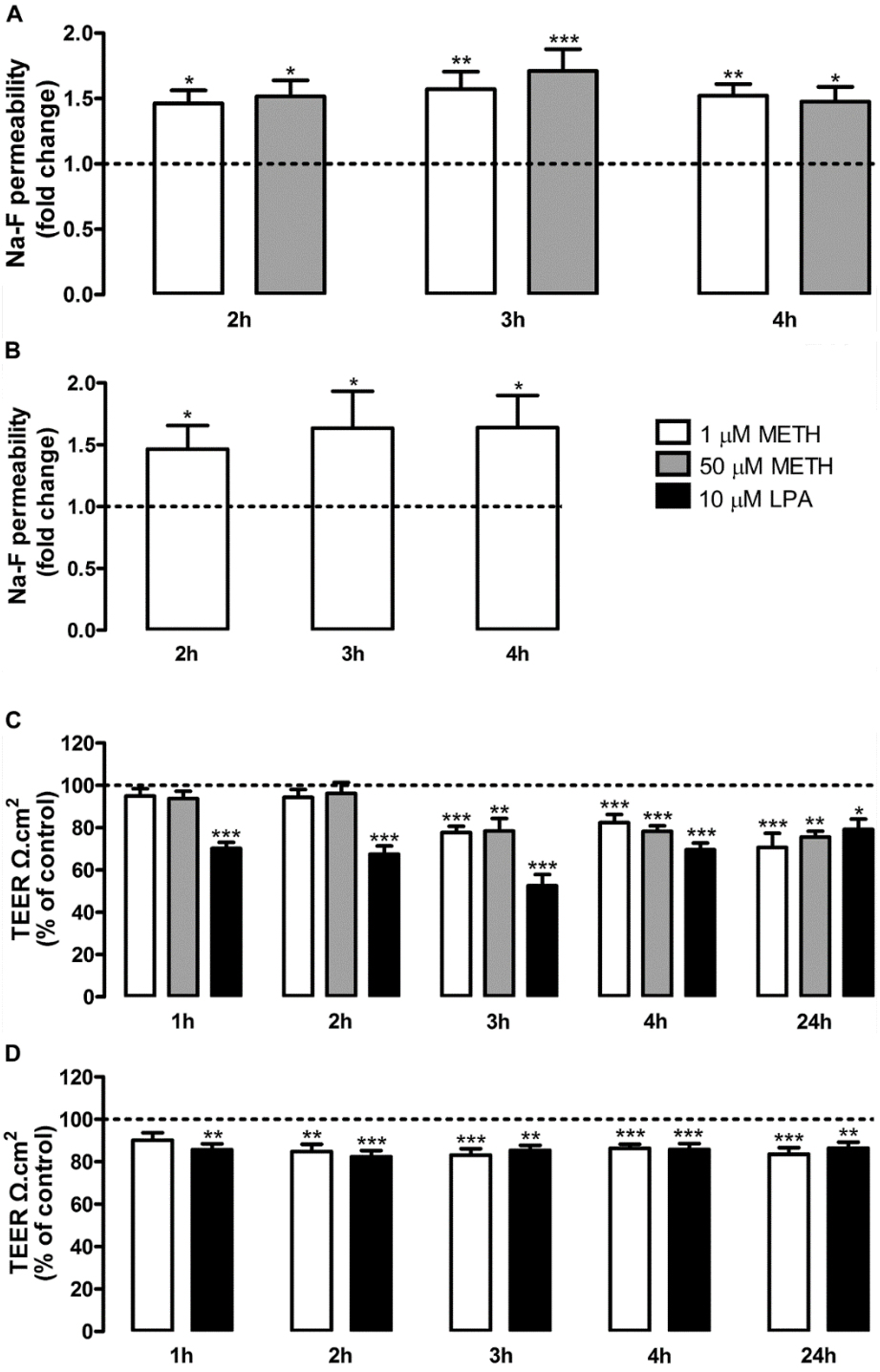

Figure 2.1. METH increases the permeability of brain microvascular endothelial cells (BMVECs). (A, B) Macromolecular flux across **(A)** rat and **(B)** human BMVECs was assessed using sodium fluorescein (Na-F, 376 Da) at different time points after METH exposure, n=5-20. **(C, D)** Transendothelial electrical resistance (TEER) of confluent **(C)** rat and **(D)** human BMVECs monolayers was analyzed under the condition of METH or lysophosphatidic acid (LPA) exposure during different time periods, n=5 to 10. All results are shown as mean + S.E.M. *P<0.05, **P<0.01, ***P<0.001 significantly different when compared with the control (dashed line) of each time point using Bonferroni's Multiple comparison test.

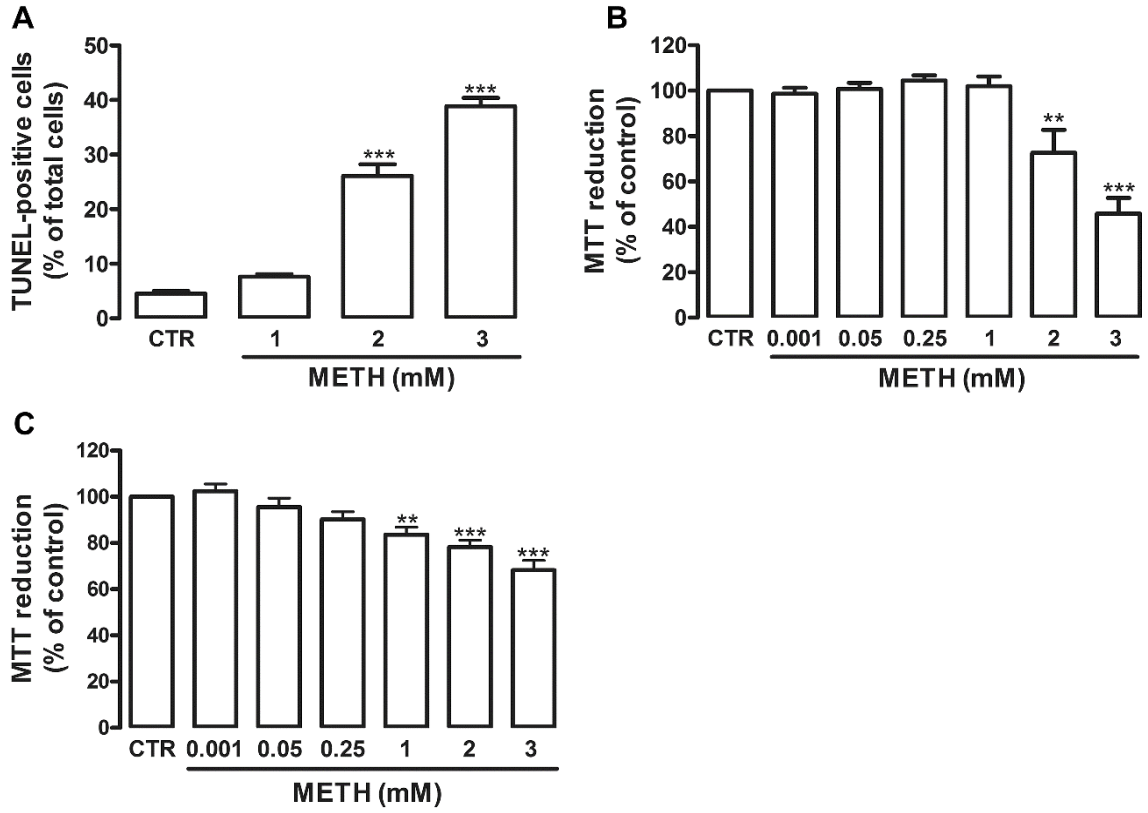

Figure 2.2. Concentration-response toxicity of METH on BMVECs. (A) METH (2 and 3 mM for 24h) increased the number of TUNEL-positive cells (apoptotic cells) in rat BMVECs. **(B)** Rat and **(C)** human BMVECs were exposed to increasing METH concentrations (0.001 mM-3 mM) for 24h, and we observed that both 2 and 3 mM METH decreased cell viability. The results are expressed as mean % of control + S.E.M., n=22-24 for TUNEL assay, n=5-9 for MTT studies. **P<0.01, ***P<0.001, significantly different when compared to control (CTR) using Dunnett's Multiple comparison test.

2.4.2. Methamphetamine Leads to Barrier Breakdown via TNF-α/ NF-κB Pathway

METH is able to trigger a pronounced neuroinflammatory response with increased release of proinflammatory cytokines (Gonçalves et al., 2010; Coelho-Santos et al., 2012). Moreover, TNF-α has been proposed as an important mediator of BBB breakdown (Candelario-Jalil et al., 2007). However, nothing is known regarding the role of TNF-α on METH-induced BBB dysfunction. Thus, we started by analyzing the effect of METH (1 μM) on TNF-α protein levels released by RBMVECs, and we observed a prominent increase

after 15 min of drug exposure (**Figure 2.3A**) that was still significantly higher than control after 1h, recovering to control values at 4h.

To clarify the possible involvement of TNF-α on METH-induced endothelial permeability, we used a specific antibody to block the effect of this proinflammatory cytokine (Ab TNF-α, 0.01 µg/ml). Under such conditions, the effect of METH on Na-F permeability (**Figure 2.3B**) and TEER (**Figure 2.3C**) was prevented. Additionally, TNF-α (0.01 µg/ml) increased Na-F permeability (**Figure 2.3B**) and decreased TEER (**Figure 2.3C**), without causing EC death (**Figure 2.4**). In fact, this proinflammatory cytokine has been described as an inductor of barrier opening (Deli et al., 1995; Aveleira et al., 2010). Importantly, it was also documented that NF-κB is a critical signaling molecule in TNF-α-induced inflammatory response (Aslam et al., 2012; Zhong et al., 2012). Thus, we further investigated the role of NF-κB in METH-induced barrier dysfunction by using an inhibitor of this pathway, BAY 11-7085 (Koedel et al., 2000). In more detail, BAY is an upstream inhibitor of NF-κB that prevents the activation of inhibitory κB kinase, an enzyme required for the activation of NF-κB (Prager et al., 2009). Moreover, the concentration used was based on the literature for the purpose of inhibiting NF- κB activation without causing toxicity (Prager et al., 2009). We concluded that blockade of NF-κB abrogated both METH- and TNF-α-induced barrier permeability (**Figure 2.3B**) and restored TEER to basal values (**Figure 2.3C**).

It is noteworthy that at 1 and 2h after METH exposure there were no alterations in TEER values (**Figure 2.3C**), although with an increase in permeability to Na-F (**Figure 2.3B**). Thus, Na-F studies give us the information regarding general permeability, whereas TEER specifically indicates alterations in paracellular transport. Taking these into consideration, we hypothesized that METH may increase EC permeability by different mechanisms. Specifically, our results show that until 2h there is no significant alteration in the paracellular pathway, demonstrated by unchanged TEER values (**Figure 2.3C**). Thus, we further investigated whether transcytosis occurred during this first period after METH exposure by measuring HRP flux across RBMVECs. Herein, we clearly show that METH (1 µM, 1h) increased HRP transport, which was once again dependent on the NF-κB

pathway since BAY completely prevented the effect of METH (**Figure 2.3D**). To further confirm the activation of the NF-κB signaling pathway, we performed an immunocytochemical assessment of the cytoplasmic and nuclear localization of p65 NF-κB subunit (**Figure 2.3E**), followed by the quantification of nuclear p65-positive cells (**Figure 2.3F**). Interestingly, we observed p65 translocation into the nucleus to be markedly increased after METH exposure (15 min), which was blocked by BAY (**Figures 2.3E and 2.3F**). This time course is in accordance with the observed increase of TNF-α levels after 15 min of METH exposure (**Figure 2.3A**), which suggest that METH triggers the release of TNF-α that will activate the NF-κB pathway. To better explain this sequence of events, we showed that the first pool of TNF-α to be release (15 min post-METH) was independent of the NF-κB pathway and so of new transcription since BAY did not prevent this effect (**Figure 2.3A**). However, at least some of the TNF-α that is being released after 1h of METH exposure is already dependent on NF-κB pathway activation (**Figure 2.3A**). Moreover, we showed that TNF-α blockade with a neutralizing antibody at 15 min after METH prevented the translocation of p65 NF-κB subunit to the cell nuclei (**Figures 2.3E and 2.3F**). Additionally, to prove the direct effect of TNF-α on NF-κB activation, we showed that this cytokine promoted p65 translocation into the nucleus, which was once again prevented by blocking the NF-κB pathway with BAY (**Figures 2.3E and 2.3F**).

Our observations prove that just after METH exposure there is an increase of vesicular transport across RBMVECs and it is dependent on NF-κB activation. However, at 3h after drug incubation it was possible to observe a decrease in TEER values, pointing to a significant alteration in the paracellular pathway after this time period. Based on these conclusions, we further evaluated the expression of TJs proteins and adhesion molecules at 4h of drug exposure. Our results show that 1 μM METH decreased claudin-5 (**Figures 2.5A and 2.5B**) and occludin (**Figures 2.5A and 2.5C**) expression, and upregulated ICAM-1 protein levels (**Figures 2.5A and 2.5D**). Then, to determine whether this effect of METH was also dependent on NF-κB activation, we once again blocked this pathway with BAY (5 μM) showing that METH-induced alterations in TJs and adhesion proteins indeed

involved the activation of the NF-κB pathway. Taken together, these data prove that TNF-α, via activation of NF-κB signaling, is involved in METH-induced barrier impairment at both transcellular and junctional/paracellular pathways across ECs.

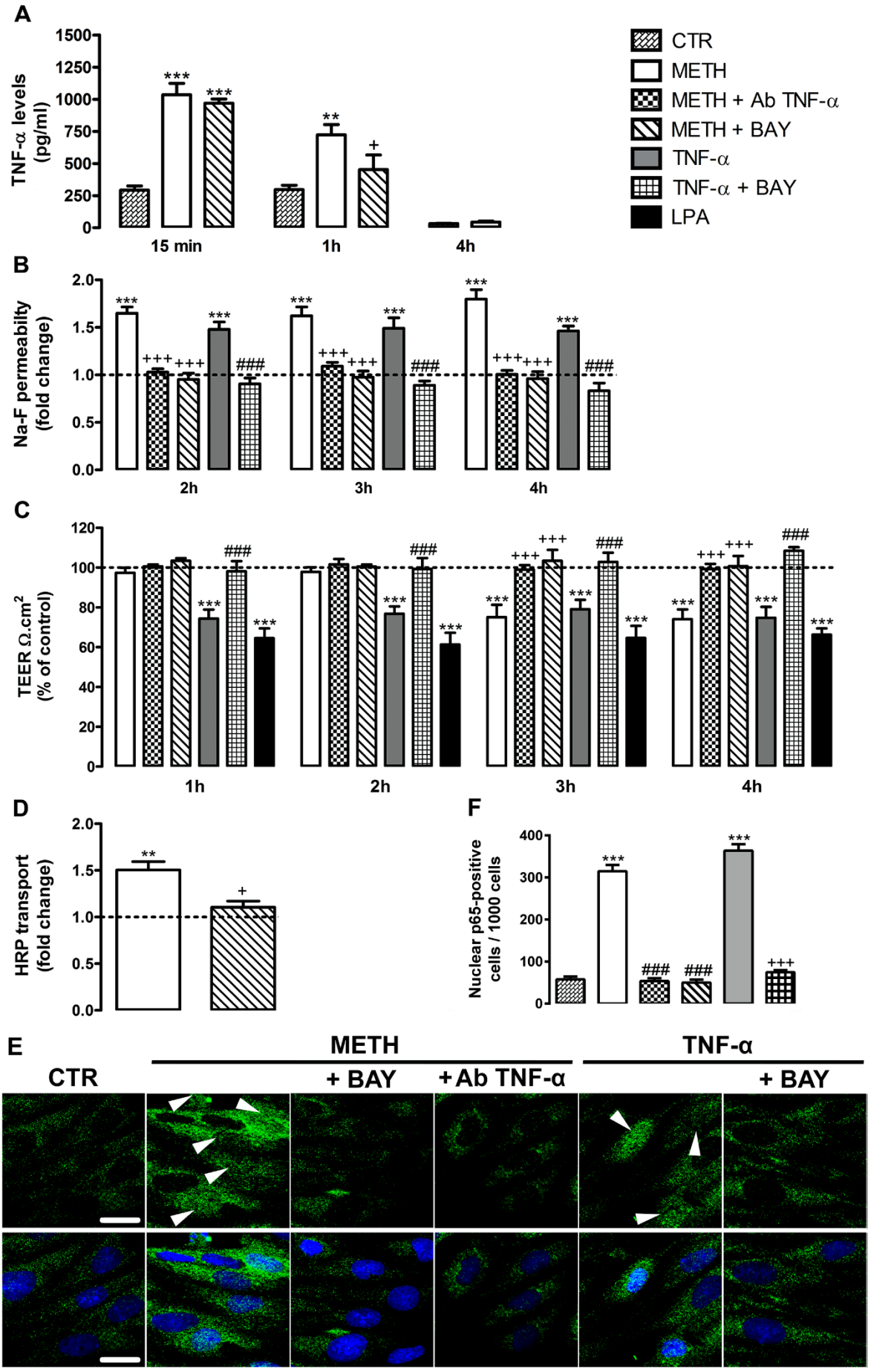
A
TNF-α levels (pg/ml)
1500
1250
1000
750
500
250
0
15 min
1h
4h
CTR
METH
METH + Ab TNF-α
METH + BAY
TNF-α
TNF-α + BAY
LPA
B
Na-F permeability (fold change)
2.0
1.5
1.0
0.5
0.0
2h
3h
4h
C
TEER Ω.cm² (% of control)
120
100
80
60
40
20
0
1h
2h
3h
4h
D
HRP transport (fold change)
2.0
1.5
1.0
0.5
0.0
F
Nuclear p65-positive cells / 1000 cells
400
300
200
100
0
E
CTR
METH
+ BAY
+Ab TNF-α
TNF-α
+ BAY

Figure 2.3. METH impairs barrier properties via TNF-α/NF-κB pathway. (A) METH (1 μM) increased TNF-α levels after 15 min, which was still observed after 1h. The blockade of NF-κB pathway with BAY only prevented TNF-α released at 1h after METH. The cytokine levels are expressed as mean pg/ml + S.E.M., n=3 to 9. **(B)** Rat endothelial cell (RBMVEC) permeability was assessed using Na-F at different time points under the following experimental conditions: 1 μM METH; METH+0.01 μg/ml Ab TNF-α; METH+5 μM BAY; 0.01 μg/ml TNF-α; TNF-α+BAY, n= 3 to 13. **(C)** Transendothelial electrical resistance (TEER) was analyzed at different time periods under the same conditions as abovementioned, n=3-8. **(D)** Horseradish peroxidase (HRP) transport across RBMVECs was evaluated in the presence of METH alone or in combination with BAY for 1h, n=3-4. The results shown are mean + S.E.M. **(E)** Representative images showing the activation of NF-κB pathway by METH (15 min exposure), which was evaluated by p65 translocation into the nucleus (arrowheads). This effect was prevented by BAY, as well as by Ab TNF-α. As a positive control, TNF-α was used which effect was also prevented by BAY. p65 (green), Hoechst 33342 (blue) and scale bars = 20 μm. **(F)** Quantification of nuclear p65-positive RBMVECs under the same experimental conditions as in **(E)**. Cells were counted within a total of 1,000 obtained from 37 to 42 visual fields acquired from 3 different slides. **P<0.01, ***P<0.001, significantly different when compared with the control (CTR or dashed line); $^{+}$P<0.05, $^{+++}$P<0.001 significantly different when compared with METH; $^{\#\#\#}$P<0.001 significantly different when compared with TNF-α from each time point using Bonferroni's Multiple comparison test.

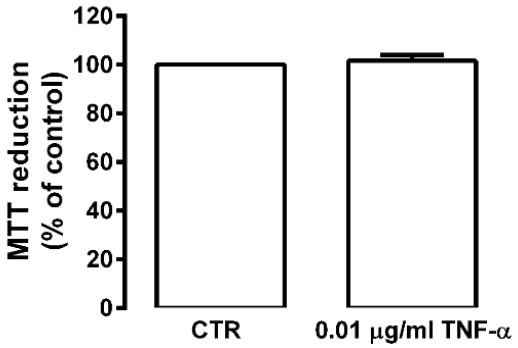

Figure 2.4. TNF-α does not interfere with brain BMVECs viability. Rat BMVECs were exposed to 0.01 μg/ml TNF-α for 24h and cell viability analyzed by MTT assay. The results are expressed as % of control + S.E.M., n=4-16.

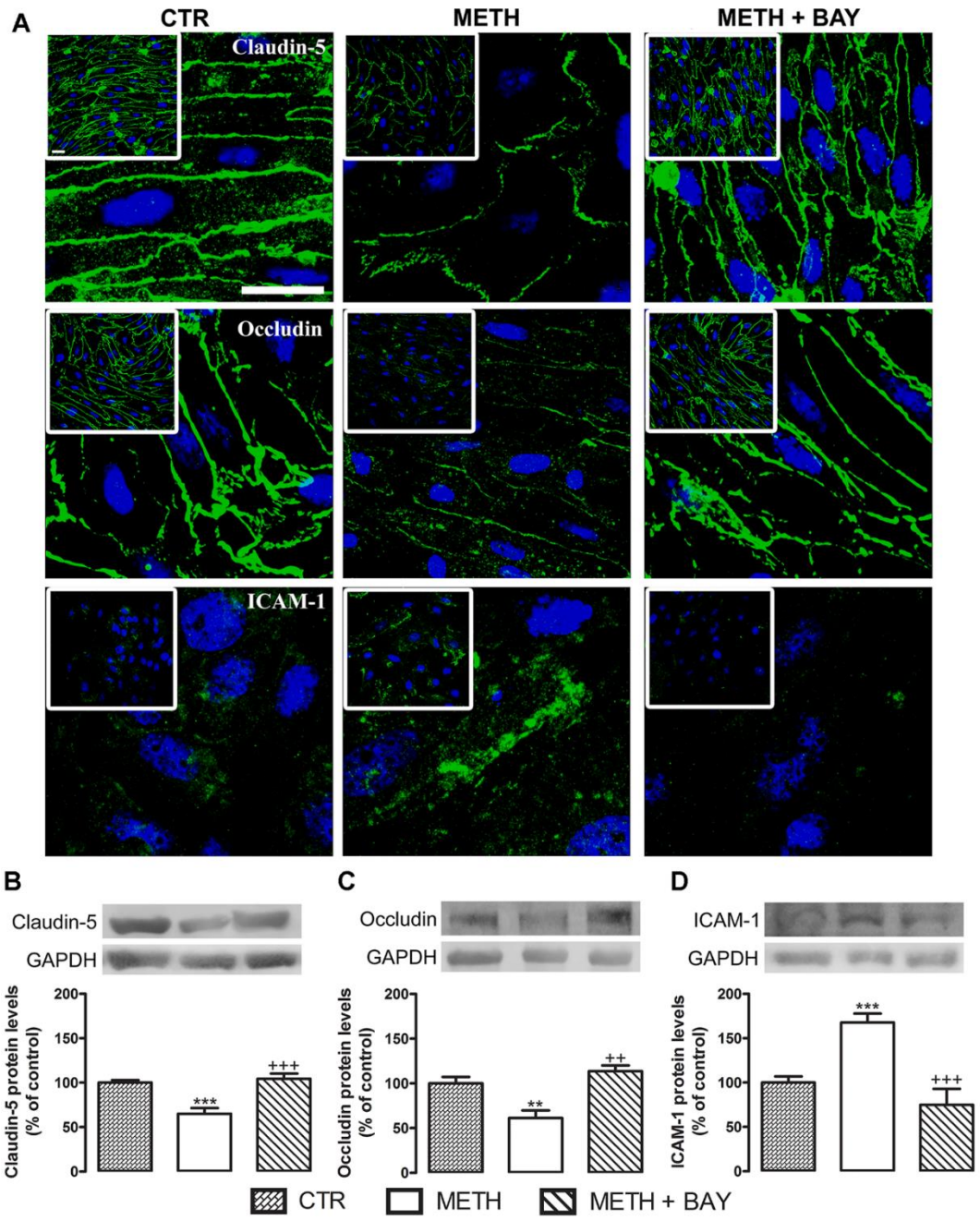

Figure 2.5. METH decreases the expression of tight junction proteins, claudin-5, and occludin, and increases the expression of intercellular adhesion molecule 1 (ICAM-1) on rat BMVECs. (A) Representative images of claudin-5, occludin, and ICAM-1 expression under different experimental conditions as follows: untreated (CTR); 1 μM METH; METH+5 μM BAY (4h of exposure). Claudin-5, occludin, and ICAM-1 (all green), Hoechst 33342 (blue), and scale bar = 20 μm. **(B–D)** Quantification of **(B)** claudin-5 (22 kDa), **(C)** occludin (65 kDa), and **(D)** ICAM-1 (110 kDa) protein levels under the same experimental conditions as previously specified in **(A)**. Above the bars, representative western blot images of the different proteins, as well as the housekeeping gene (glyceraldehyde 3-phosphate dehydrogenase, GAPDH, 37 kDa), are shown. The results are expressed as mean % of the control + S.E.M., n =5 to 16 for claudin-5, n=5 to 18 for occludin, n=3

to 10 for ICAM-1. **P<0.01, ***P<0.001 significantly different when compared with the control (CTR); ++P<0.01, +++P<0.001 significantly different when compared with METH using Bonferroni's Multiple comparison test.

2.4.3. Role of Astrocytes on Methamphetamine-Induced Barrier Dysfunction

Several studies have suggested that astrocytes modulate the structure and function of the cerebral endothelium (Kuo and Lu, 2011). In fact, these cells release several factors that determine the development and maintenance of the BBB. Thus, we also aimed to clarify whether METH alters the influence of astrocytes on ECs. We first analyzed whether METH was also able to induce TNF-α release by astrocytes, and we observed an increase triggered by 50 μM METH at 4h after exposure (**Figure 2.6A**). No significant changes were observed with a lower concentration of METH (1 μM) or at other time points (1 and 24h; **Figure 2.6A**). Additionally, we always aim to use an in vitro model as close as possible to a human condition. Taking this into consideration, we evaluated the effect of ACM on ECs permeability and TEER. As shown in **Figure 2.6**, ACM obtained from control astrocytes (not exposed to drugs) decreased RBMVECs permeability (**Figure 2.6B**) and increased TEER (**Figure 2.6C**). This corroborates previous studies demonstrating that under normal conditions astrocytes have a beneficial role in barrier properties (Kuo and Lu 2011). However, when RBMVECs were exposed to ACM obtained from astrocytes exposed to 50 μM METH during 4h (METH ACM), a significant increase in Na-F permeability (**Figure 2.6B**) and decrease in TEER (**Figure 2.6C**) were observed, when compared with CTR ACM. Importantly, from **Figure 2.6A** we know that METH ACM has increased levels of TNF-α. Thus, by using an antibody against mouse TNF-α (Ab TNF-α) we could completely prevent the increased permeability and decreased TEER induced by METH ACM at all time points analyzed (**Figures 2.6B and 2.6C**). Moreover, the inhibition of NF-κB pathway with BAY efficiently prevented the effects of METH ACM, similarly to the results obtained with Ab TNF-α (**Figures 2.6B and 2.6C**). To exclude the possibility that the remaining

METH present in the ACM was responsible for the effects on RBMVECs permeability and TEER, METH concentration was determined by ELISA in METH ACM (**Figure 2.7**). Though there are residual concentrations of both D,L-METH, the Ab TNF-α still completely prevented the BBB disruption induced by METH suggesting that TNF-α is indeed the responsible for such alterations.

Overall, these results prove that METH also triggers the release of TNF-α by astrocytes that will negatively interfere with barrier function. Additionally, the activation of NF-κB signaling was once again shown to be involved in increased permeability.

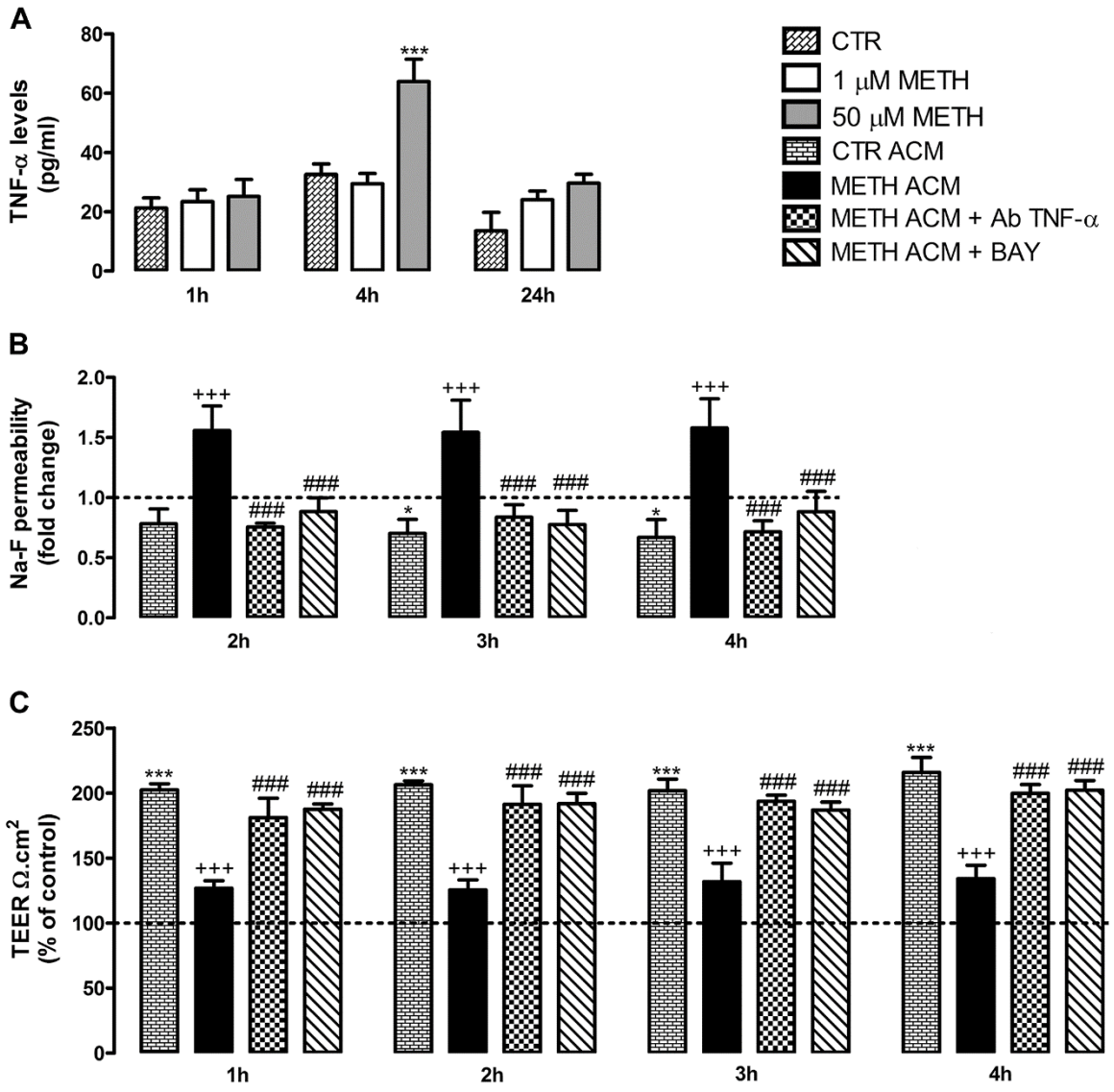

Figure 2.6. TNF-α released by astrocytes impairs the barrier properties of BMVECs via NF-κB pathway. (A) Primary cultures of mouse cortical astrocytes were exposed to 1 or 50 μM METH for 1, 4, and 24h. The results show that 50 μM METH induces a significant increase in TNF-α levels

at 4h. The TNF-α levels are expressed as mean pg/ml + S.E.M., n=4 to 10. **(B)** Macromolecular flux across primary rat BMVECs was assessed using 376 Da sodium fluorescein (Na-F) at different time points after exposure to untreated astrocyte-conditioned medium (CTR ACM), METH ACM, METH ACM+100 µg/ml Ab TNF-α, or METH ACM+5 µM BAY, n=3 to 8. **(C)** Transendothelial electrical resistance (TEER) of confluent rat BMVEC monolayers was analyzed under the same conditions of **(B)**, n=3 to 9. The results shown are mean + S.E.M. *P<0.05, ***P<0.001 significantly different when compared with the control (CTR or dashed line); $^{+++}$P<0.001 significantly different when compared with CTR ACM; $^{###}$P<0.001 significantly different when compared with METH ACM of each time point using Bonferroni's Multiple comparison test.

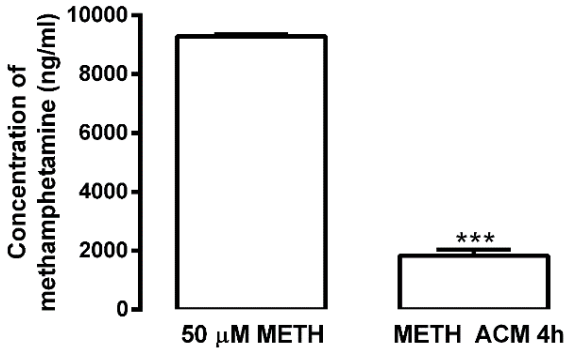

Figure 2.7. Quantification of METH in astrocyte-conditioned medium (ACM). Astrocytes were exposed to METH (50 µM) during 4h, and then its concentration in the medium was quantified. The levels of d,l-METH were residual. The results are expressed as mean ng/ml + S.E.M., n=3. ***P<0.001 significantly different when compared to 50 µM METH using Dunnet's Multiple comparison test.

2.4.4. Methamphetamine Induces *In Vivo* BBB Permeability via NF-κB Pathway

To support our in vitro results, we further used an animal model of METH-induced neurotoxicity (Grace et al., 2010). The binge administration protocol provides excellent relevance to intravenous and smoked routes of METH exposure in humans and simulates the toxic effects of METH in nontolerant users. Moreover, it was recently shown that acute METH treatment causes BBB disruption. Herein, we used albumin staining as a marker for BBB disruption (Scholler et al., 2007) since this is a blood serum protein that does not cross the BBB under normal conditions. Moreover, collagen IV is one of the most

expressed proteins in basal lamina and is responsible for the mechanical support of ECs. Thus, considering the crucial role of the striatum in METH addiction and neurotoxicity, we further investigated the alterations in collagen IV expression and the presence of albumin in the brain parenchyma of this specific brain region. A time-course study was performed, and we concluded that METH decreased collagen IV staining just 1h after the last injection, being more pronounced at 2h, and still evident after 24h. These observations indicate an altered and weakened structure of microvessels (**Figure 2.8A**). Furthermore, albumin was present in the brain parenchyma after METH administration, being a clear indicator of BBB disruption. Since a huge pick of albumin immunoreactivity was observed at 2h after the last METH injection, the following studies were performed at this time point. Noteworthy, and in accordance with our in vitro results, the blockade of the NF-κB pathway with BAY prevented the increased BBB permeability and structural alterations induced by METH (**Figures 2.8B to 2.8D**).

In an attempt to better clarify the effect of METH in animal BBB alterations, we also showed that this drug increases TNF-α levels in brain parenchyma (**Figures 2.9A and 2.9B**). Importantly, to exclude the contribution of peripheral TNF-α, we measured its levels in mouse sera and concluded that there were no alterations (**Figure 2.10**). This suggests that increased cerebrovascular permeability was not related to peripheral TNF-α production, but instead to its production in the brain (**Figures 2.9A and 2.9B**), particularly around the perivascular zone. We also evaluated astrocyte activity through GFAP immunofluorescence, but in general no significant alterations were found (**Figure 2.9C**). However, it is possible to observe a specific increase surrounding microvessels, which suggests an astrocytic recruitment and reorganization (**Figure 2.9A**). These observations lead us to hypothesize that METH may induce a perivascular astrogliosis (Alvarez et al., 2015) inflammatory status. In fact, the presence of TNF-α near both the astrocytic endfeet and capillary is notorious (**Figure 2.9A**) and corroborates ours in vitro results showing that both cells can produce TNF-α. Also, this cytokine's production was abrogated by the

treatment with BAY, demonstrating the involvement of NF-κB pathway in TNF-α production after METH binge administration.

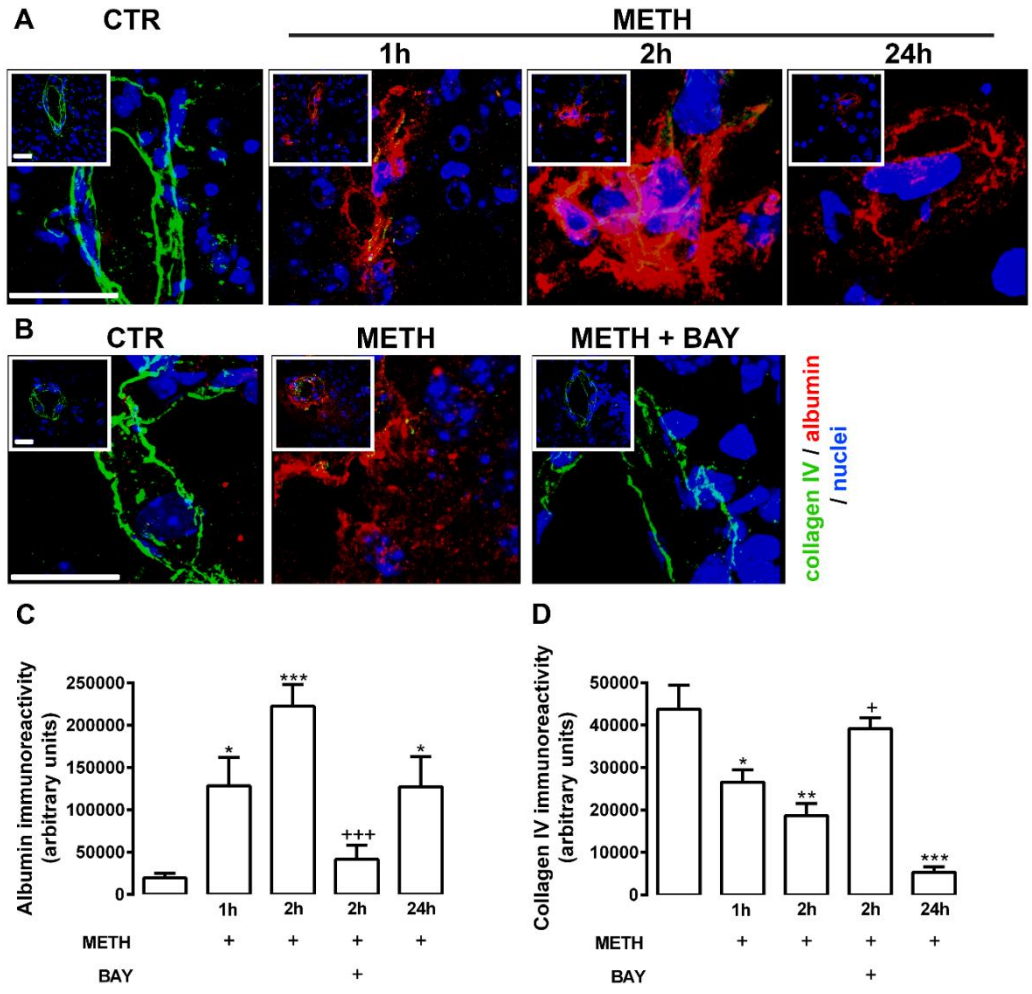

Figure 2.8. METH induces BBB disruption in the mice striatum via NF-κB pathway. Mice were administered with METH (4× 10 mg/kg, intraperitoneally (i.p.), 2h apart) and killed 1, 2, and 24h after the last injection. **(A)** Representative images of collagen IV (green), a marker of basement membrane that surrounds the brain vessels, and albumin (red) that is a marker of BBB disruption. It was clearly shown that METH triggered a decrease in collagen and an increase in albumin staining already 1h after the last METH injection, reaching a peak after 2h. Interestingly, the effect is still present after 24h of the last METH injection. **(B)** Representative images and **(C, D)** quantification of **(C)** albumin and **(D)** collagen IV immunofluorescence show that METH increases albumin extravasation and decreases collagen IV at 2h after the last injection, which was completely prevented by the blockade of NF-κB pathway with BAY treatment (20 mg/kg, i.p., 30 min before each METH injection). Total brain sections were also stained with Hoechst 33342 (blue). Scale bar = 20 μm. The results shown are mean + S.E.M., n=18 visual fields acquired from three different animals of each experimental condition. *P<0.05, **P<0.01, ***P<0.001 significantly different when compared with the control (CTR); $^{+}$P<0.01, $^{+++}$P<0.001 significantly different when compared with METH (2h) using Bonferroni's Multiple comparison test.

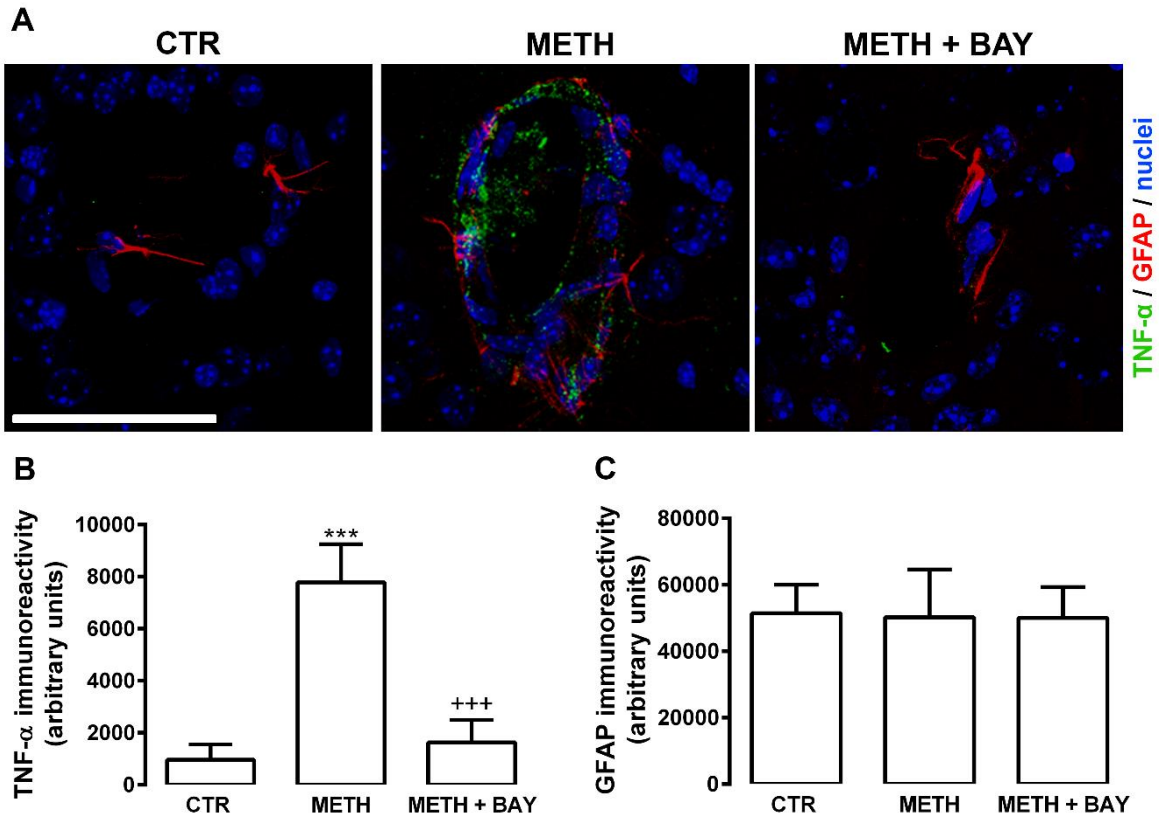

Figure 2.9. METH upregulates TNF-α levels in the mouse striatum. Mice were administered with METH (4× 10 mg/kg, intraperitoneally (i.p.), 2h apart) and killed 2h after the last injection. **(A)** Representative images of TNF-α and glial fibrillary acidic protein (GFAP) immunoreactivity showing a colocalization of the cytokine with astrocytes and vessels. **(A, B)** Quantification of both proteins shows a significant increase in **(B)** TNF-α levels that was prevented by the blockade of the NF-κB pathway with BAY, but **(C)** no alteration in general GFAP levels. Total brain sections were also stained with Hoechst 33342 (blue). Scale bar = 20 μm. The results shown are mean + S.E.M, n=18 visual fields acquired from three different animals of each experimental condition. ***P<0.001 significantly different when compared with the control (CTR); $^{+++}$P<0.001 significantly different when compared with METH using Bonferroni's Multiple comparison test.

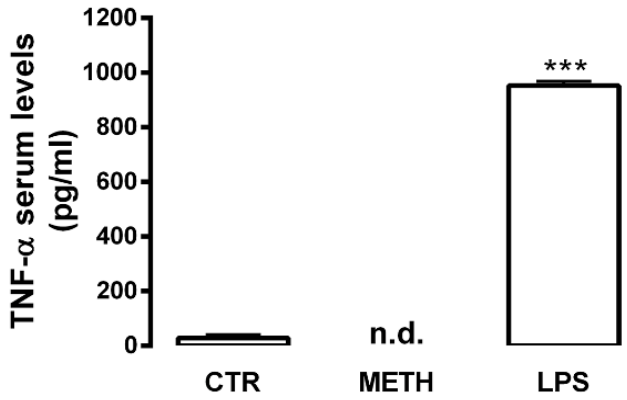

Figure 2.10. Quantification of TNF-α in mice sera. Mice were administered with METH (4× 10 mg/kg, i.p., 2h apart) and sacrificed 2h after the last injection. Control (CTR) animals were manipulated as for METH protocol but injected with saline (0.9% NaCl). As a positive control, mice were administered with lipopolysaccharide (LPS; 5 mg/kg, i.p.) and sacrificed after 1h. The cytokine levels were quantified by ELISA Ready-SET-Go kit, as specified in the datasheet and expressed as mean pg/ml + S.E.M., n=4-10. ***P<0.001 significantly different when compared to CTR using Dunnet's Multiple comparison test.

2.5. Discussion

Methamphetamine is a powerful psychostimulant drug of abuse that causes severe alterations in the CNS. In fact, the neurotoxicity triggered by this drug has been extensively studied over the last years (Thompson et al., 2004). Though its impact on BBB properties was highlighted more recently (Ramirez et al., 2009), the intracellular mechanisms involved in METH-induced cerebral endothelium dysfunction remain unknown, as well as its effect on the crosstalk between different neurovascular unit cells. Thus, to reach our goal we first took advantage of a well-established BBB in vitro model (Cardoso et al., 2012), and we observed that METH increased ECs permeability at concentrations relevant to human abuse. Considering the differences between rodents and humans, we further used human ECs (Bernas et al., 2010) to reproduce the results obtained with rat primary cultures. As it is also known that METH can induce death of various cell types (Krasnova and Cadet, 2009; Coelho-Santos et al., 2012) including ECs (Martins et al., 2013), we also considered if METH-increased endothelial permeability was due to cell death. Importantly, the concentrations used in the present study did not cause EC death or decreased cell viability. This is a key issue because, in contrast to other studies, we used METH concentrations that present a most common pattern of drug use, highlighting the importance of understanding its impact on BBB function.

Multiple studies suggest that METH triggers a pronounced neuroinflammatory response (Loftis and Janowsky, 2014), usually characterized by gliosis and increased levels of cytokines (Gonçalves et al., 2010; Coelho-Santos et al., 2012). Importantly, ECs can actively participate in inflammatory events, being also an important source of proinflammatory cytokines (Lee et al., 2001). Since we have previously shown that TNF-α has an important role in METH-induced toxicity (Gonçalves et al., 2010; Coelho-Santos et al., 2012), we hypothesized that this proinflammatory cytokine could also be involved in endothelial dysfunction induced by METH. Indeed, we proved that both brain ECs and astrocytes are an important source of TNF-α, but both cell types also showed a distinct

response to METH. It is well known that METH induces different responses according to cell type, and indeed a lower concentration of the drug triggered a faster and higher release of TNF-α by ECs when compared with astrocytes. Curiously, in ECs we also observed a fast release of TNF-α within 15 min after METH exposure that is independent of NF-κB activation, since BAY did not prevent its release. Instead, it seems that this first pool of TNF-α will trigger the p65 translocation into the nucleus, and so being itself a stimulator of subsequent cytokine synthesis. It is known that the brain endothelium is the first to interact with peripheral pathogens or harmful signals (Mai et al., 2013), and indeed ECs contain intracellular granules called Weibel-Palade bodies that store several chemokines, adhesive molecules, and inflammatory cytokines (Kim et al., 2010). These may undergo exocytosis into the extracellular space within minutes of stimulation and thus allow an immediate response of ECs (Kim et al., 2010) that is independent of gene transcription (Lowenstein et al., 2005).

Additionally, we clearly showed that the inhibition of TNF-α completely prevented the increased permeability induced by METH. Accordingly, this cytokine has been shown to participate in BBB breakdown in pathologic phenomena, such as stroke and traumatic brain injury (Tobinick et al., 2012). Namely, rat intracerebral injection of TNF-α increased BBB permeability (Candelario-Jalil et al., 2007). Similar results were observed with a short acute incubation of this proinflammatory cytokine in a BBB in vitro model of bovine cerebral ECs and rat glial cell co-cultures (Miller et al., 2005). Moreover, to unravel the intracellular signaling that culminates in BBB impairment, we targeted the NF-κB pathway. NF-κB is a potent proinflammatory nuclear transcription factor that is involved in the initiation and amplification of inflammatory responses. Additionally, TNF-α triggers signaling pathways that converge on the activation of transcription factor NF-κB (Aveleira et al., 2010; Tang et al., 2011; Zhong et al., 2012). More recently, others have shown that TNF-α activates NF-κB in both human umbilical vein ECs (Zhong et al., 2012) and dermal microvascular ECs (Clark et al., 2007). Thus, NF-κB is a transcription factor that regulates the proinflammatory responses in ECs, including ZO-1 expression as shown in lupus condition (Jacob et al.,

2011). Also, Koedel et al. (2000) showed that NF-κB inhibition had a protective effect on meningitis-associated BBB leakage. Accordingly, in the present study, we concluded that TNF-α/NF-κB blockade prevented METH- induced EC dysfunction.

Knowing that increased BBB permeability under several insult conditions can occur through different mechanisms (de Vries et al., 2012; Loftis and Janowsky, 2014), we further aimed to clarify what type of transport across ECs was being modulated by this TNF-α/NF-κB pathway. In fact, it was previously shown that METH increased both paracellular (Ramirez et al., 2009; Martins et al., 2011) and vesicular transport (Martins et al., 2013). Noteworthy, in healthy BBB endothelium, nonspecific fluid-phase transcytosis is rarely observed (Cardoso et al., 2010). However, under several types of brain injuries, the vesicular transport is increased, including in traumatic human brain edema (Castejon, 2013). Accordingly, in this study, we clearly show that just after METH exposure the transcellular permeability mediated by NF-κB is increased. Also, Tiruppathi et al. (2008) showed that NF-κB signaling was involved in LPS-increased caveolae-mediated transendothelial albumin permeability. Besides this transcellular permeability, METH also interfered with the paracellular pathway. In fact, there was a significant decrease in the expression of occludin and claudin-5, which was prevented by NF-κB pathway blockade, similarly to the vesicular transport. Accordingly, Aveleira et al. (2012) showed that, in primary cultures of bovine retinal ECs, TNF-α induced BBB impairment via NF-κB signaling, which was associated with decreased levels and changes in the cellular distribution of claudin-5 and ZO-1. Moreover, TNF-α/NF-κB pathway was shown to be responsible for ZO-1 downregulation and alteration in junctional localization that led to increased permeability of Caco-2 cells (Ma et al., 2004). Additionally, TNF-α was shown to induce NF-κB signaling in mouse brain ECs, and p65 over-expression repressed the claudin-5 promoter (Aslam et al., 2012). Importantly, NF-κB also affects the dynamic of actin cytoskeletal assembly that is crucial for the stabilization of TJs (Lee et al., 2001). All these studies emphasize the crucial role of the TNF-α/NF-κB signaling on BBB modulation, but its link with METH use has never been identified until now.

Alterations in TJs structure and organization may also affect BBB permeability, and subsequently the movement of leukocytes and immune mediators into the brain. In fact, our group has recently shown an enhancement of lymphocyte transendothelial migration after METH (Martins et al., 2013). Thus, we hypothesized that it could also upregulate the expression of cell adhesion molecules in ECs, justifying the infiltration of leukocytes. In fact, METH increased ICAM-1 expression, which was once again prevented by the blockade of the NF-κB pathway. Importantly, it was previously showed that increased levels of ICAM-1 induce ECs leakiness through alteration of cell junctions and cytoskeleton (Clark et al., 2007). Moreover, using the same concentration of TNF-α that we used, the activation of NF-κB was proven to be essential for ICAM-1 expression and the consequent increase of neutrophils adhesion onto ECs (Tang et al., 2011). Herein, we clearly show that METH has a direct effect on ECs leading to significant alterations in both vesicular and paracellular transports through TNF-α/NF-κB signaling pathway.

Despite our important findings regarding the impact of METH on ECs, BBB is a complex structure. Indeed, astrocytes have a crucial role in modulating the structure and function of the cerebral endothelium, but the effect of METH on the crosstalk between brain ECs and astrocytes has never been addressed before. Kuo and Lu (2011) showed that ACM from human astrocytes increased TEER of HBMVECs, together with a reduction of paracellular permeability. Also, ACM induced brain endothelium properties on human umbilical vein ECs, with decreased permeability to HRP and increased expression of occludin and ZO-1 (Landoni et al., 2012). Accordingly, we conclude that under control conditions astrocytes release several factors that contribute to the tightness of the barrier. However, under toxic conditions astrocytes can have a negative effect on the surrounding cells, including on ECs. Specifically, Yang et al. (2013) showed that ACM obtained from a rat cell line incubated 24h with bradykinin increased neuronal cell death due to reactive oxygen species, MMP-9, and hemeoxygenase-1/carbon monoxide present in the medium. Also, factors released by LPS- and/or Shiga toxin 1-treated astrocytes increased transendothelial permeability in human umbilical vein ECs by reducing TJs proteins

expression (Landoni et al., 2012). Importantly, these authors also showed that NF-κB inhibition or TNF-α blockade inhibited the effects of ACM (Landoni et al., 2012). Thus, considering that METH increases astrocytic reactivity as well as the expression of several cytokines in the mouse brain, including TNF-α (Gonçalves et al., 2010), we hypothesize that METH could also induce endothelium dysfunction via TNF-α released by astrocytes. Indeed, we proved that barrier dysfunction could involve not only endothelial but also astrocytic TNF-α, that again culminated in increased endothelial permeability through the activation of the NF-κB pathway.

To better support our in vitro results, we also investigated if METH binge administration to mice could cause BBB dysfunction. Importantly, this drug administration paradigm confers excellent significance to intravenous and smoked routes of METH exposure in humans (Grace et al., 2010) and the dose is similar to that detected in the blood of drug abusers (Melega et al., 2007; Ramirez et al., 2009). Additionally, this binge protocol has been widely used in animal studies and is well characterized by striatal toxicity (Beauvais et al., 2011). However, little is known about the effect of this METH regimen on BBB function. Nevertheless, Urrutia et al. (2013) showed that a similar METH binge protocol (3 × 4 mg/kg) induced BBB disruption in mouse striatum at 1, 12, and 24h after METH treatment, observed by extravasation of Immunoglobulin G (150 kDa). Herein, we showed that METH increased BBB permeability at 1, 2, and 24h after the last injection, which was evaluated by increased albumin (66 kDa) leakage and decreased expression of collagen IV. Collagen IV is the major component of the basement membrane having a decisive role in the maintenance the vessels' wall structural integrity. In fact, downregulation of this protein has been associated with the pathogenesis of BBB destruction in autoimmune Encephalomyelitis (Zhang et al., 2013) and ischemic stroke (Rosell, et al., 2008). Another interesting aspect is that MMPs, particularly MMP-9, have been implicated in collagen IV degradation (Rosell, et al., 2008; Zhang et al., 2013). Indeed, we previously showed that METH increases the expression and activity of MMP-9, being responsible for BBB breakdown (Martins et al., 2011). Moreover, we also observed an increase of TNF-α

confined to the perivascular zone, near ECs and astrocytes. Additionally, both BBB breakdown and TNF-α production were prevented by BAY, showing the involvement of NF-κB signaling in METH-induced BBB disruption. Interestingly, with our pattern of drug administration, we did not detect an increase in general GFAP immunoreactivity, which is in agreement with a previous study that showed no alterations of several proteins, including GFAP, in striatal homogenates of autopsied brains obtained from chronic METH users (Tong et al., 2014). Nevertheless, it was possible to observe a specific increase of GFAP immunoreactivity around the microvessels, which indicates an astrocytic recruitment and reorganization around the capillaries highlighting a clear perivascular astrogliosis (Alvarez et al., 2015) triggered by METH. In conclusion, the present work shows that at concentrations relevant to human abuse, METH induces the release of TNF-α by both brain ECs and astrocytes with subsequent activation of the NF-κB pathway. This sequence of events culminates in the increase of transcellular and paracellular endothelial transport.

Importantly, the blockade of TNF-α or NF-κB was able to prevent METH-induced BBB dysfunction. Moreover, these results were reproduced using rat and human cerebral ECs, as well as an animal model. So, for the first time, we show that TNF-α/NF-κB signaling pathway has a central role in METH-induced brain endothelium permeability. This observation may provide an important strategy against BBB dysfunction triggered by METH and consequent brain parenchyma alterations/infections that may occur under such conditions.

CHAPTER 3

Aquaporin-4 as a new target against methamphetamine-induced brain alterations: focus on the neurogliovascular unit and motivational behavior

3.1. Abstract

Methamphetamine (METH) abuse/misuse is a worldwide problem, and despite extensive characterization of its neurotoxicity over the last years, many questions remain unanswered. Recently, it was shown that METH compromises the blood-brain barrier (BBB) and causes a disturbance in the water homeostasis leading to brain edema. Importantly, water transport at BBB is regulated by water channels, aquaporins (AQPs), with AQP4 being expressed in astrocytic endfeet surrounding brain endothelium. Thus, the main goal of this work was to unravel the role of AQP4 under conditions of METH consumption. Our results show that METH (4× 10 mg/kg, 2h apart, i.p.) interferes with AQP4 protein levels causing brain edema and BBB breakdown in both mice striatum and hippocampus, which culminated in locomotor and motivational impairment. Furthermore, these effects were prevented by pharmacological blockade of AQP4 with a specific inhibitor (TGN-020). Moreover, siRNA knockdown of this water channel protected astrocytes from METH-induced swelling and morphologic alterations. Herein, we unraveled AQP4 as a new therapeutic target to prevent the negative impact of METH.

3.2. Introduction

METH abuse/misuse is a major problem in several countries, including the USA, Australia, Canada, and Japan but there is also an increasing concern about the situation in Europe (UNODC, 2015). METH can adversely influence human health, causing acute behavioral and physiological disturbances, as well as long-term complications (Silva et al., 2010). Most of the studies that aimed to clarify the impact of METH on the CNS have focused on oxidative stress (Toborek et al., 2013), excitotoxicity, neuroinflammation (Sharma and Kiyatkin, 2009; Silva et al., 2010; Loftis and Janowsky, 2014), and hyperthermia (Matsumoto et al., 2014). More recently, a new concept of METH-induced brain dysfunction was described based on its ability to disrupt the BBB (Ramirez et al., 2009; Martins et al., 2011). Dysfunction of BBB is likely involved in the majority of neurodegenerative diseases, and drug abuse is not an exception (Silva et al., 2010; Gonçalves et al., 2014). Specifically, we have previously demonstrated that an acute high dose of METH transiently increased BBB permeability in the mice hippocampus, which was explained by a downregulation of tight junction proteins and increased matrix metalloproteinase-9 expression and activity (Martins et al., 2011).

It has also been reported that METH causes brain edema (Beránková et al., 2005; Sharma and Kiyatkin, 2009), which occurs due to abnormally increased water content and consequent brain swelling. However, it is still unknown if this is a consequence of BBB breakdown. There are two major types of brain edema: cytotoxic (cellular) and vasogenic (leaky-vessel) (Tait et al., 2008), each involving different entry routes into the brain. The discovery of specific water channel molecules (aquaporins, AQPs) provided new insights about water movements through the plasma membrane. Since brain edema continues to be the main cause of death in several CNS diseases, the interest in AQPs as potential therapeutic targets has been increasing (Igarashi et al., 2011). The AQP4 is the most abundant and enriched AQP in the brain, specifically in astrocyte endfeet surrounding brain capillaries (Tait et al., 2008). Besides, AQP4 is expressed as two major isoforms, M1

and M23, that form heterotetramers aggregates at cell plasma membrane called orthogonal arrays of particles (OAPs), and its composition and function depend on the relative amounts of both isoforms. In fact, an increase in M1 isoform presence in the OAPs leads to a disruption of this structure causing a dysregulation in water homeostasis, while an increase of M23 presence stabilizes the supramolecular structure (Furman et al., 2003). Thus, the AQP4 expression pattern in vascular disease is a critical component since it regulates water movement during edema formation and resolution (Tait et al., 2008). In fact, several studies showed that AQP4 deficiency is associated with reduced cytotoxic brain edema in animal models of focal cerebral ischemia and bacterial meningitis (Chen et al., 2014). Contrarily, AQP4 deficiency produces more brain swelling in mouse models of vasogenic edema, including brain tumors (Tait et al., 2008). Also, there is only one study showing an increase of AQP4 expression in a human METH intoxication case (Wang et al., 2014). Importantly, the role of AQP4 in many CNS pathologies, either beneficial or deleterious, is still unclear.

Noteworthy, BBB permeability and edema formation can be associated with behavioral alterations. In fact, it was previously shown that BBB disruption led to locomotor impairment (Tomkins et al., 2007; Rapp et al., 2008; Fukuda et al., 2013) and anxiety/depressive-like behaviors (Rapp et al., 2008; Najjar et al., 2013). Moreover, there are supporting data demonstrating cognitive impairment and depression under the condition of METH use in both humans (Simon et al., 2000) and animal models (Gonçalves et al., 2012; Silva et al., 2014). Also, there is growing evidence linking brain edema with locomotor impairment (Wachter et al., 2012; Fukuda et al., 2013; Zhong et al., 2013). However, the correlation between METH-induced brain edema and behavioral abnormalities has been overlooked.

Despite the evidence showing that METH leads to BBB disruption and brain edema formation, the role of AQP4 has never been addressed before. Thus, we hypothesized that AQP4 would play a critical role on such phenomena. Additionally, we aimed to clarify the behavioral outcome of water homeostasis dysfunction.

3.3. Material and Methods

3.3.1. Animals and Treatments

Male wild-type C57BL/6J mice (8 weeks old; 24-26 g body weight; Charles River Laboratories, Barcelona, Spain) were housed under controlled environmental conditions (12h light-dark cycle, 24 ± 1°C) with food and water ad labium. Mice were divided into three groups as follows: control group [4× 0.9% NaCl, 2h apart, intraperitoneal injection (i.p.)], METH binge group (4× 10 mg/kg, 2h apart, i.p.), and METH + TGN group that received 200 mg/kg TGN (i.p.; Sigma-Aldrich, St. Louis, MO, USA) 1h before the first METH administration. Taking into consideration that this specific METH regimen causes a very significant BBB disruption at 2h after the last drug injection when compared to the other time points analyzed (1 and 24h after drug exposure; **Chapter 2**; Coelho-Santos et al., 2015), we conducted all the other experiments at 2h. The present study was approved by the Institutional Animal Care and Use Committee (FMUC/CNC, University of Coimbra, Coimbra, Portugal). Experiments were performed by certified researchers in accordance with European Community Council Directives (2010/63/EU) and Portuguese law for care and use of experimental animals (DL no. 113/2013). All efforts were made to minimize animal suffering and to reduce the number of animals used.

3.3.2. Evaluation of Brain Edema

3.3.2.1. Brain Water Content Determination

Cortical, striatal, and hippocampal water accumulation was evaluated by comparing the wet and dry weights, as previously described (Haj-Yasein et al., 2011). Specifically, to determine the wet weight (WW), mice were sacrificed and the intact brain regions were removed and weighed. Afterward, the tissue was dried for 72h at 60°C and once again weighed to obtain the dry weight (DW). The percentage of brain water was calculated using the following formula: $[(WW - DW) / WW] \times 100$.

3.3.2.2. Volume Measurements of Different Regions by in vivo Magnetic Resonance Imaging

Magnetic resonance imaging (MRI) was carried out first on the control group and then on treated animals, after 2h of the last METH administration. Mice were anesthetized with 1.5% isoflurane in air and placed on temperature controlled beds with tooth bar and head restraint to reduce motion artifact. Body temperature was maintained at 37°C and respiration was monitored. MRI was performed on a 9.4-T MR pre-clinical scanner (Bruker Biospec, Billerica MA, USA) with a transmit/receive volume coil with 40/75 mm of inner/outer diameter, respectively. High-resolution morphological images were acquired with a 2D T2-weighted turbo RARE sequence with the following parameters: TR/TE = 2500/33 ms, FOV = 20 × 20 mm, acquisition matrix = 256 × 256, echo train length = 8, echo spacing = 11 ms, and 19 axial continuous slices 0.5 mm thick. Diffusion-weighted imaging (DWI) was performed with diffusion prepared 2D spin-echo echo-planar imaging (2D SE-EPI), and the sequence parameters were as follows: TR/TE = 3000/15.8 ms, FOV = 20 × 0 mm, acquisition matrix =156 × 87, b values = 0, 100, 500, 800 (s/mm^2), with 30 averages, and 13 axial continuous slices 0.5 mm thick. Apparent diffusion coefficient (ADC) maps were calculated, using in-house developed software based on MATLAB (Mathworks, Natick, Mass, USA), using b values corrected for the amplitude of the imaging gradients (Bammer, 2003). Briefly, the ADC value per voxel was calculated by fitting the signal intensity as a function of b value to the conventional ADC equation (Sb/S0 = exp(−b ADC)), where Sb is the signal intensity corresponding to each b value and S0 is the signal intensity at b = 0. Two regions of interest were manually drawn corresponding to the striatum and the hippocampus and the average ADC value per region was extracted.

3.3.3. Western Blot Analysis

Mice were sacrificed, hippocampi and striata were dissected on ice, and western blots were performed as previously described (Gonçalves et al. 2010). Primary and secondary

antibodies used were as follows: rabbit anti-AQP4 (1:500, Millipore, Darmstadt, Germany) and goat anti-albumin (1:20000, Bethyl Laboratories Inc., Montgomery, TX, USA), and secondary antibodies were alkaline phosphatase-conjugated secondary antibody anti-rabbit (1:20,000) and anti-goat (1:10,000) (Amersham GE Healthcare Life Science, USA), respectively. Levels of glyceraldehyde 3-phosphate dehydrogenase (GAPDH, 1:500; Abcam, Cambridge, UK) were used as loading controls. Bands were visualized with enhanced chemifluorescence (ECF) reagent on the Typhoon FLA 9000 (GE Healthcare Bioscience AB, Uppsala, Sweden), and quantification performed in ImageJ 1.44o software.

3.3.4. Immunohistochemistry

Immunolabeling was performed as previously described (**Chapter 2**; Coelho-Santos et al., 2015). The antibodies used were as follows: rabbit anti-collagen IV (1:200; Abcam) and goat anti-albumin (1:2000; Bethyl Laboratories) followed by Alexa Fluor 488 anti-rabbit and Alexa Fluor 594 anti-goat (1:200; Invitrogen, Inchinnan Business Park, UK), respectively, followed by nuclei staining with 5 µg/ml Hoechst 33342 (Sigma-Aldrich). Slices were then mounted with Dako fluorescence medium (Dako, Glostrup, Denmark), and images recorded in LSM 710 Meta Confocal microscope (Carl Zeiss; Oberkochen, Germany).

3.3.5. Animal Behavior Studies

Prior to the start of behavioral tests, mice were transferred to the experimental room allowing habituation to the new environment for at least 1h. To evaluate animal locomotor activity, open field test was performed for 20 min accordingly with Joca and collaborators (Joca et al., 2014), in a 45 × 45 cm arena. The location and movement of the animals were recorded and analyzed by Anymaze Video Tracking Software (Stoelting, Wood Dale, IL, USA).

Motor coordination activity was evaluated on a rotarod Letica LI8200 (Panlab, Barcelona, Spain). As previously described (Huang et al., 2015), mice were trained for 2 sessions a day for 3 consecutive days, until they were capable of stay on the rotating drum at a speed of 25 rpm (rotations per minute) for at least 120 s. On the following day and after appropriate treatments, mice were subjected to rotarod test at an acceleration speed between 4 to 40 rpm and the latency to fall was recorded. Importantly, the cutoff time for latency to fall was 300 s (Huang et al., 2015).

For splash test, a 10% sucrose solution was squirted on the dorsal coat of mice in their home cage. Due to the viscosity of the solution, the animal coat becomes dirty and induces grooming behavior. The total time spent on grooming over a 5-min period was recorded as previously published (Boulle et al., 2014).

3.3.6. Primary Cultures of Mouse Cortical Astrocytes

Astrocytes were isolated from C57BL/6J mouse pups aged P4-5 as previously described (**Chapter 2**; Coelho-Santos et al., 2015) with minor modifications. Briefly, after brain cortices were isolated, the tissue was mechanically digested and the pellet was plated in T-75 flasks at a density of 1.2×10^5 cells/cm^2 in astrocyte medium [Dulbecco's modified Eagle's medium (DMEM) low glucose supplemented with 10% fetal bovine serum (FBS) and 1% gentamicin]. The medium was changed after 6h and then every 2 days until cells reached confluency. At this point, flasks were shaken and the adherent cells (astrocytes) were trypsinized with 0.1% Trypsin (Sigma-Aldrich) in Hank's Balanced Salt Solution (HBSS, Invitrogen). This process was stopped by incubation with astrocyte medium followed by centrifugation (143×*g*, 5 min). Cells were plated at different densities depending on the experiments.

3.3.7. AQP4 Silencing by Small-Interfering RNA-Based Knockdown

Astrocytic AQP4 knockdown was performed as previously described (Badaut et al., 2011) with minor modifications. Briefly, two optimized small interference RNA (siRNA) against AQP4 were acquired (20 nM, Invitrogen) and mixed, accordingly with the manufacturer, with ScreenFect (InCellA, Eggenstein-Leopoldshafen, Germany), diluted in Opti-MEM (1:50; Invitrogen). For negative control, non-targeted siRNAs were used (20 nM, Invitrogen). The mixture was incubated for 20 min at room temperature (RT) and then added to the respective well for 4 days.

3.3.8. Terminal Deoxynucleotidyl Transferase dUTP Nick End Labeling (TUNEL) Assay

After the appropriate treatments, the whole population of cells was collected by trypsinization. Then, cells were fixed with 4% paraformaldehyde (PFA) and adhered to superfrost microscope slides (Thermo Scientific, Menzel GmbH & Co KG, Braunschweig, Germany) by centrifugation (113×*g*, 5 min; Cellspin I, Tharmac GmbH, Waldsolms, Germany). Apoptotic cell death was further evaluated by the TUNEL assay (Roche Diagnostics GmbH, Mannheim, Germany). After that, cells were permeabilized in 0.25% Triton X-100 for 30 min at room temperature (RT), and incubated with terminal deoxynucleotidyl transferase buffer for 1h at 37ºC in a humidified chamber. Incubation with fluorescein Avidin D (1:100) was performed for 1h, followed by nuclei counterstaining with 5 µg/ml Hoechst 33342 for 5 min. Cell images were recorded using an Axiovert 200 M fluorescence microscope.

3.3.9. Immunocytochemistry

Cells were fixed with 4% PFA (Sigma-Aldrich) for 20 min at RT. Afterward, cells were permeabilized with 0.25% Triton X-100 (Sigma-Aldrich) and blocked with 5% bovine serum albumin (BSA, Sigma-Aldrich) during 1h at RT, followed by incubation with primary antibodies (rabbit anti-AQP4, 1:250, overnight at 4°C, Millipore; anti-GFAP-Cy3 conjugated, 1:1000, 1h at RT, Sigma-Aldrich). Then, cells were incubated with secondary antibody (Alexa Fluor 488, 1:200, Invitrogen) for 1h at RT in the dark and nuclei were stained with 4 µg/ml Hoechst 33342 (Sigma-Aldrich) for 5 min at RT. Finally, cells were mounted in Dako fluorescence medium (Dako) and images were recorded using a LSM 710 Meta Confocal microscope (Carl Zeiss).

3.3.10. Morphological Analysis of Astrocytes

3.3.10.1. AQP4 Quantification

Immunostaining analysis was performed in FIJI Software version 2.0 based on a previous study (**Chapter 2**; Coelho-Santos et al., 2015). In brief, all photograph area was considered as well as three different zones without staining (black) to be used for background subtraction. To determine the corrected total AQP4 fluorescence, we used the following formula: correct total fluorescence = (integrated intensity) − (area of picture × mean background). The results are expressed as mean of fluorescence intensity (arbitrary units) of five photos from three different primary cultures slides for each experimental group.

3.3.10.2. Membrane/Cytoplasm Ratio of AQP4

The alterations in AQP4 cellular localization were analyzed based on a previous study (Fernandes et al., 2016). Shortly, a line perpendicular to astrocytic membrane limits was drawn for each cell in all pictures (five pictures from three different cultures for each

experimental condition). An intensity plot profile of that line was obtained and the ratio between membrane and cytoplasmic pixel intensity was calculated.

3.3.10.3. Analysis of Astrocytic Processes

GFAP-labeled astrocytes were analyzed using the NeuronJ program, a plugin of FIJI Software, to measure the length and count the number of astrocytes processes in each experimental group as previously described by Di Benedetto and collaborators (Di Benedetto et al., 2016).

3.3.11. Water Uptake Measurements by Calcein Fluorescence Quenching Method

In order to evaluate changes in astrocytic volume and water movements, we used the calcein quenching method as previously published (Hawkins et al., 2013). This methodology consists of cell incubation with a solution of calcein-acetoxymethyl ester (Calcein-AM), which is a cell-permeable and non-fluorescent dye. Once inside the cells, the AM group is cleaved by cytoplasmic esterases and calcein becomes cell membrane impermeable and acquires fluorescence. This technique allows us to infer about the cell volume since fluorescence is proportional to cell volume. Thus, astrocytes were plated in laminin-coated (10 µg/ml in phosphate-buffered saline (PBS); Invitrogen) black 96-wells plates, and after appropriate treatments, cells were washed with 0.01 M PBS and incubated with 5 µM Calcein-AM (Invitrogen) in artificial cerebrospinal fluid (aCSF, in mM: 120 NaCl, 2.5 KCl, 25 $NaHCO_3$, 1 NaH_2PO_4, 2.5 $CaCl_2$, 1.3 $MgSO_4$, 10 glucose) for 1h at 37°C. Then, calcein solution was removed and astrocytes were maintained in aCSF for fluorescence measurements (excitation 485 nm, emission 530 nm).

3.3.12. Reactive Oxygen Species Quantification

Astrocyte cell cultures were seeded in black 96-wells plates. After appropriate treatments for 4h, cells were incubated with 2′,7′-dichlorodihydrofluorescein diacetate (H_2DCFDA; 5 μM; Invitrogen) during 1h at 37°C in the dark. Fluorescence intensity was read (ex/em 485/528 nm) and divided by the total amount of protein.

3.3.13. Statistical Analysis

Results are expressed as mean + standard error of the mean (S.E.M.). Data were analyzed using a Mann-Whitney test or one-way ANOVA followed by Dunnet's or Bonferroni's post hoc test, as indicated in figure legends. ADC values were analyzed using Wilcoxon matched-pairs test since each animal was used as its own control (before vs after drug(s) treatment). The level of significance was $P<0.05$ and the ´n´ represents the total number of animals or the total of multiwell plates obtained from at least three independent cultures. Statistical analysis was calculated using Prism 6.0 (GraphPad Software, San Diego, CA, USA).

3.4. Results

3.4.1. METH Causes Brain Edema and AQP4 Upregulation

It was previously shown that a single METH administration causes an increase in rat brain water content (Sharma and Kiyatkin, 2009). However, nothing is known about the effect of other METH regimens or the possible alterations in water channels, as well as their involvement in edema formation. Here, we show for the first time that a binge METH treatment induces striatal (**P<0.01 vs CTR) and hippocampal (*P<0.05 vs CTR) water accumulation at 2h after the post last injection, without changes at an earlier time point (1h) and on the pre-frontal cortex (**Figure 3.1A**). Moreover, we aimed to identify the type of edema observed under these conditions. Magnetic resonance imaging (MRI) analysis showed a reduction of the apparent diffusion coefficient (ADC) values in both the striatum and hippocampus (**P<0.01 vs CTR within the same region) suggesting that METH induced a cytotoxic edema (**Figures 3.1B and 3.1C**).

Some studies have demonstrated that the water channel AQP4 plays a critical role on brain edema under different pathological conditions, such as hypoxia (Chen et al., 2014) and ischemia (Igarashi et al., 2011). Thus, we analyzed the AQP4 protein levels at 2h after the last METH injection, the same time point that occurred brain edema formation, and it was possible to observe an upregulation of AQP4 total protein levels (**Figure 3.1D**; *P<0.05 and ***P<0.001 vs CTR in the striatum and hippocampus, respectively) and M1/M23 ratio (**Figure 3.1E**; **P<0.01 vs CTR within the same region).

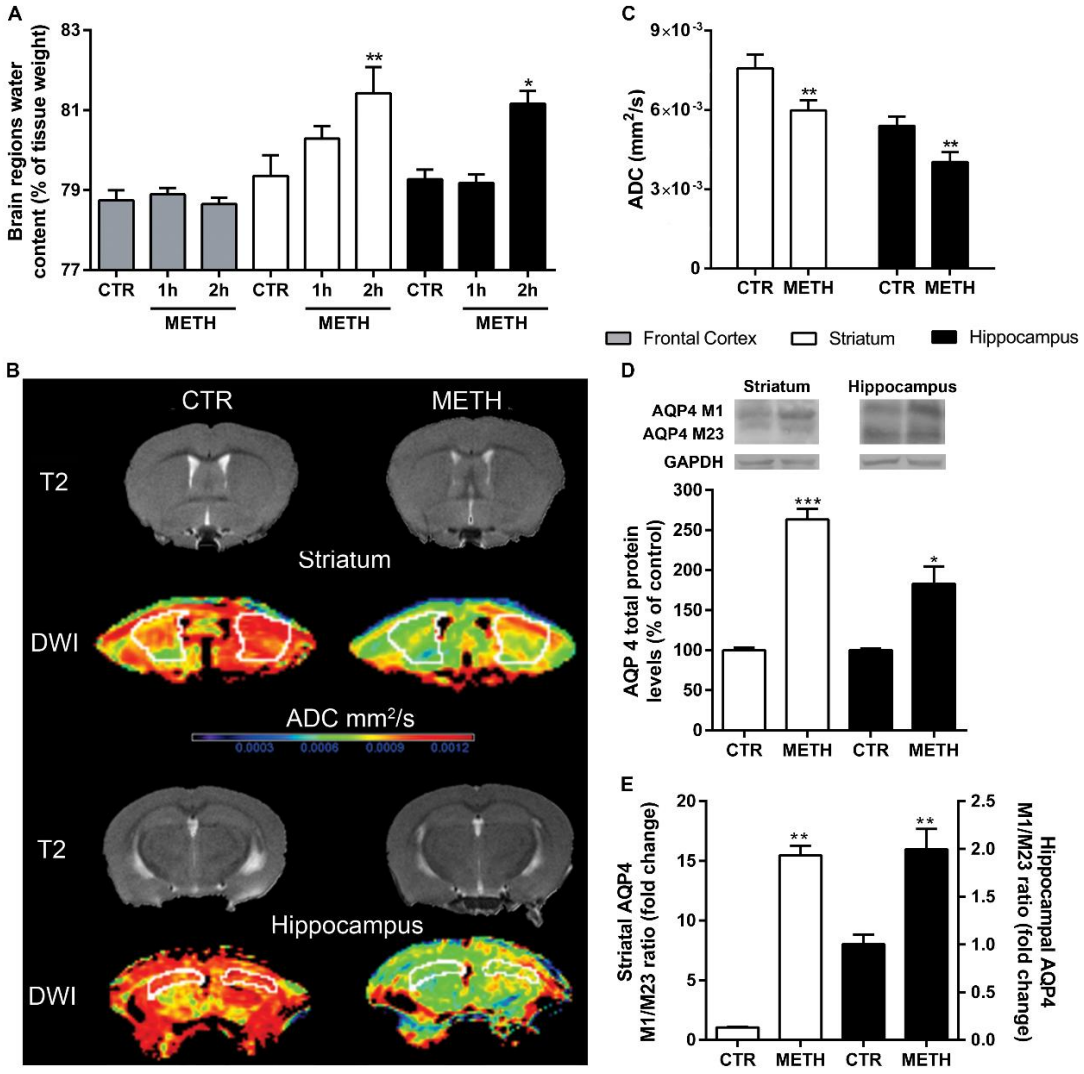

Figure 3.1. METH causes cytotoxic edema in the mice striatum and hippocampus with AQP4 upregulation. Mice were administered with METH (4× 10 mg/kg, i.p., 2h apart) and sacrificed 1 or 2h after the last injection. **(A)** METH increased brain water content in both striatum and hippocampus, specifically at 2h after drug administration, without any effect on the pre-frontal cortex water content. Results are expressed as mean % tissue weight + S.E.M., n=4-9, *P<0.05, **P<0.01 significantly different when compared to the control (CTR) within the same brain region, using one-way ANOVA followed by Bonferroni's multiple comparison test. **(B)** Representative anatomical (T2) and water content (DWI) images of both striatum and hippocampus before and after METH administration. **(C)** ADC values were decreased in both striatum and hippocampus pointing to a cytotoxic brain edema. Results are expressed as mean mm^2/s + S.E.M., n=9, **P<0.01 significantly different when compared to the control (CTR) within the same brain region, using Wilcoxon matched-pairs test. Both **(D)** AQP4 total protein levels and **(E)** M1/M23 ratio were increased by METH in the brain regions analyzed. Above the bars, representative western blot images of AQP4 (M1, 34 kDa; M23, 32 kDa) and GAPDH (37 kDa) are shown. Results are expressed as mean % of control + S.E.M., n=7–11; *P<0.05, **P<0.01, ***P<0.001 significantly different when compared to the control (CTR) within the same brain region, using Mann-Whitney test.

3.4.2. AQP4 Inhibition Protects against METH-Induced Brain Alterations

To determine the involvement of AQP4 in METH-induced brain edema, we measured the water content, as described in **Figure 3.1A**, but now in the presence of a novel AQP4 inhibitor, TGN-020 (TGN) (Igarashi et al., 2011). The blockade of this water channel, per se, did not interfere with the water content of the brain regions analyzed (**Figure 3.2A**). However, TGN was able to prevent all the effects induced by METH, specifically the water accumulation (**Figure 3.2A**; $^{###}P<0.001$ and $^{##}P<0.01$ vs METH in the striatum and hippocampus, respectively), upregulation of total AQP4 protein levels (**Figure 3.2B**; $^{###}P<0.001$ and $^{##}P<0.01$ vs METH in the striatum and hippocampus, respectively), and M1/M23 isoforms ratio (**Figure 3.2C**; $^{###}P<0.001$ vs the respective METH condition).

Additionally, we also aimed to clarify if the inhibition of AQP4, and consequently the prevention of brain edema, was capable of preventing BBB disruption triggered by METH. Interestingly, we showed that TGN also inhibited METH-induced striatal and hippocampal BBB disruption (**Figure 3.3**). In detail, TGN blocked the increase of albumin immunolabeling (**Figure 3.3A**; in red) induced by METH. These observations were confirmed by western blot analyses since METH was able to increase albumin protein levels (**Figure 3.3B**; **P<0.01 vs CTR within the same regions) and TNG once again prevented this upregulation ($^{##}P<0.01$ and $^{###}P<0.001$ vs METH in the striatum and hippocampus, respectively). Moreover, the structure of brain vessels was investigated by analyzing the major component of the basement membrane, collagen IV. We observed that METH triggered a downregulation of collagen IV immunostaining (**Figure 3.3A**; in green) together with an increase of albumin (**Figure 3.3A**; in red) in both the striatum and hippocampus. TGN was able to completely prevent collagen IV alterations and BBB disruption, as shown by the complete absence of albumin in the tissue (**Figure 3.3A**) and by its quantification (**Figure 3.3B**). Overall, these results allow us to conclude that the

blockade of AQP4 was able to maintain the physical support of brain microvasculature and consequently to avoid BBB disruption.

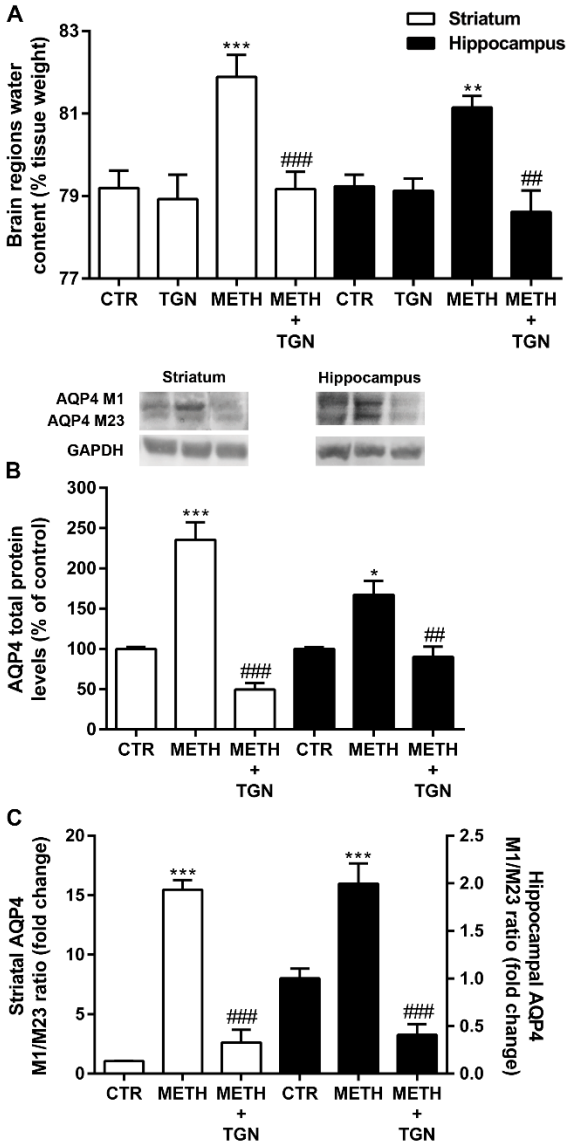

Figure 3.2. METH interferes with water homeostasis in the mice striatum and hippocampus. Animals were administered with METH alone, or co-administrated with an AQP4 specific inhibitor, TGN-020 (TGN; 200 mg/kg, i.p., 1h before the first METH injection), and sacrificed 2h after the last METH injection (4× 10 mg/kg, i.p., 2h apart). **(A)** The inhibition of AQP4 channels by TGN prevented the METH-induced edema in both brain regions analyzed. Results are expressed as mean % tissue weight + S.E.M., n=4–8. METH also increased the **(B)** total AQP4 protein levels and **(C)** M1/M23 ratio in the striatum and hippocampus, which were completely abolished by TGN. Above the bars, representative western blot images of AQP4 (M1, 34 kDa; M23, 32 kDa) and GAPDH (37 kDa) are shown. Results are expressed as mean + S.E.M., n=6–11. *P<0.05, **P<0.01, ***P<0.001 significantly different when compared to the control (CTR) within the same brain region; $^{\#\#}$P<0.01, $^{\#\#\#}$P<0.001 when compared with METH within the same brain region, using one-way ANOVA followed by Bonferroni's multiple comparison test

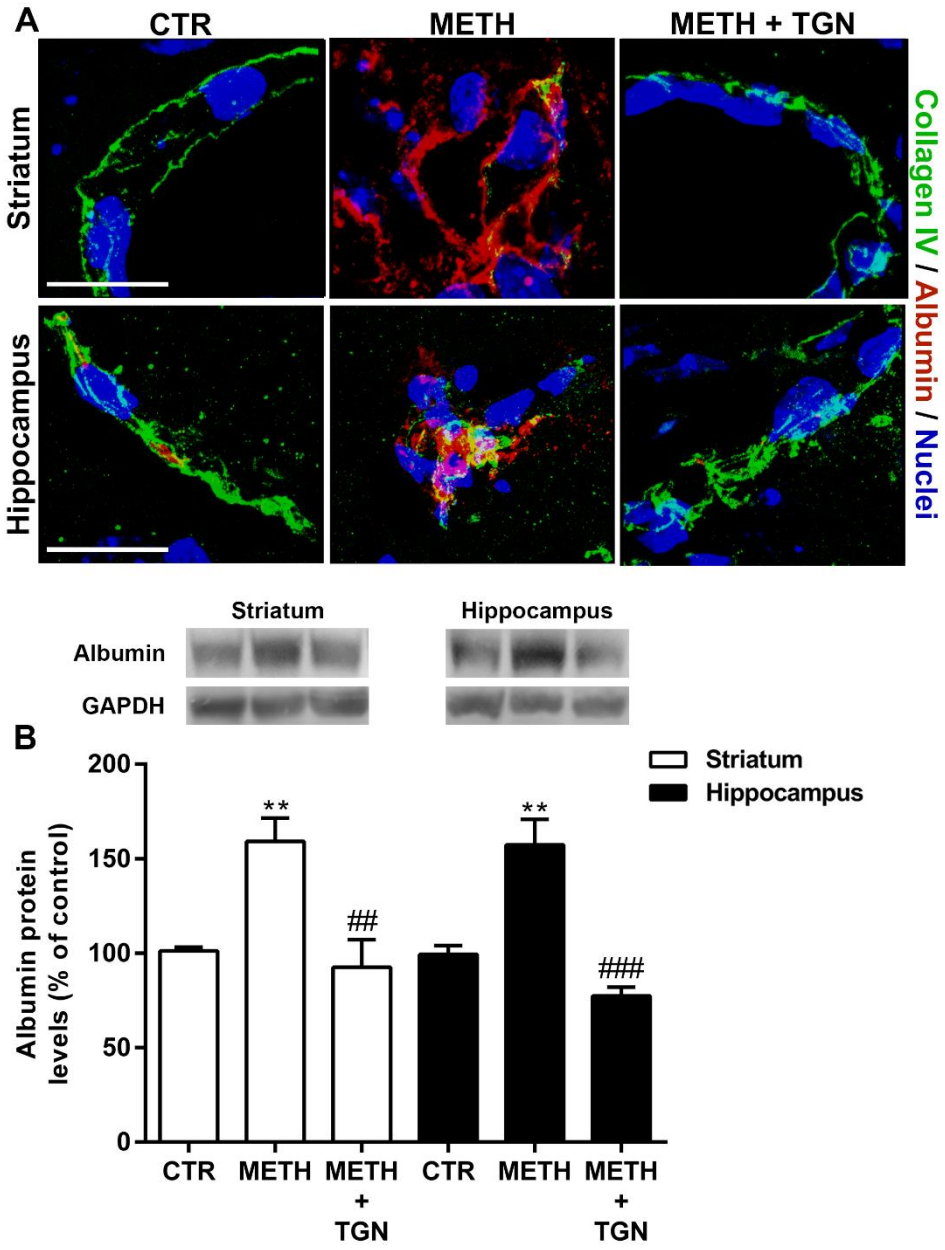

Figure 3.3. METH induces BBB disruption in the mice striatum and hippocampus. Mice were administered with METH alone (4× 10 mg/kg, i.p., 2h apart), or co-administrated with TGN-020 (200 mg/kg, i.p., 1h before the first METH injection; TGN), and sacrificed 2h after the last METH injection. **(A)** Representative images of collagen IV (green) and albumin (red) show that METH decreased and increased the immunoreactivity, respectively. Moreover, blockade of AQP4 prevented the METH effects. Total brain sections were also stained with Hoechst 33342 (blue). Scale bars = 20 μm. **(B)** METH significantly increased albumin protein levels in both striatum and hippocampus. Above the bars, representative western blot images of albumin (66 kDa) and GAPDH (37 kDa) are shown. Results are expressed as mean % of control + S.E.M., n=5. **P<0.01 significantly different when compared to the control (CTR) within the same brain region; ##P<0.01, ###P<0.001 significantly different when compared to METH within the same brain region using one-way ANOVA followed by Bonferroni's multiple comparison test

3.4.3. Behavioral Changes Triggered by METH

It has been described that METH causes behavior abnormalities, but the role of brain edema or/and BBB disruption on these alterations has never been addressed before. Thus, we performed behavioral tests to evaluate the impact of METH on mice mobility and motivation, as well as the involvement of AQP4 in such effects (**Figure 3.4**). Using the open field test, we found that METH-administrated animals showed a decrease in both total distance traveled (**Figure 3.4A**; ***P<0.001 vs CTR) and rearings (**Figure 3.4B**; ***P<0.001 vs CTR), suggesting that drug causes locomotor and exploratory impairment. Additionally, these behavioral changes were not prevented by TGN (**Figures 3.4A and 3.4C**; ***P<0.001 vs CTR). To better clarify the possible motor alterations triggered by METH, we further performed the rotarod test and observed that this drug impaired coordination since there was a significant decrease in the latency to fall (**Figure 3.4D**; ***P<0.001 vs CTR). Curiously, mice observation led us to hypothesized that METH could interfere with animal self-care and motivational behavior. Thus, by using the splash test, we demonstrated that METH decreased mice grooming, a form of motivational behavior considered to be parallel with some symptoms of depression such as apathy (**Figure 3.4E**; ***P<0.001 vs CTR). Noteworthy, in both rotarod and splash tests, TGN was able to diminish METH-induced behavioral impairment (**P<0.01 vs CTR; $^{\#\#}$P<0.01 vs METH).

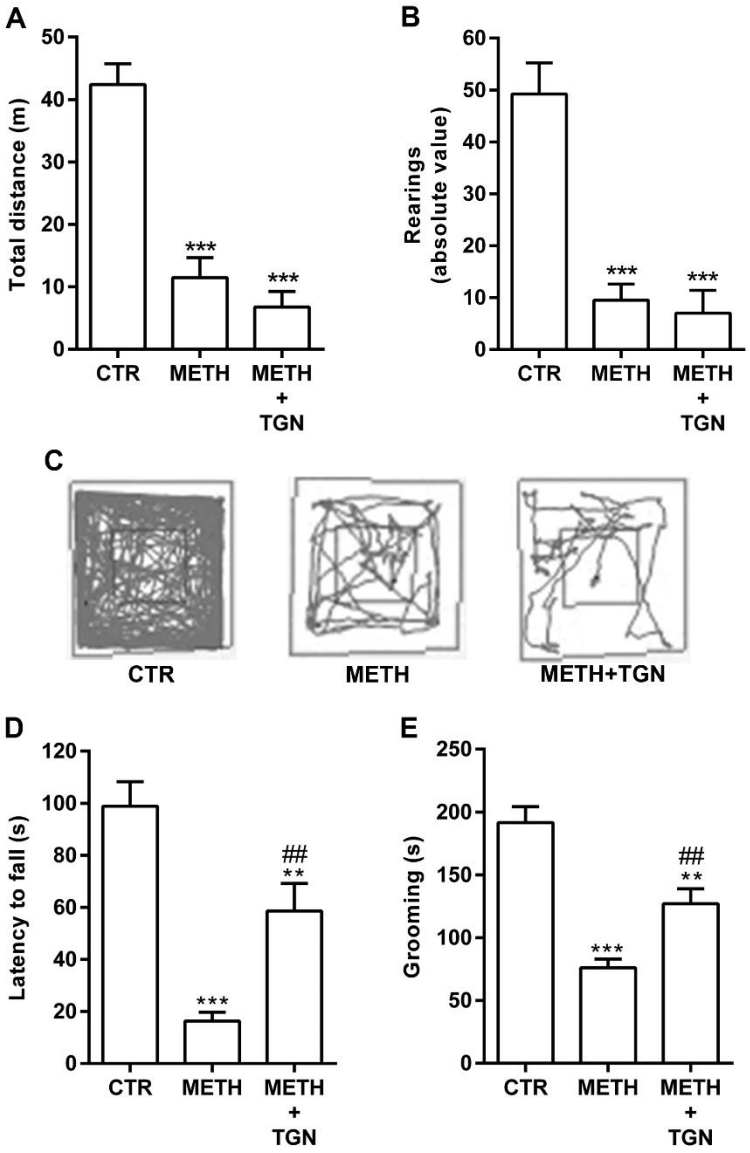

Figure 3.4. METH causes significant alterations in mice behavior. Mice were administered with METH alone (4× 10 mg/kg, i.p., 2h apart), or co-administrated with TGN-020 (200 mg/kg, i.p., 1h before the first METH injection; TGN), and **(A-C)** open field, **(D)** rotarod, and **(E)** splash tests were performed 2h after the last injection. METH impaired voluntary locomotion and exploratory behavior since mice showed a decreased in the **(A, C)** distance traveled and **(B)** rearings. **(C)** Representative track plot representing the path traveled by animals in the different groups. The inhibition of AQP4 by TGN did not prevent the drug-induced animal behavior. Additionally, METH caused a significant impairment in **(D)** motor coordination and **(E)** self-caring/motivational behavior. Interestingly, here, TGN was able to diminish both negative effect of METH on the latency to fall and grooming. The results are expressed as mean + S.E.M., n=6–9, **P<0.01, ***P<0.001 significantly different when compared to control (CTR), using one-way ANOVA followed by Dunnet's multiple comparison test, and $^{\#\#}$P<0.01 significantly different when compared to METH using one-way ANOVA followed by Bonferroni's multiple comparison test

3.4.4. Specific Role of AQP4 in METH-Induced Alterations of Astrocytes

Despite all the strength given by the animal studies abovementioned, we also aimed to clarify the specific involvement of astrocytes, since AQP4 is expressed mainly by these cells. Different in vitro models have been used to study AQP4 properties and function, such as Xenopus laevis oocytes (Assentoft et al., 2013), astrocyte cell lines (Smith et al., 2014), or astrocytes primary cultures (Coelho-Santos et al., Howe et al., 2014). Since the first two models do not endogenously express this water channel protein, we decided to use the primary cultures to dissect the specific role played by AQP4 (Howe et al., 2014; Coelho-Santos et al. 2015) under METH exposure, and so to complement the animal studies. Additionally, a concentration of METH (250 μM) that did not cause cell death (**Figure 3.5**) was used in the present study. Importantly, the METH concentration used is in accordance with previous in vitro studies (Abdul Muneer et al., 2011) and it is within the range of drug molar concentrations found in brain tissue of METH binge users (Rivière et al., 2000; Melega et al., 2007).

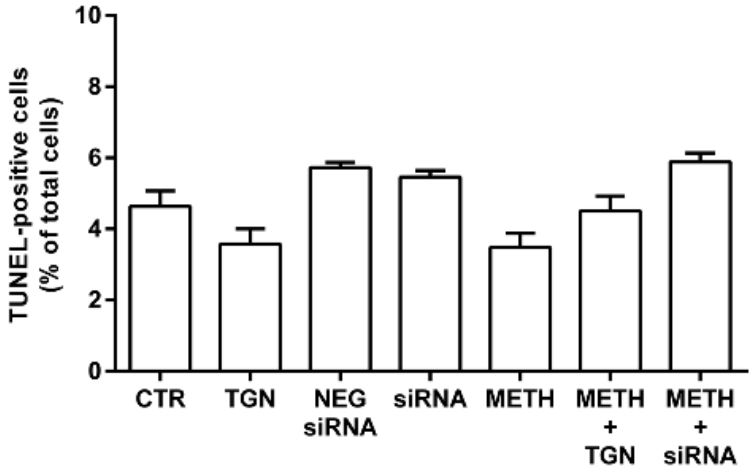

Figure 3.5. METH and AQP4 knockdown does not cause astrocyte cell death. Cells were treated during 24h with METH (250 μM) and/or TGN (25 μM), non-specific siRNA (Neg siRNA, 20 nM), AQP4 targeting siRNA (siRNA, 20 nM). Results are expressed as mean + S.E.M., n = 4.

It was possible to observe an upregulation of total AQP4 protein levels (**Figure 3.6A**; ***P<0.001 vs CTR), M1/M23 ratio (**Figure 3.6B**; ***P<0.001 vs CTR), and immunoreactivity (**Figures 3.6C and 3.6D**; **P<0.01 vs CTR), in accordance with our previous findings in mice. Interestingly, METH effects in astrocytes were completely prevented by a pharmacological blockade of AQP4 ($^{\#}$P<0.05 and $^{\#\#\#}$P<0.001 vs METH), as well as by its highly efficient knockdown (**Figure 3.7**) with small-interfering ribonucleic acid targeting AQP4 (siRNA; $^{\#\#\#}$P<0.001 vs METH). Moreover, we investigated the AQP4 cellular distribution and astrocytic morphology alterations triggered by METH. There was a clear increase in AQP4 and membrane/cytoplasm ratio (**Figures 3.6E and 3.6F**; ***P<0.001 vs CTR) that was prevented by TGN (**Figures 3.6D and 3.6E**; $^{\#\#\#}$P<0.001 vs METH). This ratio gives us indications about the cellular distribution of AQP4, and so we can conclude that there was a shift from cytoplasmic localization to the membrane after METH exposure (**Figures 3.6E and 3.6F**).

.

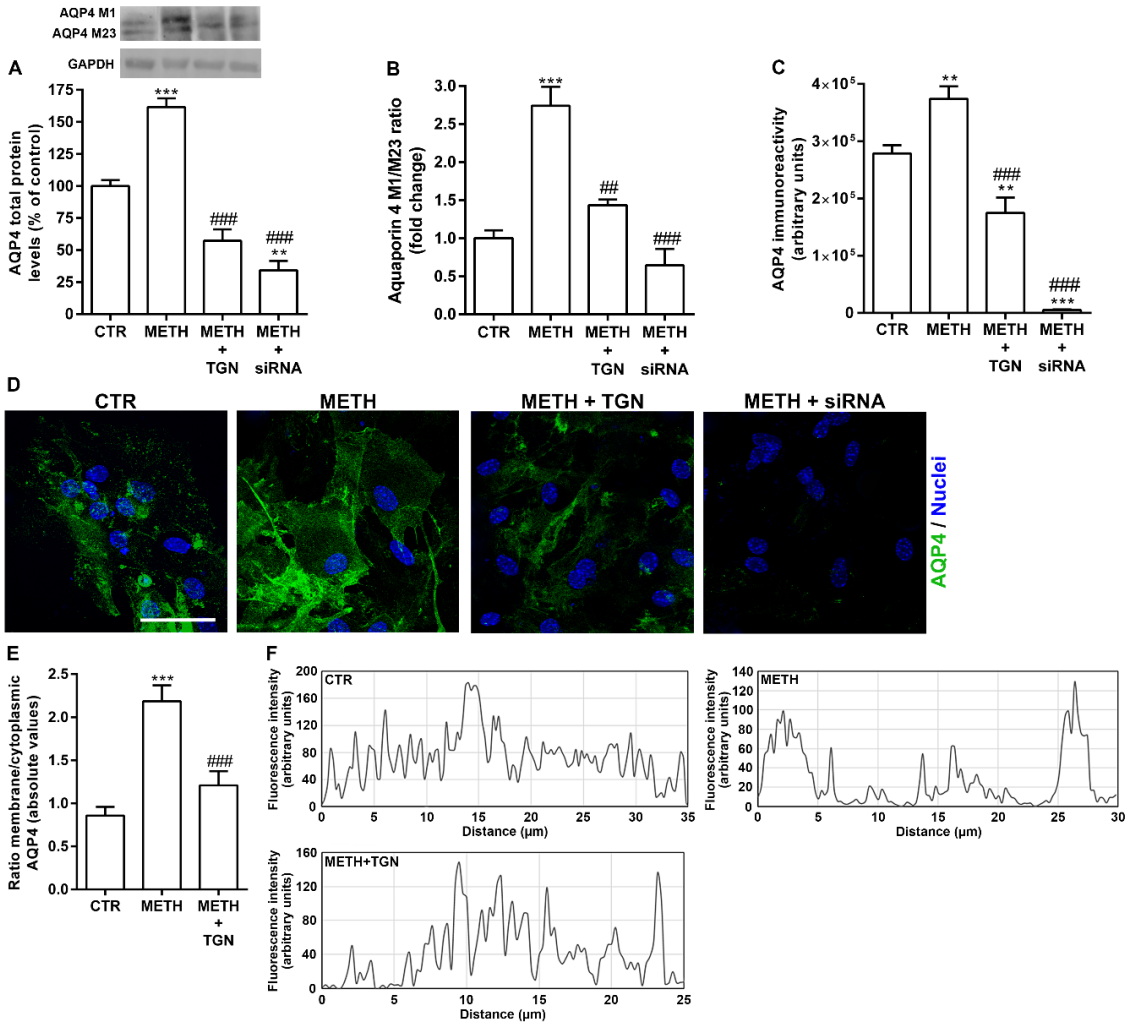

Figure 3.6. METH upregulates AQP4 expression in astrocytes. Primary cultures of mouse cortical astrocytes were exposed to 250 µM METH during 24h alone or together with TGN (25 µM, 30 min before METH exposure) or siRNA (20 nM, for 4 days before METH exposure). METH increased both **(A)** AQP4 protein total levels and **(B)** M1/M23 isoform ratio, which were prevented by pharmacological inhibition of AQP4 (TGN) and its knockdown (siRNA). Above the bars, representative western blot images of AQP4 (M1, 34 kDa; M23, 32 kDa) and GAPDH (37 kDa) are shown. Results are expressed as mean % of control + S.E.M., n=6. **(C)** In accordance, quantification of AQP4 immunoreactivity proved that METH increased its expression, which was prevented by TGN and protein knockdown. **(D)** Representative images of AQP4 (green) showing that METH increased AQP4 staining. Moreover, pharmacological inhibition and knockdown of AQP4 prevented the METH effects. Cell nuclei were also stained with Hoechst 33342 (blue). Scale bars = 20 µm. **(E)** Quantification of AQP4 membrane/cytoplasm ratio, where we observed once again a protective role of TGN against METH effects. **(F)** Representative track plots from AQP4 cellular distribution showing a switch in membrane/cytoplasm ratio from widespread in astrocytes to an accumulation on cell membrane boundaries. Results are expressed as mean + S.E.M., n=15. **P<0.01, ***P<0.001 significantly different when compared to the control (CTR); ##P<0.01, ###P<0.001 significantly different when compared to METH using one-way ANOVA followed by Bonferroni's multiple comparison test.

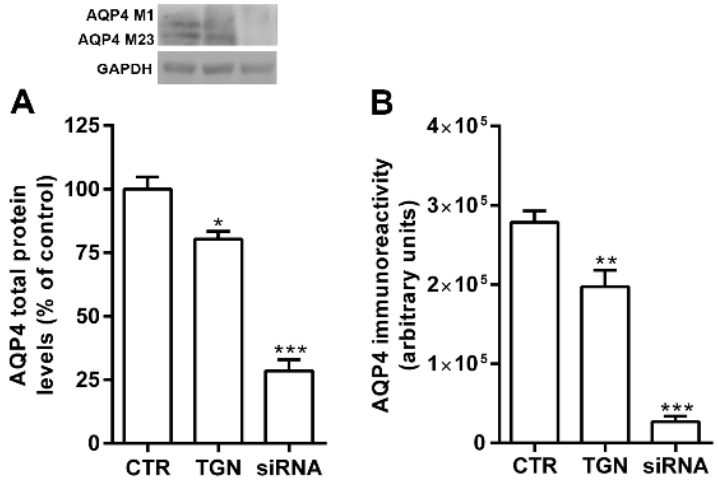

Figure 3.7. Pharmacological inhibition and knockdown of AQP4 cause a downregulation of its protein levels. Primary cultures of mouse cortical astrocytes were exposed to TGN (25 μM for 24h) or AQP4 targeting siRNA (20 nM for 4 days, siRNA). After the appropriate treatments, we observed a significant decrease in AQP4 **(A)** protein levels, by western blot analysis, and **(B)** immunoreactivity. Above the bars, representative western blot images of AQP4 (M1, 34 kDa; M23, 32 kDa) and GAPDH (37 kDa) are shown. Results are expressed as mean + S.E.M., n=4 for western blot, and n=15 for immunocytochemistry. *P<0.05, **P<0.01, ***P<0.001 significantly different when compared to the control (CTR) using one-way ANOVA followed by Dunnet's Multiple comparison test.

Morphological changes in astrocytes were also evaluated, and although METH had no effect on GFAP protein levels (**Figure 3.8**), it promoted astrocytic processes with an increase in the number (**Figures 3.9A and 3.9D**; **P<0.01 vs CTR) and the total length of cellular processes (**Figures 3.9B and 3.9D**; *P<0.05 vs CTR). Taking into consideration the morphological changes of astrocytes together with AQP4 upregulation, we hypothesized that METH could lead to cell swelling. In fact, this hypothesis was confirmed by showing that METH increased calcein fluorescence (**Figure 3.9C**; ***P<0.001 vs CTR). Once again, TGN and AQP4 knockdown were able to prevent METH-induced alterations in astrocytes ($^{\#}$P<0.05, $^{\#\#}$P<0.01, $^{\#\#\#}$P<0.001 vs METH). As controls, neither TGN nor siRNA interfere with astrocytic morphology (**Figure 3.10**), whereas siRNA targeting AQP4

or TGN decreased the cell volume confirming the specific role of AQP4 in water homeostasis (**Figure 3.11**).

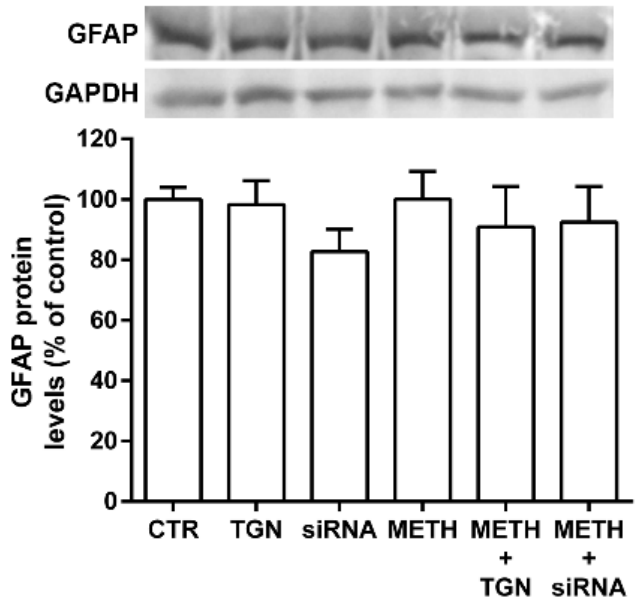

Figure 3.8. METH does not interfere with GFAP protein levels. No significant alterations were observed regarding the GFAP protein levels at 24h after the different treatments, as follows: 25 μM TGN, 20 nM AQP4 targeting siRNA (siRNA), 250 μM METH. Above the bars, representative western blot images of GFAP (50 kDa) and GAPDH (37 kDa) are shown. Results are expressed as mean + S.E.M., n=4.

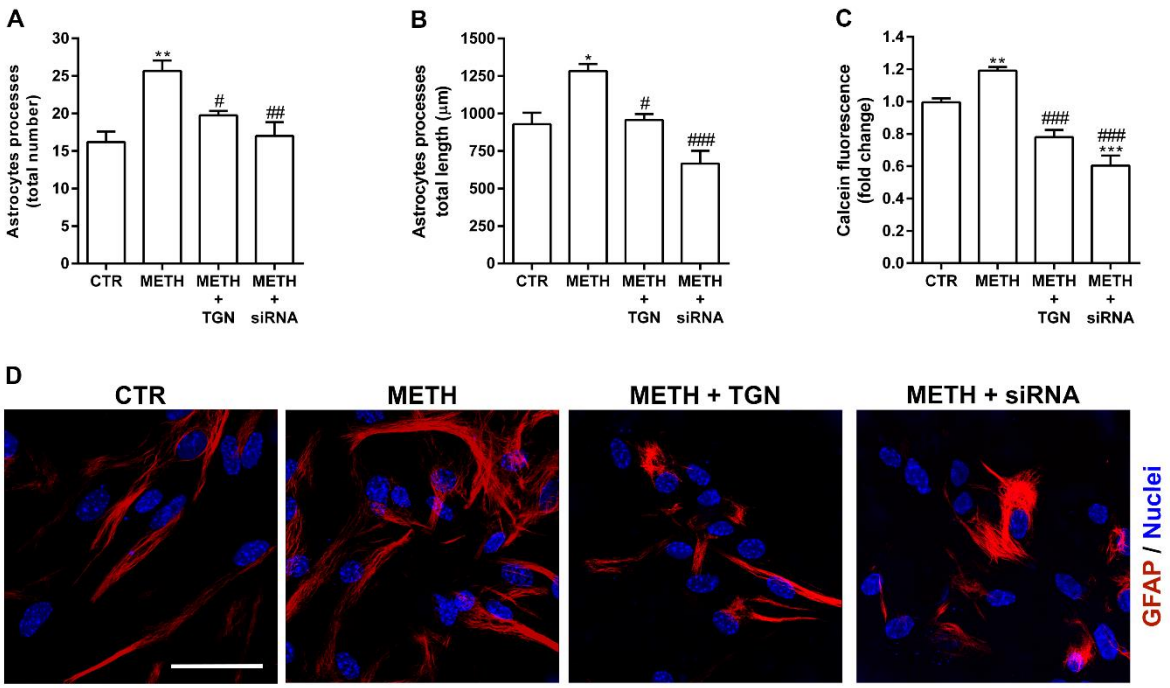

Figure 3.9. AQP4 mediates METH-induced astrocytic morphological alterations. Primary cultures of astrocytes were exposed to 250 µM METH during 24h alone or together with TGN (25 µM, 30 min before METH exposure) or siRNA (20 nM, for 4 days before METH exposure). Morphological alterations in astrocytes were analyzed in detailed by the quantification of **(A)** total number and **(B)** total length of cell processes. Results are expressed as mean + S.E.M., n=15. **(C)** Cell swelling triggered by METH was also observed by calcein fluorescence quantification. All the morphological alteration induced by the drug was prevented by both AQP4 pharmacological blockade (TGN) and knockdown (siRNA). Results are expressed as mean fold change + S.E.M., n=4–8. *P<0.05, **P<0.01, ***P<0.001 significantly different when compared to the control (CTR); $^{\#}$P<0.05, $^{\#\#}$P<0.01, $^{\#\#\#}$P<0.001 significantly different when compared to METH using one-way ANOVA followed by Bonferroni's multiple comparison test. **(D)** Representative images of GFAP (red) showing that METH does not interfere with GFAP immunoreactivity. Cell nuclei were also stained with Hoechst 33342 (blue). Scale bars = 20 µm.

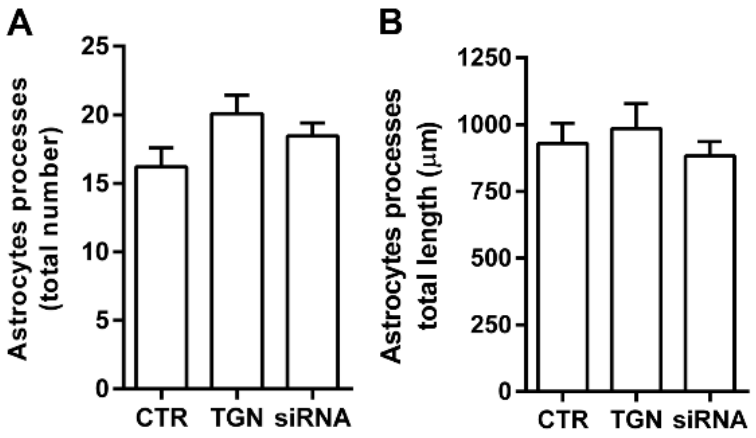

Figure 3.10. AQP4 inhibition or knockdown does not cause astrocytic morphological alterations. After the appropriate treatments [TGN (25 μM for 24h) or AQP4 targeting siRNA (20 nM for 4 days, siRNA)] we did not observe any alterations in astrocytes processes **(A)** total number or in **(B)** total length. Results are expressed as mean + S.E.M., n=15.

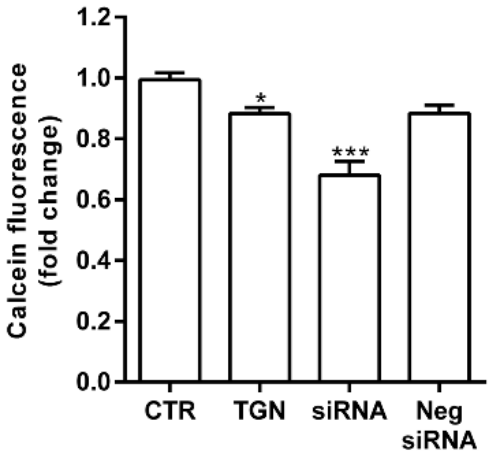

Figure 3.11. Both AQP4 inhibition and silencing decrease cell volume. AQP4 inhibition, by using TGN (25 μM for 24h) or AQP4 knockdown siRNA (20 nM for 4 days, siRNA) silencing methodology, caused a significant reduction in astrocyte cell volume. On the other hand, the Neg siRNA (20 nM non-specific siRNA) did not interfere with the cell size. Results are expressed as mean + S.E.M., n = 10. *P<0.05, ***P<0.001 significantly different when compared to the control using one-way ANOVA followed by Dunnet's Multiple comparison test.

3.4.5. METH Induces Astrocytic Swelling via Oxidative Stress

Oxidative stress is one of the most documented deleterious effects of METH exposure (Toborek et al., 2013; Leitão et al., 2016). Thus, we hypothesized whether reactive oxygen species (ROS) would have a role in cell swelling induced by METH. In fact, we found that METH exposure during 4h significantly increased ROS production (**Figure 3.12A**; ***P<0.001 vs CTR), which was prevented by TGN (25 μM) or vitamin C (200 μM; VitC) (**Figure 3.12A**; ###P<0.001 vs METH). Also, the antioxidant approach by using VitC was able to block the swelling induced by METH (**Figure 3.12B**; ###P<0.001 vs METH). Curiously, VitC even reduced calcein fluorescence to a lower level than control proving that basal levels of ROS play also a role in cell morphology (**Figure 3.12B**; ***P<0.001 vs CTR). In order to confirm the antioxidant effect of TGN and VitC, we treated astrocytes with 500 μM H_2O_2 for 4h and observed that both treatments prevented the ROS production induced by oxygen peroxide (**Figure 3.13**). Moreover, when we looked at AQP4 protein levels, we concluded that once again, the antioxidant prevented the upregulation of AQP4 (**Figure 3.12C**; ###P<0.001 vs METH) and the increase of M1/M23 ratio induced by METH (**Figure 3.12D**; ###P<0.001 vs METH).

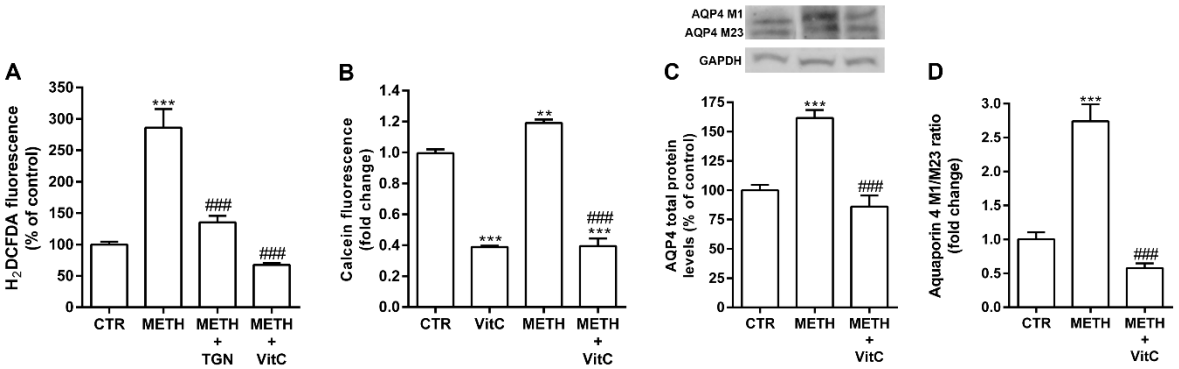

Figure 3.12. Reactive oxygen species are involved in METH-induced astrocytic cell swelling. **(A)** Primary cultures of astrocytes were treated with 250 μM METH alone or together with TGN (25 μM, 30 min before METH exposure) or vitamin C (200 μM, 30 min before METH incubation; VitC) during 4h. The significant increase in reactive oxygen species (ROS) formation triggered by METH was prevented by both TGN and VitC. Results are expressed as mean % of control + S.E.M., n=18. **(B)** Calcein quenching method was used to confirm the protective effect of VitC against cell volume

increase after 24h of METH exposure. Results are expressed as mean fold change + S.E.M., n=10. Moreover, METH-increased **(C)** AQP4 protein total levels and **(D)** M1/M23 isoform ratio were prevented by antioxidant treatment with VitC. Above the bars, representative western blot images of AQP4 (M1, 34 kDa; M23, 32 kDa) and GAPDH (37 kDa) are shown. Results are expressed as mean % of control + S.E.M., n=4. **P<0.01, ***P<0.001, significantly different when compared to the control (CTR); ###P<0.001 significantly different when compared to METH condition using one-way ANOVA followed by Bonferroni's multiple comparison test.

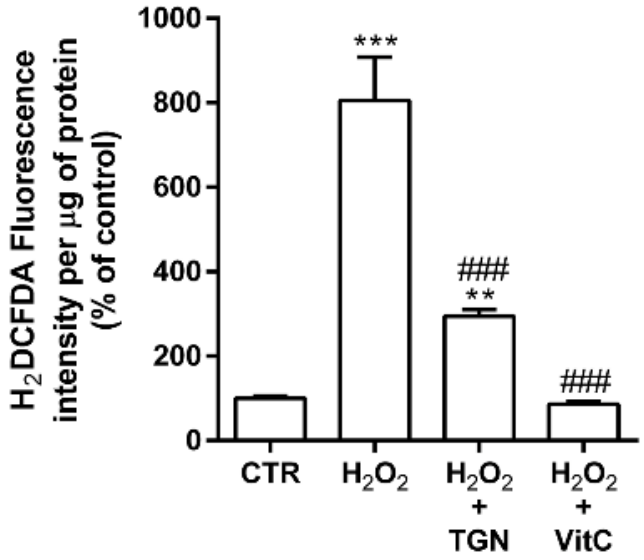

Figure 3.13. Both TGN and VitC are able to prevent the increase of ROS triggered by oxygen peroxide. Primary cultures of astrocytes were treated with 500 μM oxygen peroxide (H_2O_2) for 4h alone or together with TGN (25 μM) or vitamin C (200 μM; VitC). Here we show that TGN plays a similar role than the well-known antioxidant VitC. Results are expressed as mean % of control + S.E.M., n=10. **P<0.01, ***P<0.001, significantly different when compared to the control (CTR); ###P<0.001 significantly different when compared to METH using one-way ANOVA followed by Bonferroni's Multiple comparison test.

3.5. Discussion

Brain edema is a deleterious neuropathological condition that leads to severe disabilities and ultimately to death. Moreover, it is originated by several factors such as stroke (Chen et al., 2014), traumatic brain injury (Naderi et al., 2015), and substance abuse (Wang et al., 2014). In fact, it was demonstrated that a single dose of METH causes edema in the cortex, hippocampus, and hypothalamus (Sharma and Kiyatkin, 2009). However, nothing is known about the effects of a binge drug paradigm, which better mimics METH pharmacokinetic of smoked and intravenous route used by human abusers (Krasnova and Cadet, 2009). Also, the underlying mechanisms responsible for such edema formation were never addressed before. Herein, we describe for the first time that METH triggers brain edema formation, specifically in the striatum and hippocampus, due to alterations in the water channel AQP4. In addition, BBB dysfunction and behavioral alterations were also identified, and the blockade of AQP4 was able to prevent, or at least to diminish, the negative impact of METH. Since AQP4 is mainly expressed by astrocytes, we also investigated the impact of METH on these cells concluding that AQP4 was responsible for drug-induced astrocytic alterations.

Brain edema can be divided into two main groups: vasogenic and cytotoxic (Tait et al., 2008). Vasogenic edema occurs due to vascular leakage and it has been shown that AQP4 knockout mice have a worse outcome after edema induction by infusion of normal saline into brain parenchyma or under a condition of brain tumor (Tait et al., 2008). In the cytotoxic edema, BBB often maintains its integrity and AQP4 knockout mice do not develop brain edema under a condition of water intoxication or focal cerebral ischemia (Tait et al., 2008). Currently, MRI with ADC calculations is the only technique that allows a discrimination between vasogenic and cytotoxic edema. Thus, higher ADC values correspond to more water molecules freely moving in the extracellular space, which occurs in the vasogenic edema. On the contrary, lower ADC values indicate a cytotoxic edema characterized by the limited movements of water molecules due to cell swelling (Barzó et

al., 1997; Marmarou et al., 2006). Our results point to a cytotoxic edema at 2h post-after METH administration in both the striatum and hippocampus. Accordingly, we did not observe significant changes in the volume of brain regions analyzed, which characterize this type of edema. Also, the higher susceptibility of these regions is in accordance with other works showing that the striatum (**Chapter 2**; Coelho-Santos et al., 2015) and hippocampus (Martins et al., 2011) exhibit BBB disruption after a binge administration or single high dose of METH, respectively. In fact, several studies have demonstrated that the hippocampus (Nakajima et al., 2004; Martins et al., 2011) and striatum (Nakajima et al., 2004) can be negatively modulated by METH whereas pre-frontal cortex remained unaltered. Moreover, striatum is well known for a long time as one of the most affected brain regions by METH (Krasnova and Cadet, 2009; Grace et al., 2010; Urrutia et al., 2013; Silva et al., 2014), and the hippocampus is highly involved in depressive-like behaviors (MacQueen and Frodl, 2011) and cognitive functions (Gonçalves et al., 2012) that are two important features of METH abuse. Nevertheless, future studies are needed to better clarify the differences between brain regions.

Upregulation of AQP4 expression was described in human METH abusers (Wang et al., 2014), but a possible link with edema formation was overlooked. Our study demonstrated an increase in both total AQP4 protein levels and M1/M23 ratio together with a decrease in ADC values, which points to a dysfunction in water homeostasis and consequently a cytotoxic edema. Accordingly, others showed that transient middle cerebral artery occlusion decreased ADC values together with an upregulation of AQP4 levels (He et al., 2014). Since METH-induced AQP4 system impairment, we further aimed to understand the role of this channel. Recently, TGN was raised as an AQP4-specific inhibitor and able to prevent brain edema formation post-ischemia (Igarashi et al., 2011). Despite the lack of published studies with rodent models exposed to TGN alone, there are several papers demonstrating that AQP4 knockout animals do not show any differences when compared to wild-type animals regarding neurological, brain water content, BBB properties, nerve cell death, and pericapillary astrocyte foot process area (Tang et al., 2010). Accordingly,

we observed that TGN alone did not interfere with water content whereas it prevented brain edema induced by METH in the mice striatum and hippocampus. In fact, using primary cultures treated with METH and TGN or AQP4 siRNA, we were able to prove that drug-induced cell alterations were prevented by both pharmacological blockade of AQP4 and gene silencing. At the same time, the increase in AQP4 membrane/cytoplasm ratio demonstrated that AQP4 upregulation occurs on cellular membrane leading to an augmentation of water transport in astrocytes. Accordingly, it was previously shown that a specific AQP4 upregulation in cell membrane domain is responsible for the astrocyte volume increase (Rao et al., 2010). Additionally, it is well known that cellular swelling induces astrocytic morphology alterations (Wang et al., 2016). In fact, METH-exposed astrocytes showed a spreading in both processes number and length, as previously shown under conditions of ischemia (Yang et al, 2011), demyelination (Tourdias et al., 2009), and intracranial hypertension (Eide et al., 2016), where astrocytic hypertrophy is lastingly associated with AQP4 upregulation (Tourdias et al., 2009; Yang et al, 2011; Eide et al., 2016) and water homeostasis dysfunction (Tourdias et al., 2009). Interestingly, we were able to prevent deleterious METH-induced astrocytic alterations by direct AQP4 inhibition and so controlling the water homeostasis dysfunction observed under drug exposure.

Since TGN is formulated by conjugation of two well-known anti-inflammatory and antioxidant chemical groups, nicotinamide and thiadiazole (Burnett et al., 2015), we hypothesized that oxidative stress may have a role in controlling AQP4 protein expression and cell swelling induced by METH. In fact, Jayakumar and colleagues (Jayakumar et al., 2006) already demonstrated astrocytic cell volume reduction after treatment with several antioxidants. Herein, we demonstrated that METH promotes the release of ROS by astrocytes and VitC has a protective role on cell alterations. Importantly, oxidative stress also activates a key transcription factor for inflammatory response, NF-κB pathway, which is a putative transcription factor for the AQP4 gene (Hsu et al., 2015). In fact, it has been already shown that NF-κB pathway is responsible for AQP4 upregulation under intracerebral hemorrhage (Wang et al., 2015) or inflammatory processes (Ito et al., 2006).

Also, we have previously demonstrated that the same METH regimen used in the present study (binge protocol) activates the NF-κB signaling pathway culminating in BBB disruption (**Chapter 2**; Coelho-Santos et al., 2015).

It is known that METH induces BBB hyperpermeability (**Chapter 2**; Martins et al., 2011; Coelho-Santos et al., 2015; Northrop and Yamamoto, 2015) and brain edema (Sharma and Kiyatkin, 2009; Wang et al., 2014). However, it was unclear whether there is a link between both phenomena under conditions of METH use. In accordance with our results, others showed that in animal models of cerebral ischemia (Pillai et al., 2009; He et al., 2014) and Parkinson's disease (Wachter et al., 2012), brain edema occurred simultaneously with BBB impairment. Herein, we focused for the first time on the role of AQP4 and its correlation with edema formation and BBB disruption. Nevertheless, we have previously identified important key players responsible for METH-induced brain endothelial hyperpermeability, such as matrix metalloproteinase-9 (MMP9) (Martins et al., 2011), nitric oxide (Martins et al., 2013), and TNF-α (**Chapter 2**; Coelho-Santos et al., 2015). Additionally, Wang and collaborators (2014) showed a decrease in claudin-5 mRNA together with an increase in MMP9 and AQP4 mRNA levels in postmortem METH abusers brains. Organotypic hippocampal slice cultures treated with TNF-α also showed a huge increase in AQP4 mRNA levels (Zou et al., 2012). Thus, in the present study, we demonstrated that AQP4 inhibition prevented edema formation and BBB disruption under a condition of METH use. Such results are in accordance with previous studies, in which the AQP4 inhibition conferred protection from deleterious effects of water accumulation in cytotoxic edema conditions (Igarashi et al., 2011; Fukuda et al., 2013).

Even though the TGN protective effect strengthens the classification of cytotoxic edema, we have BBB disruption at the same time point. Noteworthy, there are studies showing the presence of both types of edema (Barzó et al., 1997), cytotoxic and vasogenic, in hypoxia/ischemia and metabolic imbalance models (Ho et al., 2012), as well as in a case report of schizophrenia (Koch et al., 2001). Other supporting data also demonstrated that cytotoxic edema appears first, followed by vasogenic edema (Lazovic et al., 2005), or both

can also occur at the same time (Dalle Lucca et al., 2012). In this work, the TGN protection against BBB breakdown was proved by assessing albumin protein levels in brain parenchyma (**Chapter 2**; Coelho-Santos et al., 2015) and collagen IV levels in brain vessels' structure. Nothing is known about the link between AQP4 and collagen, but it was described that downregulation of laminin, an important protein of basal membrane as collagen IV, leads to a disarrangement of AQP4 supramolecular structures causing an impairment in brain water homeostasis (Yao et al., 2014). Additionally, it has been demonstrated that MMP9 activity is responsible for laminin and collagen IV degradation observed in an ischemic animal model, resulting in BBB disruption (Copin et al., 2011). Here, we showed a decrease in collagen IV immunoreactivity, and Urrutia and collaborators (2013) published that METH binge induced a decrease in laminin levels at 1h after the post-last METH binge administration. Thus, we can hypothesize that the loss of collagen IV triggered by METH is associated with laminin downregulation, which can, in turn, lead to AQP4 system impairment. In fact, a decrease in laminin expression or its fiber disorganization causes a decrease in AQP4 protein levels (Hirrlinger et al., 2011) and an imbalance on water homeostasis (Menezes et al., 2014).

Besides cellular alterations triggered by METH, we also aimed to clarify if such edema formation and BBB disruption could lead to behavioral alterations. Previous works demonstrated that in different neuropathological conditions, such as ischemia or Parkinson's disease, brain edema is present together with locomotor impairment (Wachter et al., 2012; Zhong et al., 2013). Interestingly, AQP4 knockdown prevented brain edema, BBB disruption, and locomotor impairment in traumatic brain injured rats (Fukuda et al., 2013). Additionally, BBB disruption has been associated with anxiety-like behavior (Rapp et al., 2008), major depressive disorder (Najjar et al., 2013), and both locomotor and cognitive impairment (Tomkins et al., 2007; Rapp et al., 2008). Yet to date, nothing was known about the possible correlation between METH-induced brain edema or/and BBB dysfunction and behavior impairment. Here, we observed a clearly locomotor coordination impairment, as well as a depressive-like behavior induced by METH. In fact, a single high

dose of METH was able to cause cognitive impairment (Diaz-Ruiz et al., 2012; Gonçalves et al., 2012) and depressive-like behavior (Silva et al., 2014). Moreover, others showed that METH binge paradigm causes locomotor hypoactivity (Boger et al., 2007; Urrutia et al., 2013) and a depressive-like behavior (Joca et al., 2014). Despite these studies, for the first time, we showed that AQP4 inhibition not only prevented METH-induced brain edema and BBB disruption but also locomotor abnormalities and depressive-like behavior. The absence of AQP4 blockade effect on the open field test in contrast to the positive impact on rotarod can be explained as follows: the open field test reflects multiple underlying traits, including locomotor activity, exploratory activity, olfaction, and vision, as well as fear and anxiety, whereas rotarod specifically measure motor coordination and balance (Crawley, 2007). Also in the rotarod, the mice are forced to move which can overcome the lack of motivation that can highly interfere with the spontaneous activity measured in the open field. Thus, by using more specialized tests to analyzed both motor activity and motivation, we were able to improve animal performance by blocking the AQP4 water channel.

Overall, we concluded that METH interferes with AQP4 protein levels leading to brain edema, BBB disruption, and behavioral abnormalities. Moreover, astrocytic water accumulation triggered by this drug led to morphologic alterations. Thus, with the present work, we identify the water channel AQP4 as a new target involved in METH-induced brain alterations, which brings novel insights into the possible therapeutic targets in psychostimulants abuse/misuse.

CHAPTER 4

Protective effect of parthenolide against methamphetamine-induced neuroinflammation and neurogliovascular dysfunction

4.1. Abstract

Psychostimulants abuse is a worldwide concern as it causes long-term health complications with devastating consequences in the daily life of individuals and surrounded community. Among these drugs of abuse, methamphetamine (METH) is known to cause serious deleterious effects on the Central Nervous System. Herein, we aimed to clarify the possible involvement of neuroinflammation in BBB permeability and brain edema induced by METH, and to identify a new approach to counteract such negative effects. To address this issue, mice were administered with a binge regimen of METH (4× 10 mg/kg, i.p, 2h apart) and hippocampi were analyzed. We observed a neuroinflammatory response with microglial activation, astrocyte morphology alterations, and increased TNF-α protein levels. Additionally, brain edema and BBB disruption were identified through the quantification of brain water content and identification of albumin immunoreactivity in the brain parenchyma, respectively. Importantly, to uncover the signaling pathway beyond these METH effects, we neutralized the TNF-α receptor 1 (TNFR1) in astrocytes primary cultures using a monoclonal antibody, and so preventing the cell swelling induced by METH. Moreover, in an attempt to identify a protective approach against this drug-induced brain alterations, we further evaluated the effect of parthenolide (PTL), a molecule with anti-inflammatory properties present in feverfew plant extract. Interestingly, PTL prevented both neuroinflammatory processes and neurogliovascular dysfunction, as well as cell swelling triggered by METH. With this study, we provide new insights into our understanding of brain dysfunction induced by psychostimulants and suggest a new pharmacological approach to counteract such negative effects.

4.2. Introduction

Drug abuse has a major impact on society and economics. Among several drugs, METH is leading the global market of illegal synthetic drugs (UNODC, 2015), and despite the extensive characterization of METH effects (Silva et al., 2010; Gonçalves et al., 2014), several questions remain unanswered. More recently, the capability of METH to interfere with the BBB properties has been proposed as an important cause of several detrimental effects of this psychostimulant (Leitão et al., 2016). The BBB is the boundary that protects the brain parenchyma from fluctuations in the blood stream. Nevertheless, it is not a static structure but a highly dynamic interface with several transporters and receptors (Cardoso et al., 2010). Also, BBB has a proactive role on brain since endothelial cells are able to release many modulators, including proinflammatory cytokines, which will interfere with neural cells function (**Chapter 2**; Coelho-Santos et al., 2015).

Neuroinflammation has been recognized as one of the most deleterious effects of METH abuse, being responsible for causing neurodegeneration (Gonçalves et al., 2010), brain edema (Northrop and Yamamoto, 2012), and BBB hyperpermeability (**Chapter 2**; Coelho-Santos et al., 2015). The neuroinflammatory process is characterized by activation of glial cells (astrocytes and microglia), production and release of proinflammatory cytokines, such as interleukin (IL)-1β, IL-6, TNF-α, and peripheral immune cells infiltration into brain parenchyma (Sochocka et al., 2016). Recently, our group demonstrated that TNF-α was responsible for BBB disruption through the activation of the NF-κB pathway (**Chapter 2**; Coelho-Santos et al., 2015). TNF-α knockout mice also showed less motivation to METH self-administration (Yan et al., 2012), which reinforces the crucial role of this cytokine in the negative effects mediated by METH. Additionally, the manipulation of TNF-α, by using neutralizing antibodies, significantly protected the brain tissue from brain edema and BBB disruption observed after status epilepticus induction (Kim et al., 2012), acute liver failure (Wang et al., 2011), and ischemia (Hosomi et al., 2005). Importantly, there are two different TNF-α receptors, TNF-receptor 1 (TNFR1) and TNF-receptor 2 (TNFR2), and the

inhibition of TNFR1 confers protection against Alzheimer's disease (Montgomery and Bowers, 2012) and multiple sclerosis (Kassiotis and Kollias, 2001).

Despite the well-described effects of METH (Gonçalves et al., 2014; Leitão et al., 2016), there is still missing an effective pharmacological therapy for psychostimulants abuse/misuse. Interestingly, the market of plant extracts as prescribed drugs has been increasing in the last few years, with Europe representing approximately half of the global market with sales of several billion dollars per year. Moreover, the traditional Asian medical practice has also gained credibility worldwide. Particularly, parthenolide (PTL) is among the most used herbal extracts on this trendy medical practice. PTL is a sesquiterpene lactone obtained from feverfew (*Tanacetum parthenium*) that has been recently shown to have anti-cancer and anti-inflammatory properties (Mathema et al., 2012). Its anti-inflammatory characteristics seem to be linked to the inhibition of NF-κB pathway and consequently to the downregulation of TNF-α (Mathema et al., 2012).

Thereafter, with the present work, we aimed to investigate the PTL potentiality as a new therapeutic approach against noxious effects of METH, specifically the BBB dysfunction and edema formation.

4.3. Material and Methods

4.3.1. Animal Treatments

Male wild-type C57BL/6J mice (3-month-old; 24-26 g body weight; Charles River Laboratories, Barcelona, Spain) were housed under controlled environmental conditions (12h light:dark cycle, 24±1ºC) with food and water ad labium. Mice were divided into three different groups as follows: the control group received four intraperitoneal (i.p.) injections of 0.9% NaCl, 2h apart; METH binge group (4× 10 mg/kg, 2h apart, i.p.); the METH+PTL group received PTL (4× 1 mg/kg, i.p.) 30 min before each METH administration. The animals were sacrificed 2h after the last injection. Experiments were performed by certified researchers in accordance with European Community Council Directives (2010/63/EU) and Portuguese law for care and use of experimental animals (DL no. 113/2013). All efforts were made to minimize animal suffering and to reduce the number of animals used.

4.3.2. Western Blot Analysis

Western blot was performed as previously described (**Chapter 3**; Leitão et al., 2017). Primary antibodies were as follows: goat anti-albumin (1:20000, Bethyl Laboratories Inc., Montgomery, TX, USA); rabbit anti-TNF-α (1:100, Millipore, Darmstadt, Germany). Secondary antibodies were as follows: alkaline phosphatase-conjugated secondary antibody anti-rabbit (1:20,000), and anti-goat (1:10,000) (GE Healthcare Bio-Sciences, Pittsburgh, PA, USA). Immunoblots were reprobed with an antibody against glyceraldehyde 3-phosphate dehydrogenase (GAPDH) to ensure equal sample loading. Quantification of band density was performed using Image Studio (LI-COR Biosciences, Lincoln, NE, USA).

4.3.3. Evaluation of Hippocampal Edema

Tissue water accumulation was evaluated by comparing the hippocampal wet and dry weights, as previously described (**Chapter 3**; Leitão et al., 2017). Specifically, mice were sacrificed and the intact hippocampi were removed and weighed, corresponding to the wet weight (WW). Afterward, the brain region was dried for 72h at 60ºC, and once again weighed to obtain the dry weight (DW). The percentage of brain water was calculated using the following formula: [(WW – DW)/WW] x 100.

4.3.4. Immunohistochemistry

Immunostaining studies were performed as previously published (**Chapters 2 and 3**; Coelho-Santos et al., 2015; Leitão et al., 2017). Brain slices were incubated with rabbit anti-GFAP (1:1000, Sigma-Aldrich; St. Louis, MO, USA) and rat anti-CD11b (1:200, AbD Serotec, Kidlington, United Kingdom) primary antibodies followed by rabbit Alexa Fluor 594 and rat Alexa Fluor 488 secondary antibodies (1:200; Invitrogen, Inchinnan Business Park, UK) for 1h at RT, and 5 µg/ml Hoechst 33342 (Sigma-Aldrich) for 5 min in the dark at RT. Finally, slices were mounted with Dako fluorescence medium (Dako, Glostrup, Denmark), and images were recorded using the LSM 710 Meta Confocal microscope (Carl Zeiss; Oberkochen, Germany). Quantification of GFAP and CD11b immunoreactivity was accomplished using the NIH ImageJ 1.47 analysis software. To define the corrected total fluorescence, we used the following formula: correct total fluorescence = (integrated intensity) − (total area × mean background). The results are expressed as mean of fluorescence intensity (arbitrary units) of five brain slices obtained from three different animals for each experimental group.

4.3.5. Morphological Analysis of Astrocytic Processes

GFAP-labeled astrocytes were analyzed using the NeuronJ program, a plugin of FIJI Software, to measure the length (total and mean) and count the number of astrocytes

processes in each experimental group as previously described by Di Benedetto and collaborators (Di Benedetto et al., 2016; **Chapter 3**).

4.3.6. Primary Cultures of Mouse Cortical Astrocytes

Astrocyte primary cultures were obtained as previously described (**Chapter 2**; Coelho-Santos et al., 2015). Briefly, brains of C57BL/6J mouse pups aged P4 were used. After proper mechanic digestion cell pellet was plated in T-75 flasks at a density of 1.2 × 105 cells/cm^2. After confluence, flasks were shaking with the non-astrocytic cells discarded (detached cells) and the astrocytes (adherent cells) plated at different densities depending on the experiments.

4.3.7. Enzyme-Linked Immunosorbent Assay

Astrocytes culture medium was collected from control (CTR) or cell treated with METH (250 µM, for 24h) alone or together with PTL (10 µM, for 24h). The released levels of TNF-α were quantified by ELISA Ready-SET-Go kit (eBioscience, San Diego, CA, USA), as specified in the datasheet. The results were expressed as pg/ml.

4.3.8. Cell Volume Measurements

The evaluation of astrocytic volume due to water movements was performed as previously published (**Chapter 3**; Leitão et al., 2017). Briefly, astrocytes were plated in laminin-coated black 96-well plates. After the appropriate treatments cells were washed with PBS and incubated with 5 µM calcein-AM for 1h at 37ºC. Afterward, culture medium with calcein-AM was replaced by calcein-free medium and the fluorescence was measured on a fluorescence plate reader (excitation 485 nm, emission 530 nm). The results were expressed as fold change from CTR condition.

4.3.9. Statistical Analysis

Results are expressed as mean + standard error of the mean (SEM). Data were analyzed using one-way ANOVA followed by Bonferroni's post hoc test, as indicated in figure legends. The level of significance was $P<0.05$ and the 'n' represents the total number of animals or the total of multiwell plates obtained from at least three independent cultures. Statistical analysis was calculated using Prims 6.0 (GraphPad Software, San Diego, CA, USA).

4.4. Results

Very recently, our group showed that METH binge (4× 10 mg/kg, i.p., 2h intervals) causes BBB disruption mediated by TNF-α and NF-κB pathway activation (**Chapter 2**; Coelho-Santos et al., 2015). Thus, we decided to investigate a new approach in an attempt to counteract the deleterious effects of METH. Parthenolide (PTL) is obtained from feverfew plants and is known to have anti-inflammatory properties (Mathema et al., 2012). The animals exposed to PTL (4× 1 mg/kg, i.p., 30 min before each METH injection) showed a prevention against METH-induced BBB disruption, as can be observed by a decrease in albumin protein levels in isolated hippocampi (**Figure 4.1A**; **P<0.01 vs CTR; ###P<0.001 vs METH). Regarding brain edema, PTL also protected hippocampus from the water accumulation observed under METH conditions (**Figure 4.1B**; **P<0.01 vs CTR; ###P<0.001 vs METH).

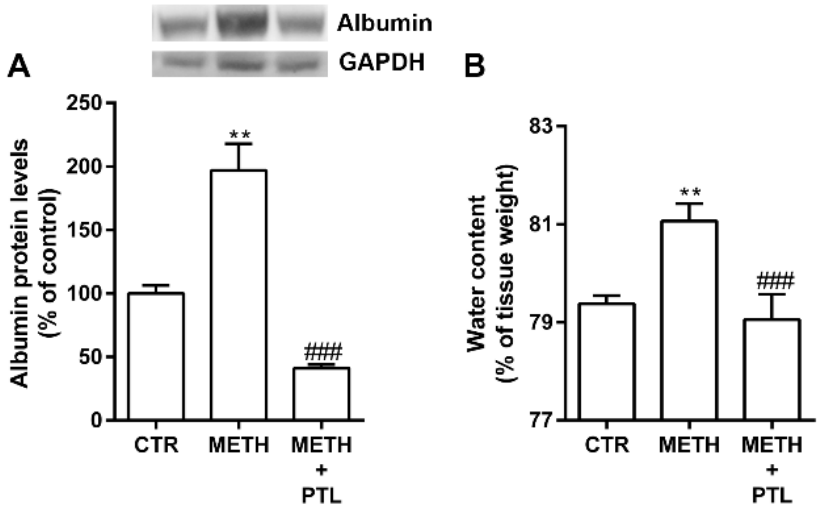

Figure 4.1. Parthenolide (PTL) prevents neurogliovascular dysfunction induced by METH in the mice hippocampus. PTL significantly prevented **(A)** BBB disruption, observed by increased albumin protein levels, and **(B)** brain edema induced by METH. Above the bars, representative western blot images of albumin (66 kDa), and GAPDH (37 kDa) are shown. The results are expressed as mean + S.E.M., n=5, **P<0.01 significantly different when compared to the control (CTR), ###P<0.001 significantly different when compared to METH condition using one-way ANOVA followed by Bonferroni's Multiple comparison test.

Further, to clarify whether PTL also acts as an anti-inflammatory molecule, we looked to possible alterations in astrocytes and microglia, by GFAP and CD11b immunoreactivity, respectively. Interestingly, we did not observe any differences in GFAP immunoreactivity (**Figure 4.2A and 4.2C**) between experimental groups. Nevertheless, alterations in the astrocytes morphology induced by METH were proved by the increase in the total number of astrocytic processes (**Figure 4.2D**; ***P<0.001 vs CTR), as well as the total (**Figure 4.2E**; ***P<0.001 vs CTR) and the mean (**Figure 4.2F**; ***P<0.001 vs CTR) length of those processes. Importantly, PTL exerted its protective effect mainly on the length of the astrocytic processes (**Figure 4.2E** and **4.2F;** *P<0.05 vs CTR; $^{###}$P<0.001 vs METH), without a statistical significant effect on the total number of the cell processes (**Figure 4.2D**) although a tendency to a decrease can be observed. On the other hand, the significant increase in CD11b immunoreactivity triggered by METH (**Figures 4.2B and 4.2G**; ***P<0.001 vs CTR) was completely prevented by PTL (**Figures 4.2B and 4.2G**; $^{###}$P<0.001 vs METH).

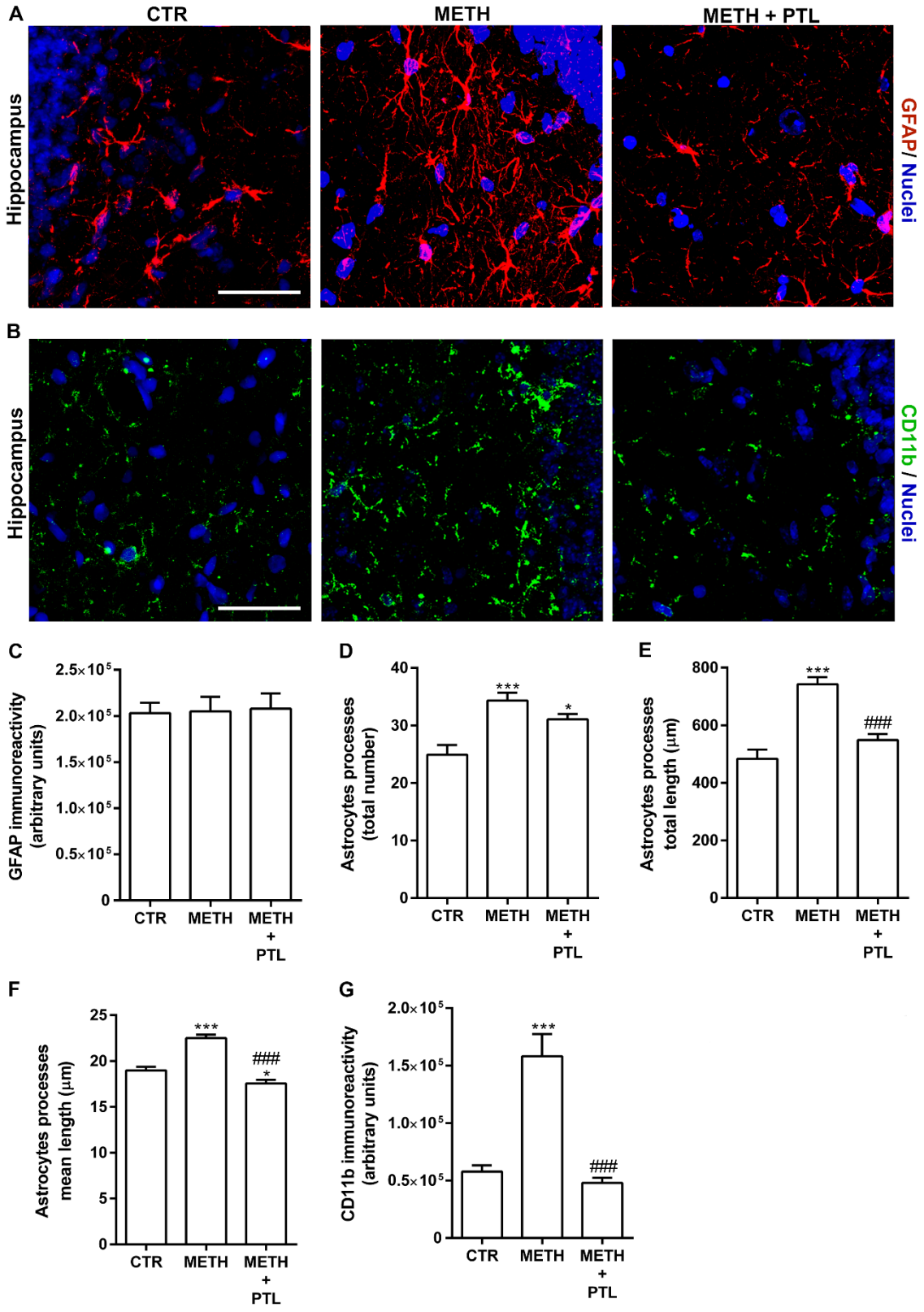

Figure 4.2. METH causes astrocytic morphological alterations and microglia activation in the mice hippocampal CA3 sub-region. Representative immunohistochemistry images for **(A)** GFAP

(red, astrocytes), **(B)** CD11b (green, microglia), and Hoechst (blue, nuclei). Scale bar = 40 µm. Neither METH nor PTL interferes with **(A, C)** GFAP immunostaining. However, the increase in **(D)** astrocytes processes induced by METH was not prevented by PTL. Nevertheless, METH-induced increase in **(E)** total length and **(F)** mean length of processes was both prevented by PTL exposure. Moreover, METH promoted the activation of microglial cells and PTL blocked the increase in **(B, G)** CD11b staining (a marker of microglial cells) induced by the drug. Results are expressed as mean + S.E.M., n=10-15, *P<0.05, ***P<0.001 significantly different when compared to the control (CTR), $^{###}$P<0.001 significantly different when compared to METH condition using one-way ANOVA followed by Bonferroni's Multiple comparison test.

Since glial cells are an important source of inflammatory mediators, we also measured the TNF-α protein levels (**Figure 4.3A**) and once again concluded that PTL was able to prevent the upregulation of this cytokine induced by METH (**P<0.01 vs CTR; $^{##}$P<0.01 vs METH). Besides the abovementioned increase of TNF-α protein levels in the hippocampus of mice administered with METH, we have also previously shown that this drug leads to TNF-α release by both endothelial cells and astrocytes (**chapter 2**; Coelho-Santos et al., 2015), as well as to cell swelling (**chapter 3**; Leitão et al., 2017). However, the role of TNF-α in METH-induced cell swelling has never been investigated. Thus, we further demonstrate that the release of this cytokine by astrocytes was prevented by PTL (**Figure 4.3B**; ***P<0.001 vs CTR; $^{###}$P<0.001 vs METH). This protective effect was also observed when we analyzed astrocytic cell swelling (**Figure 4.4A**; ***P<0.001 vs CTR; $^{###}$P<0.001 vs METH). Then, we hypothesize whether TNF-α could have a direct effect on water regulation. In fact, astrocytes incubated with a TNF-α or TNFR1 neutralizing antibody together with METH showed a cell volume lower than in CTR condition (**Figure 4.4A**; ***P<0.001 vs CTR; $^{###}$P<0.001 vs METH). To prove the direct involvement of TNF-α on astrocyte volume changes, we also showed that 1 ng/ml of this cytokine significantly increased the cell volume (**Figure 4.4B**; ***P<0.001 vs CTR), which was prevented by PTL (*P<0.05 vs CTR; $^{###}$P<0.001 vs TNF-α) or a neutralizing antibody against TNFR1 (**P<0.01 vs CTR; $^{###}$P<0.001 vs TNF-α). The decrease of calcein fluorescence below

control values also suggests that there is basal alterations in cell volume intrinsic to experimental conditions and somehow involving TNF-α signaling.

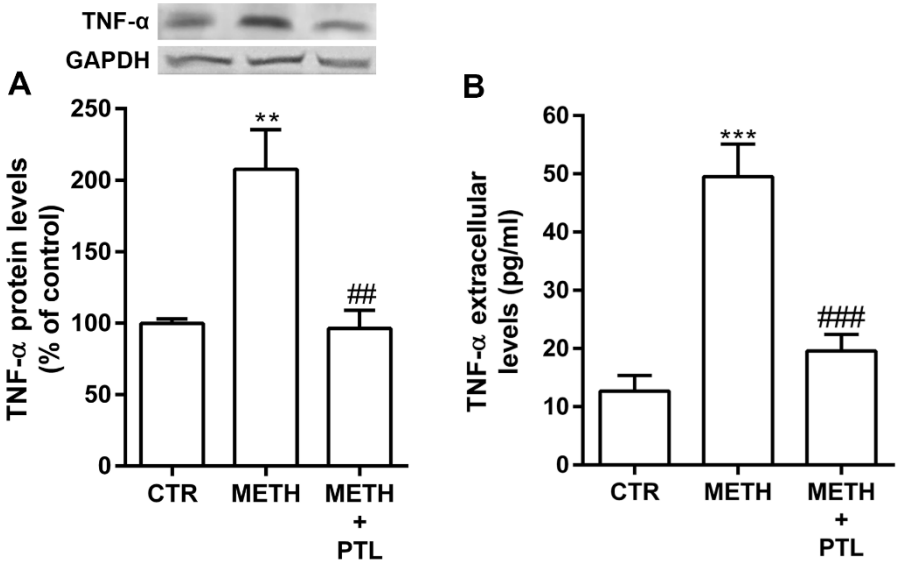

Figure 4.3. METH-induced TNF-α upregulation and release is prevented by parthenolide. (A) PTL (4× 1 mg/kg, 1h before each METH injection) prevented the TNF-α upregulation induced by METH (4× 10 mg/kg, 2h apart) in mice hippocampus. Above the bars, representative western blot images of TNF-α (16 kDa), and GAPDH (37 kDa) are shown. The results are expressed as mean % of control + S.E.M., n=4. **(B)** Once again, PTL (10 µM, 30 min before METH incubation) prevented the astrocytic TNF-α released induced by METH (250 µM for 4h). The results are expressed as pg/ml+S.E.M., n=8. **P<0.01, ***P<0.001 significantly different when compared to the control; ##P<0.01, ###P<0.001 significantly different when compared to METH condition using one-way ANOVA followed by Bonferroni's Multiple comparison test.

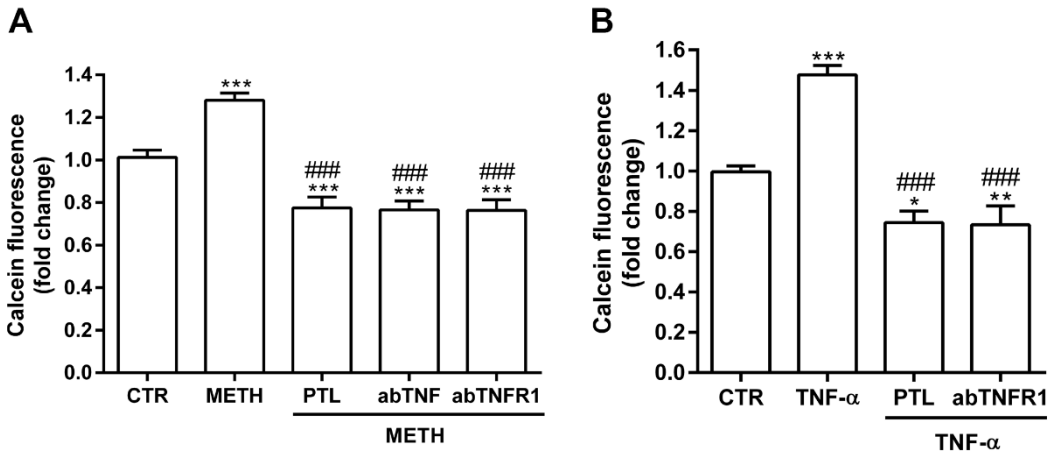

Figure 4.4. Protective role of parthenolide in METH-induced astrocyte swelling. (A) Cell swelling induced by METH was also prevented by PTL, as well as by both neutralizing monoclonal antibody against TNF-α (abTNF, 100 µg/ml; 30 min before METH incubation) and TNFR1 (abTNFR1, 20 µg/ml; 30 min before METH incubation). Moreover, **(C)** PTL and ab TNFR1 prevented the cell swelling triggered by TNF-α (1 ng/ml). Results are expressed as mean fold change + S.E.M., n=5. *P<0.05, **P<0.01, ***P<0.001 significantly different when compared to the control; ###P<0.001 significantly different when compared to METH condition using one-way ANOVA followed by Bonferroni's Multiple comparison test.

4.5. Discussion

Almost 4% of European adults admitted consuming amphetamines at least once in their lives, turning this into a serious society problem (UNODC, 2015). Despite several pathways that are known to be related to METH-induced brain dysfunction, an effective pharmacological approach against the deleterious effects of this drug is still missing. Yet, we have previously demonstrated that the inhibition of TNF-α/NF-κB pathway is able to protect against neurovascular dysfunction induced by METH (**Chapter 2**; Coelho-Santos, et al., 2015). Additionally, the administration of a nonsteroidal anti-inflammatory drug (indomethacin) prevented the neurodegeneration and gliosis induced by METH (Gonçalves et al., 2010). Very recently our group has also demonstrated that the inhibition of the water channel aquaporin 4 prevented both METH-induced BBB disruption and behavioral alterations (**Chapter 3**; Leitão et al., 2017).

Taking into consideration that the therapeutic use of natural products has gained prominence among the population, we further explored the role of PTL, an extract from feverfew plants. In fact, PTL exposure has been shown to have several benefits, including protection against brain edema and stroke induced by middle cerebral artery occlusion (Dong et al., 2013) and prevention of anxiety-like behavior in a diabetic rat model (Khare et al., 2017). Moreover, PTL treatment was capable of preventing the activation of the NF-κB pathway (Rummel et al., 2011; Dong et al., 2013), as well as the upregulation of proinflammatory cytokines TNF-α and IL-1β (Rummel et al., 2011; Khare et al., 2017). Accordingly, we demonstrated that PTL prevented the BBB hyperpermeability induced by METH. As a consequence of BBB impairment, water molecules can accumulate within astrocytes, causing cytotoxic brain edema (**Chapter 3**; Adeva et al., 2012; Leitão et al., 2017), or in extracellular space, originating vasogenic edema (Adeva et al., 2012). To date, the possible protective role of PTL on water accumulation has been overlooked. There is only one study clearly demonstrating that PTL prevented brain edema formation induced by middle cerebral artery occlusion, a rat model of stroke/ischemia (Dong et al., 2013).

Moreover, Ohnishi and collaborators (2014) showed that PTL prevented AQP4 upregulation induced by high-mobility group box 1, a non-histone nucleoprotein that has proinflammatory cytokine-like effects. Notably, our group already proved that AQP4 upregulation is involved in water content augmentation triggered by METH in both mice striatum and hippocampus (**Chapter 3**; Leitão et al., 2017). Herein, we proved that PTL prevents brain edema observed under METH exposure.

It is well known that METH causes an increase in TNF-α mRNA (Gonçalves et al., 2008) and protein levels (**Chapter 2**; Gonçalves et al., 2010; Coelho-Santos et al., 2015) in microglia cells (Coelho-Santos et al., 2012). Accordingly, we demonstrated that METH increased TNF-α protein levels in the hippocampus and promoted its release by astrocytes. Both effects were once again prevented by PTL. Then, we hypothesize whether the TNF-α pathway could be also involved in the deleterious effects of METH. Indeed, the neutralization of TNF-α by a monoclonal antibody prevented the astrocytic cell swelling induced by METH, which is in accordance with previous studies demonstrating that neutralizing antibodies prevented brain edema and BBB disruption after status epilepticus induction (Kim et al., 2012), acute liver failure (Wang et al., 2011), and ischemia (Hosomi et al., 2005). Also, it is of crucial importance to uncover the TNF-α receptor involved on cell swelling induced by METH. Gonçalves and collaborators (2010) proved that a single high dose of METH only causes an upregulation of TNFR1 without any effect on TNFR2 (Gonçalves et al., 2010). Others, by using knockout mice for TNFR1, showed that this receptor is involved in neutrophils infiltration into brain parenchyma, AQP4 upregulation, and brain edema induced by lipopolysaccharide administration (Alexander et al., 2008). In accordance with these results, we demonstrated that TNFR1 was involved in astrocytic cell swelling induced by METH.

In sum, the present work presents parthenolide as a possible therapeutic drug against the negative effects of METH, highlighting a new pharmacologic approach by using plant extracts.

CHAPTER 5

General discussion

5.1. General Discussion

Drug abuse costs more than 7 billion euros to European healthcare system (Lievens et al., 2014) and amphetamine group of drugs is the fourth most consumed type of illicit drugs in Europe. Moreover, 3.8% of European adults consumed amphetamines at least once in their lives (UNODC, 2015), and 0.5% of Portuguese general population (from 15 to 64 years old) or 7% of 18-years-old males have admitted the consumption of amphetamine-like drugs (EMCDDA, 2016; SICAD, 2016). These numbers enlighten the importance of improving our knowledge in this field.

Neurotoxicity of METH, recognized as the most powerful psychostimulant drug of abuse, has been extensively studied over the last years (**Figure 5.1**; Leitão et al., 2016), and the present thesis gave an important contribution by uncovering the involvement of neuroinflammation and oxidative stress in BBB disruption and brain edema induced by this psychostimulant.

One of the most striking findings in this thesis was the role of brain endothelial cells (ECs) as key players in neuroinflammatory processes induced by METH. In fact, ECs are the first cells to interact with pathogens or peripheral signals, being sentinels of the innate immune system (Mai et al., 2013), and also have a pro-active role by the release of inflammatory mediators that will trigger an immune and physiological response in the brain parenchyma (Stanley and Lacy, 2010). Accordingly, we demonstrated that ECs have a quickest and stronger response to METH-induced TNF-α release than astrocytes. Further, microglia cells exposed to METH can also release TNF-α (Coelho-Santos et al., 2012). Thus, it is well established that glial cells are involved in proinflammatory cytokines production and release, but herein we demonstrated that ECs have also an important role in inflammatory processes and immune surveillance under METH exposure.

Despite the importance of ECs in brain parenchyma and blood stream separation and homeostasis, the NVU properties are also influenced by surrounding cells, such as astrocytes. The role of astrocytes in the induction and maintenance of barrier properties

have been extensively demonstrated (Abbott et al., 2006; Kuo and Lu, 2011; Landoni et al., 2012). However, under certain types of injury astrocytes can exert a deleterious response, by releasing several inflammatory mediators. In fact, we demonstrated that TNF-α released by astrocytes was also responsible for the hyperpermeability observed under METH exposure, and we unraveled the NF-κB pathway as the downstream signaling pathway involved in such TNF-α effects.

Importantly, one of the main roles of astrocytes is the control of water homeostasis through the water channel AQP4 (Nag et al., 2009). A dysfunction in this water channel leads to a pathological condition known as brain edema, which is characterized by water accumulation in extracellular (vasogenic edema) or in intracellular (cytotoxic edema) compartments. Unquestionably METH leads to brain edema in both humans (Beránková et al., 2005; Ago et al., 2006) and rats (Kiyatkin et al., 2007; Sharma and Kiyatkin, 2009; Northrop and Yamamoto, 2012). However, until now the molecular mechanism(s) behind such effect, and pharmacological approaches to treat it, are still unknown. Thus, we demonstrated that METH specifically induced a cytotoxic brain edema, and the AQP4 inhibition not only prevented the edema formation but also BBB disruption and behavioral abnormalities, as well as the astrocytic morphological aberrations, induced by this psychostimulant.

Oxidative stress is also part of the inflammatory mediators' group of molecules and is capable of activate one of the key transcription factors on the neuroinflammatory response, the NF-κB pathway (Schreck et al., 1992). In fact, a cocktail of antioxidants (catalase, vitamin E, superoxide dismutase) was shown to be protective against cell swelling induced by hyperammonemia (Jayakumar et al., 2006). Accordingly, we proved that an antioxidant treatment, using vitamin C, was able to prevent the astrocytic water accumulation as well as the AQP4 upregulation induced by METH. Importantly, it has already been demonstrated that activation of the NF-κB pathway by ROS leads to an upregulation of AQP4 levels (Ito et al., 2006). Additionally, the *aqp4* gene has indeed a putative transcription factor site for NF-κB subunits (Ito et al., 2006). Thus, we further identified

parthenolide (PTL), a recognized NF-κB inhibitor (Mathema et al., 2012), as a new drug capable of preventing the deleterious effects of METH. Specifically, PTL prevented not only the BBB disruption and brain edema but also the astrocytic morphologic alterations and cell swelling induced by METH.

In conclusion, the present thesis shows that inflammatory mediators including TNF-α/NF-κB pathway and oxidative stress have a key role in METH deleterious effects. Moreover, we uncover ECs as one the earliest inflammatory players after METH insult and also identified a crucial role of AQP4 in BBB properties and water homeostasis, with associated behavioral impact. Finally, we unveiled PTL as a new pharmacological approach to counteract METH-induced neurovascular dysfunctions.

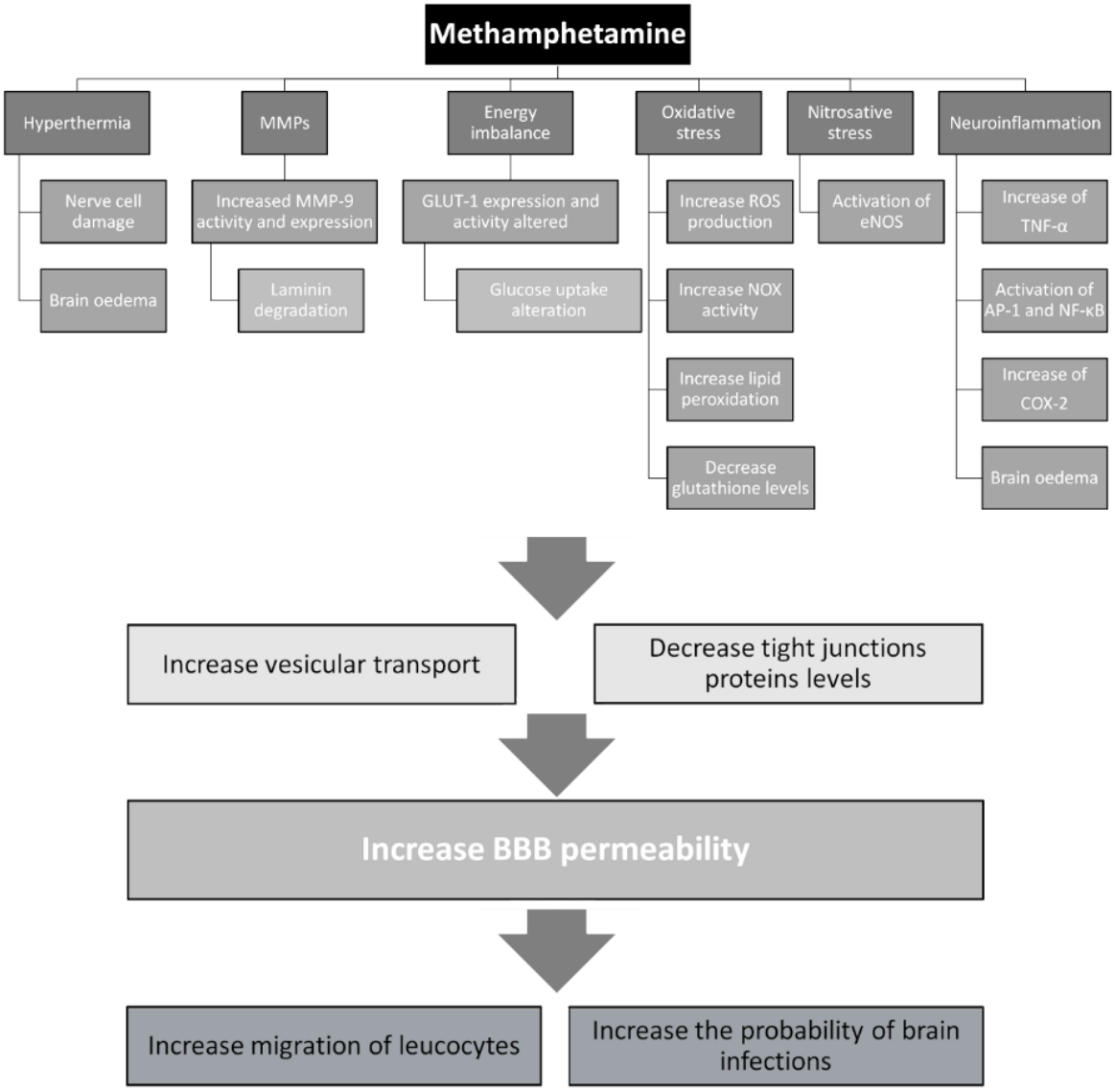

Figure 5.1. Schematic summary of the methamphetamine effects on the blood-brain barrier. The scheme summarizes the main effects on brain endothelial cells triggered by METH such as energy imbalance, oxidative and nitrosative stress, hyperthermia and neuroinflammation. AP-1: Activator protein 1; BBB: blood-brain barrier; COX-2: cyclooxygenase 2; eNOS: endothelial nitric oxide synthase; GLUT-1: glucose transporter 1; MMP-9: matrix metalloproteinase 9; NF-κB: nuclear factor kappa B; NOX: NADPH oxidase; ROS: reactive oxygen species; TNF-α: tumour necrosis factor alpha; ZO-1: zonula occludens 1 (taken from Leitão et al., 2016 with permission).

5.2. Main conclusions

- METH promotes vesicular and paracellular transport across brain endothelial cells.
- METH-induced BBB disruption involves the TNF-α/NF-KB pathway.
- METH causes a cytotoxic brain edema together with AQP4 upregulation.
- AQP4 inhibition prevents both BBB disruption and depressive-like behavior induced by METH.
- Oxidative stress and TNF-α, *via* its TNFR1, are involved in astrocytic cell swelling induced by METH.
- Parthenolide, a feverfew plant extract, prevents both METH-induced BBB disruption and brain edema.

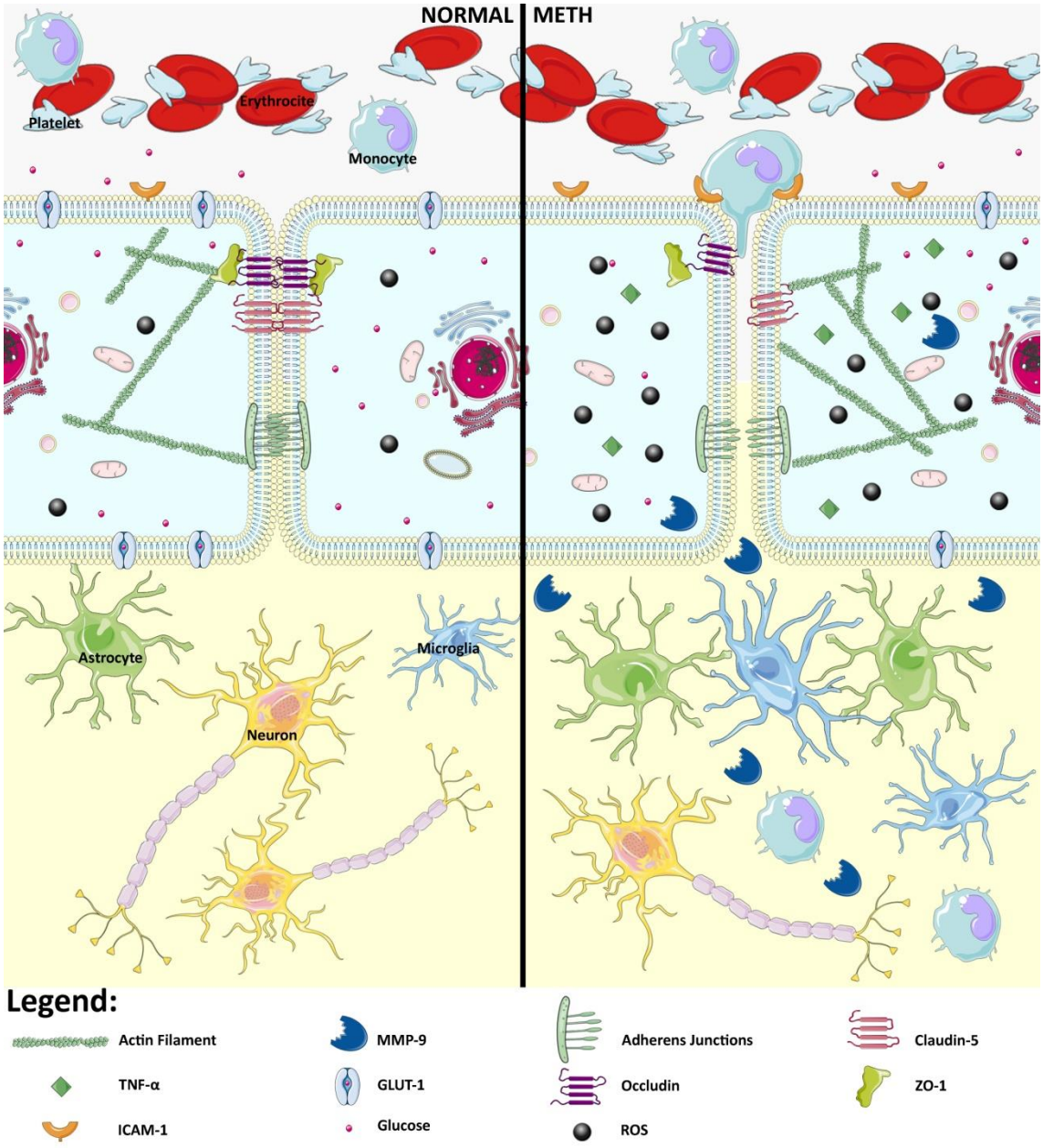

Figure 5.2. Schematic representation of key players involved in methamphetamine-induced blood-brain barrier dysfunction. Picture showing the differences in brain endothelial cells between a physiological (normal) situation and under METH exposure (METH), where is possible to observe an increase in ROS, an impairment of tight junction proteins and glucose uptake, and alterations in the actin cytoskeleton. GLUT-1: glucose transporter-1; ICAM-1: intercellular adhesion molecule-1; MMP-9: matrix metalloproteinase-9; ROS: reactive oxygen species; TNF-α: tumor necrosis factor-alpha; ZO-1: zonula occludens 1 (taken from Leitão et al., 2016 with permission).

CHAPTER 6

References

6.1. References

Abbott NJ, Friedman A. (2012) Overview and introduction: the blood-brain barrier in health and disease. Epilepsia, 53 Suppl 6, 1-6.

Abbott NJ, Patabendige AA, Dolman DE, Yusof SR, Begley DJ. (2010) Structure and function of the blood-brain barrier. Neurobiol Dis, 37: 13-25.

Abbott NJ, Ronnback L, Hansson E. (2006) Astrocyte–endothelial interactions at the blood–brain barrier. Nat Rev Neurosci, 7: 41-53.

Abbott NJ. (2002) Astrocyte-endothelial interactions and blood-brain barrier permeability. J Anat, 200: 629-638

Abdul Muneer PM, Alikunju S, Szlachetka AM, Haorah J (2011) Methamphetamine inhibits the glucose uptake by human neurons and astrocytes: stabilization by acetyl-L-carnitine. PLoS One 6:e19258.

Abdul Muneer PM, Chandra N, Haorah J. (2015) Interactions of Oxidative Stress and Neurovascular Inflammation in the Pathogenesis of Traumatic Brain Injury. Mol Neurobiol. 51:966-79.

Adeva MM, Souto G, Donapetry C, Portals M, Rodriguez A, Lamas D. (2012) Brain edema in diseases of different etiology. Neurochem Int, 61: 166-74.

Ago M, Ago K, Hara K, Kashimura S, Ogata M. (2006) Toxicological and histopathological analysis of a patient who died nine days after a single intravenous dose of methamphetamine: a case report. Leg Med (Tokyo), 8: 235-239.

Agrawal SM, Lau L, Yong VW. (2008) MMPs in the central nervous system: where the good guys go bad. Semin Cell Dev Biol, 19: 42-51.

Alexander JJ, Jacob A, Cunningham P, Hensley L, Quigg RJ. (2008). TNF is a key mediator of septic encephalopathy acting through its receptor, TNF receptor-1. Neurochem Int, 52: 447-456.

Allaman I, Bélanger M, Magistretti PJ. (2011) Astrocyte-neuron metabolic relationships: for better and for worse. Trends Neurosci, 34: 76-87.

Alvarez JI, Saint-Laurent O, Godschalk A, Terouz S, Briels C, Larouche S, Bourbonniere L, Larochelle C, Prat A. (2015) Focal disturbances in the blood-brain barrier are associated with formation of neuroinflammatory lesions. Neurobiol Dis, 74: 14–24.

Amiry-Moghaddam M, Frydenlund DS, Ottersen OP. (2004) Anchoring of aquaporin-4 in brain: molecular mechanisms and implications for the physiology and pathophysiology of water transport. Neuroscience, 129: 999-1010.

Amiry-Moghaddam M, Lindland H, Zelenin S, Roberg BA, Gundersen BB, Petersen P, Rinvik E, Torgner IA, Ottersen OP. (2005) Brain mitochondria contain aquaporin water channels: evidence for the expression of a short AQP9 isoform in the inner mitochondrial membrane. FASEB J, 19: 1459-67.

Amiry-Moghaddam M, Ottersen OP. (2003) The molecular basis of water transport in the brain. Nat Rev Neurosci, 4: 991-1001.

Argaw AT, Gurfein BT, Zhang Y, Zameer A, John GR. (2009) VEGF-mediated disruption of endothelial CLN-5 promotes blood-brain barrier breakdown. Proc Natl Acad Sci USA, 106: 1977-82.

Armulik A, Genové G, Mäe M, Nisancioglu MH, Wallgard E, Niaudet C, He L, Norlin J, Lindblom P, Strittmatter K, Johansson BR, Betsholtz C. (2010) Pericytes regulate the blood-brain barrier. Nature, 468: 557-561.

Asai H, Kakita H, Aoyama M, Nagaya Y, Saitoh S, Asai K. (2013) Diclofenac enhances proinflammatory cytokine-induced aquaporin-4 expression in cultured astrocyte. Cell Mol Neurobiol, 33: 393-400.

Aslam M, Ahmad N, Srivastava R, Hemmer B. (2012) TNF-alpha induced NF-kappaB signaling and p65 (RelA) overexpression repress Cldn5 promoter in mouse brain endothelial cells. Cytokine, 57: 269–275.

Assentoft M, Kaptan S, Fenton RA, Hua SZ, de Groot BL, MacAulay N (2013) Phosphorylation of rat aquaporin-4 at Ser(111) is not required for channel gating. Glia 61:1101–1112.

Aveleira CA, Lin CM, Abcouwer SF, Ambrosio AF, Antonetti DA. (2010) TNF-alpha signals through PKCzeta/NF-kappaB to alter the tight junction complex and increase retinal endothelial cell permeability. Diabetes, 59: 2872–2882.

Ayus JC, Achinger SG, Arieff A. (2008) Brain cell volume regulation in hyponatremia: role of sex, age, vasopressin, and hypoxia. Am J Physiol renal Physiol, 295: 619-24.

Badaut J, Ashwal S, Adami A, Tone B, Recker R, Spagnoli D, Ternon B, Obenaus A (2011) Brain water mobility decreases after astrocytic aquaporin-4 inhibition using RNA interference. J Cereb Blood Flow Metab 31:819–831.

Bagshaw SM, Peets AD, Hameed M, Boiteau PJ, Laupland KB, Doig CJ. (2004) Dialysis Disequilibrium Syndrome: brain death following hemodialysis for metabolic acidosis and acute renal failure – a case report. BMC Nephrol, 5: 9.

Ballabh P, Braun A, Nedergaard M. (2004) The blood–brain barrier: an overview Structure, regulation, and clinical implications. Neurobiol Dis, 16: 1-13.

Bammer R (2003) Basic principles of diffusion-weighted imaging. Eur J Radiol 45:169–184.

Banerjee A, Zhang X, Manda KR, Banks WA, Ercal N. (2010) HIV proteins (gp120 and Tat) and methamphetamine in oxidative stress-induced damage in the brain: potential role of the thiol antioxidant N-acetylcysteine amide. Free Radic Biol Med, 48: 1388-1398.

Barata-Antunes S, Cristóvão AC, Pires J, Rocha MS, Bernardino L. (2017) Dual role of histamine on microglia-induced neurodegeneration. Biochim Biophys Acta, 1863: 764-769.

Barzó P, Marmarou A, Fatouros P, Hayasaki K, Corwin F. (1997) Contribution of vasogenic and cellular edema to traumatic brain swelling measured by diffusion-weighted imaging. J Neurosurg, 87: 900-907.

Bastide M, Ouk T, Plaisier F, Pétrault O, Stolc S, Bordet R. (2007) Neurogliovascular unit after cerebral ischemia: is the vascular wall a pharmacological target. Psychoneuroendocrinology, 32 Suppl 1: S36-S39.

Beauvais G, Atwell K, Jayanthi S, Ladenheim B, Cadet JL. (2011) Involvement of dopamine receptors in binge methamphetamine-induced activation of endoplasmic reticulum and mitochondrial stress pathways. PLoS ONE, 6: e28946.

Bell RD, Winkler EA, Sagare AP, Singh I, LaRue B, Deane R, Zlokovic BV. (2010) Pericytes control key neurovascular functions and neuronal phenotype in the adult brain and during brain aging. Neuron, 68: 409-427.

Bendayan R, Ronaldson PT, Gingras D, Bendayan M. (2006) In situ localization of P-glycoprotein (ABCB1) in human and rat brain. J Histochem Cytochem, 54: 1159-1167.

Benga O, Huber VJ. (2012) Brain water channel proteins in health and disease. Mol Aspects Med, 33: 562-78.

Beránková K, Habrdová V, Baliková M, Strejc P. (2005) Methamphetamine in hair and interpretation of forensic findings in a fatal case. Forensic Sci Int, 153: 93-97.

Bernardino L, Agasse F, Silva B, Ferreira R, Grade S, Malva JO. (2008) Tumor necrosis factor-alpha modulates survival, proliferation, and neuronal differentiation in neonatal subventricular zone cell cultures. Stem Cells, 26: 2361-2371.

Bernas MJ, Cardoso FL, Daley SK, Weinand ME, Campos AR, Ferreira AJ, Hoying JB, Witte MH, Brites D, Persidsky Y, Ramirez SH, Brito MA. (2010) Establishment of primary cultures of human brain microvascular endothelial cells to provide an in vitro cellular model of the blood-brain barrier. Nat Protoc, 5: 1265–1272.

Binder DK, Yao X, Verkman AS, Manley GT. (2006) Increased seizure duration in mice lacking aquaporin-4 water channels. Acta Neurochir Suppl, 96: 389-92.

Boger HA, Middaugh LD, Patrick KS, Ramamoorthy S, Denehy ED, Zhu H, Pacchioni AM, Granholm AC, McGinty JF. (2007) Long-term consequences of methamphetamine exposure in young adults are exacerbated in glial cell line-derived neurotrophic factor heterozygous mice. J Neurosci 27:8816–8825.

Boulle F, Massart R, Stragier E, Paizanis E, Zaidan L, Marday S, Gabriel C, Mocaer E (2014) Hippocampal and behavioral dysfunctions in a mouse model of environmental stress: normalization by agomelatine. Transl Psychiatry 4:e485.

Bowyer JF, Ali S. (2006) High doses of methamphetamine that cause disruption of the blood-brain barrier in limbic regions produce extensive neuronal degeneration in mouse hippocampus. Synapse, 60: 521-532.

Bowyer JF, Robinson B, Ali S, Schmued LC. (2008) Neurotoxic-related changes in tyrosine hydroxylase, microglia, myelin, and the blood-brain barrier in the caudate-putamen from acute methamphetamine exposure. Synapse, 62: 193-204.

Braun AA, Herring NR, Schaefer TL, Hemmerle AM, Dickerson JW, Seroogy KB, Vorhees CV, Williams MT. (2011) Neurotoxic (+)-methamphetamine treatment in rats increases brain-derived neurotrophic factor and tropomyosin receptor kinase B expression in multiple brain regions. Neuroscience, 184: 164-171.

Brown RC, Davis TP. (2005) Hypoxia/aglycemia alters expression of occludin and actin in brain endothelial cells. Biochem Biophys Res Commun, 327: 1114-23.

Buchanan JB, Sparkman NL, Johnson RW. (2010) Methamphetamine sensitization attenuates the febrile and neuroinflammatory response to a subsequent peripheral immune stimulus. Brain Behav Immun, 24: 502-511.

Burnett ME, Johnston HM, Green KN (2015) Structural characterization of the aquaporin inhibitor 2-nicotinamido-1,3,4-thiadiazole. Acta Cryst C71:1074–1079.

Buttner A. (2011) The neuropathology of drug abuse. Neuropathol and Appl Neurobiol, 37: 118-134.

Cadet JL, Krasnova IN, Jayanthi S, Lyles J. (2007) Neurotoxicity of substituted amphetamines: molecular and cellular mechanisms. Neurotox Res, 11: 183-202

Candelario-Jalil E, Taheri S, Yang Y, Sood R, Grossetete M, Estrada EY, Fiebich BL, Rosenberg GA. (2007) Cyclooxygenase inhibition limits blood-brain barrier disruption following intracerebral injection of tumor necrosis factor-alpha in the rat. J Pharmacol Exp Ther, 323: 488-498.

Cardoso FL, Brites D, Brito MA. (2010) Looking at the blood-brain barrier: molecular anatomy and possible investigation approaches. Brain Res Rev, 64: 328-363.

Cardoso FL, Kittel A, Veszelka S, Palmela I, Toth A, Brites D, Deli MA, Brito MA. (2012) Exposure to lipopolysaccharide and/or unconjugated bilirubin impair the integrity and function of brain microvascular endothelial cells. PLoS ONE, 7: e35919.

Castejon OJ. (2013) Increased vesicular and vacuolar transendothelial transport in traumatic human brain oedema. A review. Folia Neuropathol, 51: 93–102.

Chen F, Ohashi N, Li W, Eckman C, Nguyen JH. (2009) Disruptions of occludin and claudin-5 in brain endothelial cells in vitro and in brains of mice with acute liver failure. Hepatology, 50: 1914-1923.

Chen SJ, Yang JF, Kong FP, Ren JL, Hao K, Li M, Yuan Y, Chen XC, Yu RS, Li JF, Leng G, Chen XQ, Du JZ. (2014) Overactivation of corticotropin-releasing factor receptor type 1 and aquaporin-4 by hypoxia induces cerebral edema. Proc Natl Acad Sci U S A 111: 13199–13204.

Cheng WS, Garfein RS, Semple SJ, Strathdee SA, Zians JK, Patterson TL. (2010) Binge use and sex and drug use behaviors among HIV(-), heterosexual methamphetamine users in San Diego. Subst Use Misuse, 45:116-133.

Choi YK, Kim K. (2008) Blood-neural barrier: its diversity and coordinated cell-to-cell communication. BMB Reports, 41: 345-352.

Clark PR, Manes TD, Pober JS, Kluger MS. (2007) Increased ICAM-1 expression causes endothelial cell leakiness, cytoskeletal reorganization and junctional alterations. J Invest Dermatol, 127: 762–774.

Claudio L, Kress Y, Norton WT, Brosnan CF. (1989) Increased vesicular transport and decreased mitochondrial content in blood-brain barrier endothelial cells during experimental autoimmune encephalomyelitis. Am J Pathol, 135: 1157-1168.

Coelho-Santos V, Gonçalves J, Fontes Ribeiro C, Silva AP. (2012) Prevention of methamphetamine-induced microglial cell death by TNF-alpha and IL-6 through activation of the JAK-STAT pathway. J Neuroinflammation, 9: 103.

Coelho-Santos V*, Leitão RA*, Cardoso FL, Palmela I, Rito M, Barbosa M, Brito MA, Fontes-Ribeiro CA, Silva AP. (2015) The TNF-α/NF-κB signaling pathway has a key role in methamphetamine-induced blood-brain barrier dysfunction. J Cereb Blood Flow Metab, 35: 1260-1271. (*These authors contribute equally to work).

Coelho-Santos V, Socodato R, Portugal C, Leitão RA, Rito M, Barbosa M, Couraud PO, Romero IA, Weksler B, Minshall RD, Fontes-Ribeiro C, Summavielle T, Relvas JB, Silva AP. (2016) Methylphenidate-triggered ROS generation promotes caveolae-mediated transcytosis via Rac1 signaling and c-Src-dependent caveolin-1 phosphorylation in human brain endothelial cells. Cell Mol Life Sci, 73: 4701-4716.

Collins JS, Perry RT, Watson B Jr, Harrell LE, Acton RT, Blacker D, Albert MS, Tanzi RE, Bassett SS, McInnis MG, Campbell RD, Go RC. (2000) Association of a haplotype for tumor necrosis factor in siblings with late-onset Alzheimer disease: the NIMH Alzheimer Disease Genetics Initiative. Am J Med Genet, 96: 823-830.

Collins MA, Neafsey EJ. (2012) Neuroinflammatory pathways in binge alcohol-induced neuronal degeneration: oxidative stress cascade involving aquaporin, brain edema, and phospholipase A2 activation. Neurotox Res, 21: 70-78.

Colombo E, Farina C. (2016) Astrocytes: Key Regulators of Neuroinflammation. Trends Immunol, 37: 608-620.

Connors NC, Adams ME, Froehner SC, Kofuji P. (2004) The potassium channel Kir4.1 associates with the dystrophin-glycoprotein complex via alpha-syntrophin in glia. J Biol Chem, 279: 28387-28392.

Copin JC, Bengualid DJ, Silva RF, Kargiotis O, Schaller K, Gasche Y (2011) Recombinant tissue plasminogen activator induces blood–brain barrier breakdown by a matrix metalloproteinase-9-independent pathway after transient focal cerebral ischemia in mouse. Eur J Neurosci 34:1085–1092.

Correale J. (2014) The role of microglial activation in disease progression. Mult Scler, 20: 1288-1295.

Crawley JN (2007) What's wrong with my mouse: behavioral phenotyping of transgenic and knockout mice, 2nd edn. John Wiley & Sons, Inc., Hoboken, NJ

Cruickshank CC, Dyer KR. (2009) A review of the clinical pharmacology of methamphetamine. Addiction, 104: 1085-1099.

Dalle Lucca JJ, Chavko M, Dubick MA, Adeeb S, Falabella MJ, Slack JL, McCarron R, Li Y. (2012) Blast-induced moderate neurotrauma (BINT) elicits early complement activation and tumor necrosis factor α (TNFα) release in a rat brain. J Neurol Sci, 318: 146-154.

Darke S, Kaye S, McKetin R, Duflou J. (2008) Major physical and psychological harms of methamphetamine use. Drug Alcohol Rev, 27: 253-262.

de la Torre R, Yubero-Lahoz S, Pardo-Lozano R, Farré M. (2012) MDMA, methamphetamine, and CYP2D6 pharmacogenetics: what is clinically relevant? Front Genet, 3: 235.

De Stefano D. (2011) Oligonucleotides decoy to NF-kappaB: becoming a reality? Discov Med, 12: 97-105.

Deli MA, Descamps L, Dehouck MP, Cecchelli R, Joo F, Abraham CS, Torpier G. (1995) Exposure of tumor necrosis factor-alpha to luminal membrane of bovine brain capillary endothelial cells cocultured with astrocytes induces a delayed increase of permeability and cytoplasmic stress fiber formation of actin. J Neurosci Res, 41: 717–726.

Di Benedetto B, Malik VA, Begum S, Jablonowski L, Gómez-Gonzáles GB, Neumann ID, Rupprecht R (2016) Fluoxetine requires the endfeet protein aquaporin-4 to enhance plasticity of astrocyte processes. Front Cell Neurosci 10:8.

Diaz-Ruiz O, Zhang Y, Shan L, Malik N, Hoffman AF, Ladenheim B, Cadet JL, Lupica CR, Tagliaferro A, Brusco A, Bäckman CM. (2012) Attenuated response to methamphetamine sensitization and deficits in motor learning and memory after selective deletion of β-catenin in dopamine neurons. Learn Mem 19:341–350.

Dietrich JB. (2009) Alteration of blood-brain barrier function by methamphetamine and cocaine. Cell Tissue Res, 336: 385-392.

Dong L, Qiao H, Zhang X, Zhang X, Wang C, Wang L, Cui L, Zhao J, Xing Y, Li Y, Liu Z, Zhu C. (2013) Parthenolide is neuroprotective in rat experimental stroke model: downregulating NF-κB, phospho-p38MAPK, and caspase-1 and ameliorating BBB permeability. Mediators Inflamm, 2013: 370804.

Du L, Zhang Y, Chen Y, Zhu J, Yang Y, Zhang HL. (2016) Role of Microglia in Neurological Disorders and Their Potentials as a Therapeutic Target. Mol Neurobiol, doi:10.1007/s12035-016-0245-0 (Epub ahead of print).

Eide PK, Eidsvaag VA, Nagelhus EA, Hansson HA (2016) Cortical astrogliosis and increased perivascular aquaporin-4 in idiopathic intracranial hypertension. Brain Res 1644:161–175.

European Monitoring Centre for Drugs and Drug Addiction (EMCDDA). (2013). Europpean Drug Report 2013. Publications Office of the European Union, Luxembourg.

European Monitoring Centre for Drugs and Drug Addiction (EMCDDA). (2016) European Drug Report 2016: Trends and Developments. Publications Office of the European Union, Luxembourg.

Emmanouil M, Taoufik E, Tseveleki V, Vamvakas SS, Tselios T, Karin M, Lassmann H, Probert L. (2009) Neuronal I kappa B kinase beta protects mice from autoimmune encephalomyelitis by mediating neuroprotective and immunosuppressive effects in the central nervous system. J Immunol, 183: 7877-7889.

Engelhardt B. (2006) Molecular mechanisms involved in T cell migration across the blood-brain barrier. J Neural Transm, 113: 477-485.

Ennis SR, Keep RF. (2006) Effects of 2,4-dinitrophenol on ischemia-induced blood-brain barrier disruption. Acta Neurochir Suppl, 96: 295-298.

Eugenin EA, Greco JM, Frases S, Nosanchuk JD, Martinez LR. (2013) Methamphetamine alters blood brain barrier protein expression in mice, facilitating central nervous system infection by neurotropic Cryptococcus neoformans. J Infect Dis, 208: 699-704.

Fernandes S, Salta S, Bravo J, Silva AP, Summavielle T (2016) Acetyl-L-carnitine prevents methamphetamine-induced structural damage on endothelial cells via ILK-related MMP-9 activity. Mol Neurobiol 53:408–422.

Fleckenstein AE, Volz TJ, Riddle EL, Gibb JW, Hanson GR. (2007) New insights into the mechanism of action of amphetamines. Annu Rev Pharmacol Toxicol, 47: 681-698.

Francesca B, Rezzani R. (2010) Aquaporin and Blood Brain Barrier. Curr Neuropharmacol, 8: 92-96.

Fraser PA. (2011) The role of free radical generation in increasing cerebrovascular permeability. Free Radic Biol Med, 51: 967-977.

Fukuda AM, Adami A, Pop V, Bellone JA, Coats JS, Hartman RE, Ashwal S, Obenaus A, Badaut J. (2013) Posttraumatic reduction of edema with aquaporin-4 RNA interference improves acute and chronic functional recovery. J Cereb Blood Flow Metab 33:1621–1632.

Furman CS, Gorelick-Feldman DA, Davidson KG, Yasumura T, Neely JD, Agre P, Rash JE. (2003) Aquaporin-4 square array assembly: opposing actions of M1 and M23 isoforms. Proc Natl Acad Sci USA, 100: 13609-13614.

Ghatol A, Kazory A. (2012) Ecstasy-associated acute severe hyponatremia and cerebral edema: a role for osmotic diuresis? J Emerg Med, 42: e137-140.

Gonçalves A, Ambrosio AF, Fernandes R. (2013) Regulation of claudins in blood-tissue barriers under physiological and pathological states. Tissue Barriers, 1: e24782.

Gonçalves J, Baptista S, Martins T, Milhazes N, Borges F, Ribeiro CF, Malva JO, Silva AP. (2010) Methamphetamine-induced neuroinflammation and neuronal dysfunction in the mice hippocampus: preventive effect of indomethacin. Eur J Neurosci, 31: 315-326.

Gonçalves J, Baptista S, Olesen MV, Fontes-Ribeiro C, Malva JO, Woldbye DP, Silva AP. (2012) Methamphetamine-induced changes in the mice hippocampal neuropeptide Y system: implications for memory impairment. J Neurochem 123: 1041-1053.

Gonçalves J, Baptista S, Silva AP. (2014) Psychostimulants and brain dysfunction: A review of the relevant neurotoxic effects. Neuropharmacology, 87C: 135-149.

Gonçalves J, Martins T, Ferreira R, Milhazes N, Borges F, Ribeiro CF, Malva JO, Macedo TR, Silva AP. (2008) Methamphetamine-induced early increase of IL-6 and TNF-alpha mRNA expression in the mouse brain. Ann N Y Acad Sci, 1139: 103-111.

Grace CE, Schaefer TL, Herring NR, Graham DL, Skelton MR, Gudelsky GA, Williams MT, Vorhees CV. (2010) Effect of a neurotoxic dose regimen of (+)-methamphetamine on behavior, plasma corticosterone, and brain monoamines in adult C57BL/6 mice. Neurotoxicol Teratol, 32: 346–355.

Graham DL, Herring NR, Schaefer TL, Holland KD, Vorhees CV, Williams MT. (2012) Electroencephalographic and convulsive effects of binge doses of (+)-methamphetamine, 5-methoxydiisopropyltryptamine, and (±)-3,4-methylenedioxymethamphetamine in rats. Open Neuropsychopharmacol J, 5: 1-8.

Grände PO, Romner B. (2012) Osmotherapy in brain edema: a questionable therapy. J Neurosurg Anesthesiol, 24:407-412.

Gualtierotti R, Guarnaccia L, Beretta M, Navone SE, Campanella R, Riboni L, Rampini P, Marfia G. (2017) Modulation of Neuroinflammation in the Central Nervous System: Role of Chemokines and Sphingolipids. Adv Ther, doi:10.1007/s12325-016-0474-7 (Epub ahead of print).

Gunnarson E, Axehult G, Baturina G, Zelenin S, Zelenina M, Aperia A. (2005) Lead induces increased water permeability in astrocytes expressing aquaporin 4. Neuroscience, 136: 105-114.

Gunnarson E, Zelenina M, Axehult G, Song Y, Bondar A, Krieger P, Brismar H, Zelenin S, Aperia A. (2008) Identification of a molecular target for glutamate regulation of astrocyte water permeability. Glia, 56: 587-596.

Hackett PH. (1999) High altitude cerebral edema and acute mountain sickness. A pathophysiology update. Adv Exp Med Biol, 474: 23-45.

Haj-Yasein NN, Vindedal GF, Eilert-Olsen M, Gundersen GA, Skare Ø, Laake P, Klungland A, Thorén AE, Burkhardt JM, Ottersen OP, Nagelhus EA. (2011) Glial-conditional deletion of aquaporin-4 (Aqp4) reduces blood-brain water uptake and confers barrier function on perivascular astrocyte endfeet. Proc Natl Acad Sci U S A 108:17815–17820.

Hanisch UK, Kettenmann H. (2007) Microglia: active sensor and versatile effector cells in the normal and pathologic brain. Nat Neurosci, 10: 1387-1394.

Hawkes M, Kitai I, Blaser S, Cohen E, Bitnun A, Fluss J, Tran D. (2008) Neuroimaging findings in isoniazid central nervous system toxicity, presumed intramyelinic edema. Eur J Paediatr Neurol, 12: 512-515.

Hawkins BT, Davis TP. (2005) The Blood-Brain Barrier/Neurovascular Unit in Health and Disease. Pharmacol Rev, 57: 173-185.

Hawkins BT, Gu YH, Izawa Y, Zoppo GJ (2013) Disruption of dystroglycan-laminin interactions modulates water uptake by astrocytes. Brain Res 1503: 89–96.

Hazama A, Kozono D, Guggino WB, Agre P, Yasui M. (2002) Ion permeation of AQP6 water channel protein. Single channel recordings after Hg2+ activation. J Biol Chem, 277: 29224-29230.

He Z, Wang X, Wu Y, Jia J, Hu Y, Yang X, Li J, Fan M, Zhang L, Guo J, Leung MC. (2014) Treadmill pre-training ameliorates brain edema in ischemic stroke via down-regulation of aquaporin-4: an MRI study in rats. PLoS One 9:e84602.

Heiss JD, Papavassiliou E, Merrill MJ, Nieman L, Knightly JJ, Walbridge S, Edwards NA, Oldfield EH. (1996) Mechanism of dexamethasone suppression of brain tumor-associated vascular permeability in rats. Involvement of the glucocorticoid receptor and vascular permeability factor. J Clin Invest, 98: 1400–1408.

Helms HC, Abbott NJ, Burek M, Cecchelli R, Couraud PO, Deli MA, Förster C, Galla HJ, Romero IA, Shusta EV, Stebbins MJ, Vandenhaute E, Weksler B, Brodin B. (2016) In vitro models of the blood-brain barrier: An overview of commonly used brain endothelial cell culture models and guidelines for their use. J Cereb Blood Flow Metab, 36: 862-890.

Herring NR, Gudelsky GA, Vorhees CV, Williams MT. (2010) (+)-Methamphetamine-induced monoamine reductions and impaired egocentric learning in adrenalectomized rats is independent of hyperthermia. Synapse, 64: 773-785.

Hirrlinger PG, Pannicke T, Winkler U, Claudepierre T, Varshney S, Schulze C, Reichenbach A, Brunken WJ, Hirrlinger J. (2011) Genetic deletion of laminin isoforms β2 and γ3 induces a reduction in Kir4.1 and aquaporin-4 expression and function in the retina. PLoS One 6:e16106.

Ho ML, Rojas R, Eisenber RL. (2012) Cerebral edema. Am J Roentgenol, 199: w258-w273.

Hosomi N, Ban CR, Naya T, Takahashi T, Guo P, Song XY, Kohno M. (2005) Tumor necrosis factor-alpha neutralization reduced cerebral edema through inhibition of matrix metalloproteinase production after transient focal cerebral ischemia. J Cereb Blood Flow Metab, 25: 959-967.

Howe CL, Kaptzan T, Magaña SM, Ayers-Ringler JR, LaFrance-Corey RG, Lucchinetti CF (2014) Neuromyelitis optica IgG stimulates an immunological response in rat astrocyte cultures. Glia 62:692–708.

Huang WJ, Lee HJ, Chen HL, Fan PC, Ku YL, Chiou LC (2015) Hispidulin, a constituent of Clerodendrum inerme that remitted motor tics, alleviated methamphetamine-induced hyperlocomotion without motor impairment in mice. J Ethnopharmacol 166:18–22.

Huber JD, Hau VS, Borg L, Campos CR, Egleton RD, Davis TP. (2002) Blood-brain barrier tight junctions are altered during a 72-h exposure to lambda-carrageenan-induced inflammatory pain. Am J Physiol Heart Circ Physiol, 283: H1531-1537.

Hsu Y, Tran M, Linninger AA. (2015) Dynamic regulation of aquaporin-4 water channels in neurological disorders. Croat Med J, 56: 401-421.

Igarashi H, Huber VJ, Tsujita M, Nakada T. (2011) Pretreatment with a novel aquaporin 4 inhibitor, TGN-020, significantly reduces ischemic cerebral edema. Neurol Sci, 32: 113-116.

International Narcotics Control Board (INCB). (2005) List of psychotropic substances under international control. United Nations Publications, Sales No. E/F/S.93/XI.2

Ito H, Yamamoto N, Arima H, Hirate H, Morishima T, Umenishi F, Tada T, Asai K, Katsuya H, Sobue K. (2006) Interleukin-1beta induces the expression of aquaporin-4 through a nuclear factor-kappaB pathway in rat astrocytes. J Neurochem, 99: 107-118.

Itoh T, Rai T, Kuwahara M, Ko SB, Uchida S, Sasaki S, Ishibashi K. (2005) Identification of a novel aquaporin, AQP12, expressed in pancreatic acinar cells. Biochem Biophys Res Commun, 330: 832-838.

Jacob A, Hack B, Chen P, Quigg RJ, Alexander JJ. (2011) C5a/CD88 signaling alters blood-brain barrier integrity in lupus through nuclear factor-kappaB. J Neurochem, 119: 1041–1051.

Jansson D, Rustenhoven J, Feng S, Hurley D, Oldfield RL, Bergin PS, Mee EW, Faull RL, Dragunow M. (2014) A role for human brain pericytes in neuroinflammation. J Neuroinflammation, 11: 104.

Jayakumar AR, Panickar KS, Murthy ChR, Norenberg MD. (2006) Oxidative stress and mitogen-activated protein kinase phosphorylation mediate ammonia-induced cell swelling and glutamate uptake inhibition in cultured astrocytes. J Neurosci, 26: 4774-4784.

Joca L, Zuloaga DG, Raber J, Siegel JA (2014) Long-term effects of early adolescent methamphetamine exposure on depression-like behavior and the hypothalamic vasopressin system in mice. Dev Neurosci 36:108–118.

Jung JS, Bhat RV, Preston GM, Guggino WB, Baraban JM, Agre P. (1994) Molecular characterization of an aquaporin cDNA from brain: candidate osmoreceptor and regulator of water balance. Proc Natl Acad Sci USA, 91: 13052-13056.

Kadohira I, Abe Y, Nuriya M, Sano K, Tsuji S, Arimitsu T, Yoshimura Y, Yasui M. (2008) Phosphorylation in the C-terminal domain of Aquaporin-4 is required for Golgi transition in primary cultured astrocytes. Biochem Biophys Res Commun, 377: 463-468.

Kaltschmidt B, Widera D, Kaltschmidt C. (2005) Signaling via NF-kappaB in the nervous system. Biochim Biophys Acta, 1745:287-299.

Kassiotis G, Kollias G. (2001) Uncoupling the proinflammatory from the immunosuppressive properties of tumor necrosis factor (TNF) at the p55 TNF receptor level: implications for pathogenesis and therapy of autoimmune demyelination. J Exp Med, 193: 427-434.

Kettenmann H, Kirchhoff F, Verkhratsky A. (2013) Microglia: new roles for the synaptic stripper. Neuron, 77 (1): 10-18.

Khare P, Datusalia AK, Sharma SS. (2017) Parthenolide, an NF-κB Inhibitor Ameliorates Diabetes-Induced Behavioural Deficit, Neurotransmitter Imbalance and Neuroinflammation in Type 2 Diabetes Rat Model. Neuromolecular Med, 19: 101-112.

Kim JE, Ryu HJ, Choi SY, Kang TC. (2012) Tumor necrosis factor-α-mediated threonine 435 phosphorylation of p65 nuclear factor-κB subunit in endothelial cells induces vasogenic edema and neutrophil infiltration in the rat piriform cortex following status epilepticus. J Neuroinflammation, 9: 6.

Kim JE, Ryu HJ, Kang TC. (2013) Status epilepticus induces vasogenic edema via tumor necrosis factor-alpha/ endothelin-1-mediated two different pathways. PLoS One, 8: e74458.

Kim JH, Kim JH, Park JA, Lee S, Kim WJ, Yu YS, Kim K. (2006) Blood-neural Barrier: Intercellular Communication at Glio-Vascular Interface. J Biochem Mol Biol, 39: 339-345.

Kim KS, Park JY, Jou I, Park SM. (2010) Regulation of Weibel-Palade body exocytosis by alpha-synuclein in endothelial cells. J Biol Chem, 285: 21416–21425.

Kinoshita Y, Matsumura H, Igisu H, Yokota A. (2000) Hexachlorophene-induced brain edema in rat observed by proton magnetic resonance. Brain Res, 873: 127-130.

Kish SJ. (2008) Pharmacologic mechanisms of crystal meth. CMAJ, 178: 1679-1682.

Kitamura O, Takeichi T, Wang EL, Tokunaga I, Ishigami A, Kubo S. (2010) Microglial and astrocytic changes in the striatum of methamphetamine abusers. Leg Med (Tokyo), 12: 57-62.

Kitamura O. (2009) Detection of methamphetamine neurotoxicity in forensic autopsy cases. Leg Med (Tokyo), 11 Suppl 1: S63-65.

Kiyatkin EA, Brown PL, Sharma HS. (2007) Brain edema and breakdown of the blood-brain barrier during methamphetamine intoxication: critical role of brain hyperthermia. Eur J Neurosci, 26: 1242-1253.

Kiyatkin,EA, Sharma HS. (2011) Expression of heat shock protein (HSP 72 kDa) during acute methamphetamine intoxication depends on brain hyperthermia: neurotoxicity or neuroprotection? J Neural Transm, 118: 47-60.

Koch S, Rabinstein A, Falcone S, Forteza A. (2001) Diffusion-weighted imaging shows cytotoxic and vasogenic edema in eclampsia. Am J Neuroradiol, 22: 1068-1070.

Koedel U, Bayerlein I, Paul R, Sporer B, Pfister HW. (2000) Pharmacologic interference with NF-kappaB activation attenuates central nervous system complications in experimental Pneumococcal meningitis. J Infect Dis, 182: 1437–1445.

Kontoyiannis D, Pasparakis M, Pizarro TT, Cominelli F, Kollias G. (1999) Impaired on/off regulation of TNF biosynthesis in mice lacking TNF AU-rich elements: implications for joint and gut-associated immunopathologies. Immunity, 10: 387-398.

Kovac A, Erickson MA, Banks WA. (2011) Brain microvascular pericytes are immunoactive in culture: cytokine, chemokine, nitric oxide, and LRP-1 expression in response to lipopolysaccharide. J Neuroinflammation, 8: 139.

Krasnova IN, Cadet JL. (2009) Methamphetamine toxicity and messengers of death. Brain Res Rev, 60: 379–407.

Kuczenski R, Everall IP, Crews L, Adame A, Grant I, Masliah E. (2007) Escalating dose-multiple binge methamphetamine exposure results in degeneration of the neocortex and limbic system in the rat. Exp Neurol, 207: 42-51.

Kuo YC, Lu CH. (2011) Effect of human astrocytes on the characteristics of human brain microvascular endothelial cells in the blood-brain barrier. Colloids Surf B Biointerfaces, 86: 225–231.

Landoni VI, Schierloh P, de Campos Nebel M, Fernandez GC, Calatayud C, Lapponi MJ Isturiz MA. (2012) Shiga toxin 1 induces on lipopolysaccharide-treated astrocytes the release of tumor necrosis factor-alpha that alter brain-like endothelium integrity. PLoS Pathog, 8: e1002632.

Lazovic J, Basu A, Lin HW, Rothstein RP, Krady JK, Smith MB, Levison SW. (2005) Neuroinflammation and both cytotoxic and vasogenic edema are reduced in interleukin-1 type 1 receptor-deficient mice conferring neuroprotection. Stroke, 36: 2226-2231.

Lee KS, Kim SR, Park SJ, Min KH, Lee KY, Jin SM, Yoo WH, Lee YC. (2006) Antioxidant down-regulates interleukin-18 expression in asthma. Mol Pharmacol, 70: 1184–1193.

Lee YW, Hennig B, Yao J, Toborek M. (2001) Methamphetamine induces AP-1 and NF-kappaB binding and transactivation in human brain endothelial cells. J Neurosci Res, 66: 583-591.

Leitão RA, Coelho-Santos V, Silva AP (2016) Methamphetamine and the blood-brain barrier. In Victor R Preedy (ed) Neuropathology of Drug Addictions and Substance Misuse Volume 2: Part I Stimulants, 1st edn Academic Press-Elsevier, London, pp 155-168.

Leitão RA, Sereno J, Castelhano JM, Gonçalves SI, Coelho-Santos V, Fontes-Ribeiro C, Castelo-Branco M, Silva AP. (2017) Aquaporin-4 as a new target against methamphetamine-induced brain alterations: focus on the neurogliovascular unit and motivational behavior. Mol Neurobiol, doi: 10.1007/s12035-017-0439-0 (in press).

Lievens D, Vander Laenen F, Christiaens J. (2014) Public spending for illegal drug and alcohol treatment in hospitals: an EU cross-country comparison. Subst Abuse Treat Prev Policy, 9: 26.

Liu S, Zhu S, Zou Y, Wang T, Fu X. (2015) Knockdown of IL-1beta Improves Hypoxia-ischemia Brain Associated with IL-6 Up-regulation in Cell and Animal Models. Mol Neurobiol, 51: 743-752.

Loftis JM, Janowsky A. (2014) Neuroimmune basis of methamphetamine toxicity. Int Rev Neurobiol, 118: 165–197.

Lowenstein CJ, Morrell CN, Yamakuchi M. (2005) Regulation of Weibel-Palade body exocytosis. Trends Cardiovasc Med, 15: 302–308.

Luo Y, Wang Y, Kuang SY, Chiang YH, Hoffer B. (2010) Decreased level of Nurr1 in heterozygous young adult mice leads to exacerbated acute and long-term toxicity after repeated methamphetamine exposure. PLoS One, 5: e15193.

Ma TY, Iwamoto GK, Hoa NT, Akotia V, Pedram A, Boivin MA, Said HM. (2004) TNF-alpha induced increase in intestinal epithelial tight junction permeability requires NF kappa B activation. Am J Physiol Gastrointest Liver Physiol, 286: G367–G376.

MacQueen G, Frodl T. (2011) The hippocampus in major depression: evidence for the convergence of the bench and bedside in psychiatric research? Mol Psychiatry, 16: 252-264.

Madrid R, Le Maout S, Barrault MB, Janvier K, Benichou S, Mérot J. (2001) Polarized trafficking and surface expression of the AQP4 water channel are coordinated by serial and regulated interactions with different clathrin-adaptor complexes. EMBO J, 20: 7008-7021.

Mahajan SD, Aalinkeel R, Sykes DE, Schwartz SA. (2008) Methamphetamine alters blood-brain barrier permeability via the modulation of tight junction expression: implication for HIV-1 neuropathogenesis in the context of drug abuse. Brain Res 2008; 1203: 133-148.

Mai J, Virtue A, Shen J, Wang H, Yang XF. (2013) An evolving new paradigm: endothelial cells-conditional innate immune cells. J Hematol Oncol, 6: 61.

Manley GT, Fujimura M, Ma T, Noshita N, Filiz F, Bollen AW, Chan P, Verkman AS. (2000) Aquaporin-4 deletion in mice reduces brain edema after acute water intoxication and ischemic stroke. Nat Med, 6: 159-163.

Mark KA, Soghomonian JJ, Yamamoto BK. (2004) High-dose methamphetamine acutely activates the striatonigral pathway to increase striatal glutamate and mediate long-term dopamine toxicity. J Neurosci, 24: 11449-11456.

Marmarou A, Signoretti S, Fatouros PP, Portella G, Aygok GA, Bullock MR (2006) Predominance of cellular edema in traumatic brain swelling in patients with severe head injuries. J Neurosurg 104:720–730.

Marshall JF, O'Dell SJ. (2012) Methamphetamine influences on brain and behavior: unsafe at any speed? Trends Neurosci, 35: 536-545.

Martins T, Baptista S, Gonçalves J, Leal E, Milhazes N, Borges F, Ribeiro CF, Quintela O, Lendoiro E, López-Rivadulla M, Ambrósio AF, Silva AP. (2011) Methamphetamine transiently increases the blood-brain barrier permeability in the hippocampus: role of tight junction proteins and matrix metalloproteinase-9. Brain Res, 1411: 28-40.

Martins T, Burgoyne T, Kenny BA, Hudson N, Futter CE, Ambrósio AF, Silva AP, Greenwood J, Turowski P. (2013) Methamphetamine-induced nitric oxide promotes vesicular transport in blood-brain barrier endothelial cells. Neuropharmacology, 65: 74-82.

Mathema VB, Koh YS, Thakuri BC, Sillanpää M. (2012) Parthenolide, a sesquiterpene lactone, expresses multiple anti-cancer and anti-inflammatory activities. Inflammation, 35: 560-565.

Matsumoto RR, Seminerio MJ, Turner RC, Robson MJ, Nguyen L, Miller DB, O'Callaghan JP (2014) Methamphetamine-induced toxicity: an updated review on issues related to hyperthermia. Pharmacol Ther 144:28–40.

McCoy ES, Haas BR, Sontheimer H. (2010) Water permeability through aquaporin-4 is regulated by protein kinase C and becomes rate-limiting for glioma invasion. Neuroscience, 168: 971-981.

McCoy MK, Martinez TN, Ruhn KA, Szymkowski DE, Smith CG, Botterman BR, Tansey KE, Tansey MG. (2006) Blocking soluble tumor necrosis factor signaling with dominant-negative tumor necrosis factor inhibitor attenuates loss of dopaminergic neurons in models of Parkinson's disease. J Neurosci, 26: 9365-9375.

Melega WP, Cho AK, Harvey D, Lacan G. (2007) Methamphetamine blood concentrations in human abusers: application to pharmacokinetic modeling. Synapse, 61: 216–220.

Menezes MJ, McClenahan FK, Leiton CV, Aranmolate A, Shan X, Colognato H (2014) The extracellular matrix protein laminin α2 regulates the maturation and function of the blood–brain barrier. J Neurosci 34:15260–15280.

Miller F, Fenart L, Landry V, Coisne C, Cecchelli R, Dehouck MP, Buée-Scherrer V. (2005) The MAP kinase pathway mediates transcytosis induced by TNF-alpha in an in vitro blood brain barrier model. Eur J Neurosci, 22: 835–844.

Moe SE, Sorbo JG, Sogaard R, Zeuthen T, Petter Ottersen O, Holen T. (2008) New isoforms of rat Aquaporin-4. Genomics, 91: 367-377.

Montgomery SL, Bowers WJ. (2012) Tumor necrosis factor-alpha and the roles it plays in homeostatic and degenerative processes within the central nervous system. J Neuroimmune Pharmacol, 7: 42-59.

Muller WA. (2013) Getting leukocytes to the site of inflammation. Vet Pathol, 50: 7-22.

Muneer PM, Alikunju S, Szlachetka AM, Haorah J. (2011) Methamphetamine Inhibits the Glucose Uptake by Human Neurons and Astrocytes: Stabilization by Acetyl-L-Carnitine. PLoS One, 6: e19258.

Naderi V, Khaksari M, Abbasi R, Maghool F (2015) Estrogen provides neuroprotection against brain edema and blood brain barrier disruption through both estrogen receptors α and β following traumatic brain injury. Iran J Basic Med Sci 18:138–144.

Nag S, Manias JL, Stewart DJ. (2009) Pathology and new players in the pathogenesis of brain edema. Acta Neuropathol, 118: 197-217.

Nagelhus EA, Ottersen OP. (2013) Physiological roles of aquaporin-4 in brain. Physiol Rev, 93: 1543-1562.

Nakajima A, Yamada K, Nagai T, Uchiyama T, Miyamoto Y, Mamiya T, He J, Nitta A, Mizuno M, Tran MH, Seto A, Yoshimura M, Kitaichi K, Hasegawa T, Saito K, Yamada Y, Seishima M,

Sekikawa K, Kim HC, Nabeshima T. (2004) Role of tumor necrosis factor-alpha in methamphetamine-induced drug dependence and neurotoxicity. J Neurosci, 24: 2212-2225.

Nakama H, Chang L, Cloak C, Jiang C, Alicata D, Haning W. (2008) Association between Psychiatric symptoms and craving in methamphetamine users. Am. J. Addict, 17: 441-446.

Najjar S, Pearlman DM, Devinsky O, Najjar A, Zagzag D (2013) Neurovascular unit dysfunction with blood-brain barrier hyperpermeability contributes to major depressive disorder: a review of clinical and experimental evidence. J Neuroinflamm 10:142.

National Highway Traffic Safety Administration (NHTSA). (2015) http://www.nhtsa.gov/people/injury/research/job185drugs/methamphetamine.htm Retrieved February 2017.

Navarro P, Ruco L, Dejana E. (1998) Differential localization of VE- and N-cadherins in human endothelial cells: VE-cadherin competes with N-cadherin for junctional localization. J Cell Biol, 140: 1475-1484.

Nawashiro H, Tasaki K, Ruetzler CA, Hallenbeck JM. (1997) TNF-alpha pretreatment induces protective effects against focal cerebral ischemia in mice. J Cereb Blood Flow Metab, 17: 483-490.

Neely JD, Amiry-Moghaddam M, Ottersen OP, Froehner SC, Agre P, Adams ME. (2001) Syntrophin-dependent expression and localization of Aquaporin-4 water channel protein. Proc Natl Acad Sci USA, 98: 14108-14113.

Neurath MF, Pettersson S, Meyer zum Büschenfelde KH, Strober W. (1996) Local administration of antisense phosphorothioate oligonucleotides to the p65 subunit of NF-kappa B abrogates established experimental colitis in mice. Nat Med, 2: 998-1004.

Nicchia GP, Frigeri A, Liuzzi GM, Santacroce MP, Nico B, Procino G, Quondamatteo F, Herken R, Roncali L, Svelto M. (2000) Aquaporin-4-containing astrocytes sustain a temperature- and mercury-insensitive swelling in vitro. Glia, 31: 29-38.

Nicchia GP, Rossi A, Mola MG, Pisani F, Stigliano C, Basco D, Mastrototaro M, Svelto M, Frigeri A. (2010) Higher order structure of aquaporin-4. Neuroscience, 168: 903-914.

Nicchia GP, Rossi A, Mola MG, Procino G, Frigeri A, Svelto M. (2008) Actin cytoskeleton remodeling governs aquaporin-4 localization in astrocytes. Glia, 56: 1755-1766.

Nitta T, Hata M, Gotoh S, Seo Y, Sasaki H, Hashimoto N, Tsukita S. (2003) Size-selective loosening of the blood-brain barrier in claudin-5-deficient mice. J Cell Biol, 161: 653-660.

Northrop NA, Yamamoto BK. (2012) Persistent neuroinflammatory effects of serial exposure to stress and methamphetamine on the blood-brain barrier. J Neuroimmune Pharmacol, 7: 951-968.

Northrop NA, Yamamoto BK (2015) Methamphetamine effects on blood-brain barrier structure and function. Front Neurosci 9:69.

Ohnishi M, Monda A, Takemoto R, Fujimoto Y, Sugitani M, Iwamura T, Hiroyasu T, Inoue A. (2014) High-mobility group box 1 up-regulates aquaporin 4 expression via microglia-astrocyte interaction. Neurochem Int, 75: 32-38.

Ohtsuki S, Sato S, Yamaguchi H, Kamoi M, Asashima T, Terasaki T. (2007) Exogenous expression of claudin-5 induces barrier properties in cultured rat brain capillary endothelial cells. J Cell Physiol, 210: 81-86.

Panahpour H, Dehghani GA, Bohlooli S. (2014) Enalapril attenuates ischaemic brain oedema and protects the blood-brain barrier in rats via an anti-oxidant action. Clin Exp Pharmacol Physiol, 41: 220-226.

Papadopoulos MC, Manley GT, Krishna S, Verkman AS. (2004) Aquaporin-4 facilitates reabsorption of excess fluid in vasogenic brain edema. FASEB J, 18: 1291-1293.

Papadopoulos MC, Verkman AS. (2005) Aquaporin-4 gene disruption in mice reduces brain swelling and mortality in pneumococcal meningitis. J Biol Chem, 280: 13906-13912.

Papadopoulos MC, Verkman AS. (2007) Aquaporin-4 and brain edema. Pediatr Nephrol, 22: 778-784.

Papadopoulos MC, Verkman AS. (2013) Aquaporin water channels in the nervous system. Nat Rev Neurosci, 14: 265-277.

Park BJ, Wannemuehler KA, Marston BJ, Govender N, Pappas PG, Chiller TM. (2009) Estimation of the current global burden of cryptococcal meningitis among persons living with HIV/AIDS. AIDS, 23: 525-530.

Park M, Hennig B, Toborek M. (2012) Methamphetamine alters occludin expression via NADPH oxidase-induced oxidative insult and intact caveolae. J Cell Mol Med, 16: 362-375.

Park M, Kim HJ, Lim B, Wylegala A, Toborek M. (2013) Methamphetamine-induced occludin endocytosis is mediated by the Arp2/3 complex-regulated actin rearrangement. J Biol Chem, 288: 33324-33334.

Patel D, Desai GM, Frases S, Cordero RJB, DeLeon-Rodriguez CM, Eugenin EA, Martinez LR. (2013) Methamphetamine Enhances Cryptococcus neoformans Pulmonary Infection and Dissemination to the Brain. MBio, 4: e00400-00413.

Persidsky Y, Ramirez SH, Haorah J, Kanmogne GD. (2006) Blood-brain barrier: structural components and function under physiologic and pathologic conditions. J Neuroimmune Pharmacol, 1: 223-236.

Petty MA, Lo EH. (2002) Junctional complexes of the blood-brain barrier: permeability changes in neuroinflammation. Prog Neurobiol, 68: 311-323.

Pillai DR, Dittmar MS, Baldaranov D, Heidemann RM, Henning EC, Schuierer G, Bogdahn U, Schlachetzki F (2009) Cerebral ischemia-reperfusion injury in rats-a 3 T MRI study on biphasic blood-brain barrier opening and the dynamics of edema formation. J Cereb Blood Flow Metab 29:1846–1855.

Pozniak PD, White MK, Khalili K. (2014) TNF-α/NF-Kb signaling in the CNS: possible connection to EPHB2. J Neuroimmune Pharmacol, 9: 133-141.

Prager GW, Mihaly J, Brunner PM, Koshelnick Y, Hoyer-Hansen G, Binder BR. (2009) Urokinase mediates endothelial cell survival via induction of the X-linked inhibitor of apoptosis protein. Blood, 113: 1383–1390.

Preston GM, Jung JS, Guggino WB, Agre P. (1994) Membrane topology of aquaporin CHIP. Analysis of functional epitope-scanning mutants by vectorial proteolysis. J Biol Chem, 269: 1668-1673.

Pubill D, Canudas AM, Pallas M, Camins A, Camarasa J, Escubedo E. (2003) Different glial response to methamphetamine- and methylenedioxymethamphetamine-induced neurotoxicity. Naunyn Schmiedebergs Arch Pharmacol, 367: 490-499.

Quinton MS, Yamamoto BK. (2006) Causes and consequences of methamphetamine and MDMA toxicity. The AAPS Journal, 8: E337-E347.

Ramirez SH, Potula R, Fan S, Couraud PO, Persidsky Y. (2009) Methamphetamine disrupts blood-brain barrier function by induction of oxidative stress in brain endothelial cells. J Cereb Blood Flow Metab, 29: 1933-1945.

Ransohoff RM, Perry VH. (2009) Microglial physiology: unique stimuli, specialized responses. Annu Rev Immunol, 27: 119-145.

Rao KV, Jayakumar AR, Reddy PV, Tong X, Curtis KM, Norenberg MD (2010) Aquaporin-4 in manganese-treated cultured astrocytes. Glia 58:1490–1499.

Rapp JH, Pan XM, Neumann M, Hong M, Hollenbeck K, Liu J (2008) Microemboli composed of cholesterol crystals disrupt the blood-brain barrier and reduce cognition. Stroke 39: 2354–2361.

Rawson R, Huber A, Brethen P, Obert J, Gulati V, Shoptaw S, Ling W. (2000) Methamphetamine and cocaine users: differences in characteristics and treatment retention. J Psychoactive Drugs, 32: 233-238.

Rempe RG, Hartz AM, Bauer B. (2016) Matrix metalloproteinases in the brain and blood-brain barrier: Versatile breakers and makers. J Cereb Blood Flow Metab, 36: 1481-1507.

Rivière GJ, Gentry WB, Owens SM. (2000) Disposition of methamphetamine and its metabolite amphetamine in brain and other tissues in rats after intravenous administration. J Pharmacol Exp Ther, 292: 1042-1047.

Rojek A, Praetorius J, Frøkiaer J, Nielsen S, Fenton RA. (2008) A current view of the mammalian aquaglyceroporins. Annu Rev Physiol, 70: 301-327.

Rosell A, Cuadrado E, Ortega-Aznar A, Hernandez-Guillamon M, Lo EH, Montaner J. (2008) MMP-9-positive neutrophil infiltration is associated to blood-brain barrier breakdown and basal lamina type IV collagen degradation during hemorrhagic transformation after human ischemic stroke. Stroke, 39: 1121–1126.

Rosenberg GA. (2002) Matrix Metalloproteinases in Neuroinflammation. Glia, 39: 279-291.

Rossi D, Volterra A. (2009) Astrocytic dysfunction: insights on the role in neurodegeneration. Brain Res Bull, 80: 224-232.

Rothman RB, Baumann MH, Dersch CM, Romero DV, Rice KC, Carroll FI, Partilla JS. (2001) Amphetamine-type central nervous system stimulants release norepinephrine more potently than they release dopamine and serotonin. Synapse, 39: 32-41.

Rummel C, Gerstberger R, Roth J, Hübschle T. (2011) Parthenolide attenuates LPS-induced fever, circulating cytokines and markers of brain inflammation in rats. Cytokine, 56: 739-748.

Saitou M, Furuse M, Sasaki H, Schulzke JD, Fromm M, Takano H, Tsukita S. (2000) Complex phenotype of mice lacking occludin, a component of tight junction strands. Mol Biol Cell, 11: 4131-4142.

Sharma HS, Kiyatkin EA (2009) Rapid morphological brain abnormalities during acute methamphetamine intoxication in the rat: an experimental study using light and electron microscopy. J Chem Neuroanat 37:18–32.

Scholler K, Trinkl A, Klopotowski M, Thal SC, Plesnila N, Trabold R, Hamann GF, Schmid-Elsaesser R, Zausinger S. (2007) Characterization of microvascular basal lamina damage and blood-brain barrier dysfunction following subarachnoid hemorrhage in rats. Brain Res, 1142: 237–246.

Schreck R, Albermann K, Baeuerle PA. (1992) Nuclear factor kappa-B - an oxidative stress-responsive transcription factor of eukaryotic cells (a review). Free Radic Res Commun, 17: 221–237.

Serviço de Intervenção nos Comportamentos Aditivos e nas Dependências (SICAD). (2016) Relatório Anual 2015 - A Situação do País em Matéria de Drogas e Toxicodependências. SICAD Lisboa

Sharma HS, Kiyatkin EA. (2009) Rapid morphological brain abnormalities during acute methamphetamine intoxication in the rat: An experimental study using light and electron microscopy. J Chem Neuroanat, 37: 18-32.

Shi LB, Verkman AS. (1996) Selected cysteine point mutations confer mercurial sensitivity to the mercurial-insensitive water channel MIWC/AQP-4. Biochemistry, 35: 538-544.

Silberstein C, Bouley R, Huang Y, Fang P, Pastor-Soler N, Brown D, Van Hoek AN. (2004) Membrane organization and function of M1 and M23 isoforms of aquaporin-4 in epithelial cells. Am J Physiol Renal Physiol, 287: F501-511.

Silva AP, Martins T, Baptista S, Gonçalves J, Agasse F, Malva JO. (2010) Brain injury associated with widely abused amphetamines: neuroinflammation, neurogenesis and blood-brain barrier. Curr Drug Abuse Ver, 3: 239-254.

Silva CD, Neves AF, Dias AI, Freitas HJ, Mendes SM, Pita I, Viana SD, de Oliveira PA, Cunha RA, Fontes-Ribeiro CA, Prediger RD, Pereira FC. (2014) A single neurotoxic dose of methamphetamine induces a long-lasting depressive-like behaviour in mice. Neurotox Res 25: 395-304.

Simões PF, Silva AP, Pereira FC, Marques E, Grade S, Milhazes N, Borges F, Ribeiro CF, Macedo TR. (2007) Methamphetamine induces alterations on hippocampal NMDA and AMPA receptor subunit levels and impairs spatial working memory. Neuroscience, 150: 433-441.

Simões PF, Silva AP, Pereira FC, Marques E, Milhazes N, Borges F, Ribeiro CF, Macedo TR. (2008) Methamphetamine changes NMDA and AMPA glutamate receptor subunit levels in the rat striatum and frontal cortex. Ann N Y Acad Sci, 1139: 232-241.

Simon SL, Domier C, Carnell J, Brethen P, Rawson R, Ling W (2000) Cognitive impairment in individuals currently using methamphetamine. Am J Addict 9: 222–231.

Simon SL, Domier CP, Sim T, Richardson K, Rawson RA, Ling W. (2002) Cognitive performance of current methamphetamine and cocaine abusers. J Addict Dis, 21: 61-74.

Smith AJ, Jin BJ, Ratelade J, Verkman AS (2014) Aggregation state determines the localization and function of M1- and M23-aquaporin-4 in astrocytes. J Cell Biol 204:559–573.

Smith BL, Agre P. (1991) Erythrocyte Mr 28,000 transmembrane protein exists as a multisubunit oligomer similar to channel proteins. J Biol Chem, 266: 6407-6415.

Sochocka M, Diniz BS, Leszek J. (2016) Inflammatory Response in the CNS: Friend or Foe? Mol Neurobiol, doi:10.1007/s12035-016-0297-1 (Epub ahead of print).

Sochocka M, Koutsouraki ES, Gasiorowski K, Leszek J. (2013) Vascular oxidative stress and mitochondrial failure in the pathobiology of Alzheimer's disease: a new approach to therapy. CNS Neurol Disord Drug Targets, 12: 870-881.

Sofroniew MV. (2015) Astrocyte barriers to neurotoxic inflammation. Nat Rev Neurosci, 16: 249-263.

Sorbo JG, Moe SE, Ottersen OP, Holen T. (2008) The molecular composition of square arrays. Biochemistry, 47: 2631-2637.

Sriram K, O'Callaghan JP. (2007) Divergent roles for tumor necrosis factor-α in the brain. J Neuroimmune Pharmacol, 2: 140-153.

Srivastava SK, Ramana KV. (2009) Focus on molecules: nuclear factor-kappaB. Exp Eye Res, 88: 2-3.

Stanley AC, Lacy P. (2010) Pathways for cytokine secretion. Physiology (Bethesda), 25: 218-229.

Strbian D, Meretoja A, Putaala J, Kaste M, Tatlisumak T. (2012) Cerebral edema in acute ischemic stroke patients treated with intravenous thrombolysis. Int J Stroke, 8: 529-534.

Tait MJ, Saadoun S, Bell BA, Papadopoulos MC. (2008) Water movements in the brain: role of aquaporins. Trends Neurosci, 31: 37-43.

Tak PP, Firestein GS. (2001) NF-kappaB: a key role in inflammatory diseases. J Clin Invest, 107: 7-11.

Tang C, Xue HL, Bai CL, Fu R. (2011) Regulation of adhesion molecules expression in TNF-alpha-stimulated brain microvascular endothelial cells by tanshinone IIA: involvement of NF-kappaB and ROS generation. Phytother Res, 25: 376–380.

Tang Y, Wu P, Su J, Xiang J, Cai D, Dong Q (2010) Effects of aquaporin-4 on edema formation following intracerebral hemorrhage. Exp Neurol 223:485–495

Thomas DM, Dowgiert J, Geddes TJ, Francescutti-Verbeem D, Liu X, Kuhn DM. (2004) Microglial activation is a pharmacologically specific marker for the neurotoxicity amphetamines. Neurosci Lett, 367: 349-354.

Thompson PM, Hayashi KM, Simon SL, Geaga JA, Hong MS, Sui Y, Lee JY, Toga AW, Ling W, London ED. (2004) Structural abnormalities in the brains of human subjects who use methamphetamine. J Neurosci, 24: 6028–6036.

Tiruppathi C, Shimizu J, Miyawaki-Shimizu K, Vogel SM, Bair AM, Minshall RD, Predescu D, Malik AB. (2008) Role of NF-kappaB-dependent caveolin-1 expression in the mechanism of increased endothelial permeability induced by lipopolysaccharide. J Biol Chem, 283: 4210–4218.

Tobias MC, O'Neill J, Hudkins M, Bartzokis G, Dean AC, London ED. (2010) White-matter abnormalities in brain during early abstinence from methamphetamine abuse. Psychopharmacology (Berl), 209: 13-24.

Tobinick E, Kim NM, Reyzin G, Rodriguez-Romanacce H, DePuy V. (2012) Selective TNF inhibition for chronic stroke and traumatic brain injury: an observational study involving 629 consecutive patients treated with perispinal etanercept. CNS drugs, 26: 1051–1070.

Toborek M, Seelbach MJ, Rashid CS, Andras IE, Chen L, Park M, Esser KA. (2013) Voluntary exercise protects against methamphetamine-induced oxidative stress in brain microvasculature and disruption of the blood--brain barrier. Mol Neurodegener, 8: 22.

Tomkins O, Friedman O, Ivens S, Reiffurth C, Major S, Dreier JP, Heinemann U, Friedman A (2007) Blood–brain barrier disruption results in delayed functional and structural alterations in the rat neocortex. Neurobiol Dis 25: 367–377.

Tong J, Fitzmaurice P, Furukawa Y, Schmunk GA, Wickham DJ, Ang LC, Sherwin A, McCluskey T, Boileau I, Kish SJ. (2014) Is brain gliosis a characteristic of chronic methamphetamine use in the human? Neurobiol Dis, 67: 107–118.

Tourdias T, Dragonu I, Fushimi Y, Deloire MS, Boiziau C, Brochet B, Moonen C, Petry KG, Dousset V. (2009) Aquaporin 4 correlates with apparent diffusion coefficient and hydrocephalus severity in the rat brain: a combined MRI-histological study. NeuroImage 47:659–666.

Trevisan E, Bertero L, Bosa C, Magistrello M, Pellerino A, Ruda R, Soffietti R. (2014) Antiangiogenic therapy of brain tumors: the role of bevacizumab. Neurol Sci, 35: 507-514.

United Nations Office on Drugs and Crime (UNODC). (2007) World Drug Report Volume 1 Analysis. United Nations Office on Drugs and Crime: Vienna.

United Nations Office on Drugs and Crime (UNODC). (2014) World Drug Report. United Nations Office on Drugs and Crime: Vienna.

United Nations Office on Drugs and Crime (UNODC). (2015) World Drug Report. United Nations publication, Sales No. E.15.XI

United States Food and Drug Administration (US-FDA). (2013) http://www.accessdata.fda.gov/drugsatfda_docs/label/2013/005378s028lbl.pdf. Retrieved February 2017.

Urrutia A, Rubio-Araiz A, Gutierrez-Lopez MD, ElAli A, Hermann DM, O'Shea E, Colado MI. (2013) A study on the effect of JNK inhibitor, SP600125, on the disruption of blood-brain barrier induced by methamphetamine. Neurobiol Dis, 50: 49-58.

Urschel K, Cicha I. (2015) TNF-α in the cardiovascular system: From physiology to therapy. Int J Interferon Cytokine Mediator Res, 7: 9-25.

Vajda Z, Pedersen M, Füchtbauer EM, Wertz K, Stødkilde-Jørgensen H, Sulyok E, Dóczi T, Neely JD, Agre P, Frøkiaer J, Nielsen S. (2002) Delayed onset of brain edema and mislocalization of aquaporin-4 in dystrophin-null transgenic mice. Proc Natl Acad Sci USA, 99: 13131-13136.

van Loo G, De Lorenzi R, Schmidt H, Huth M, Mildner A, Schmidt-Supprian M, Lassmann H, Prinz MR, Pasparakis M. (2006) Inhibition of transcription factor NF-kappaB in the central nervous system ameliorates autoimmune encephalomyelitis in mice. Nat Immunol, 7: 954-961.

Venero JL, Vizuete ML, Machado A, Cano J. (2001) Aquaporins in the central nervous system. Prog Neurobiol, 63: 321-336.

Vorbrodt AW, Dobrogowska DH. (2003) Molecular anatomy of intercellular junctions in brain endothelial and epithelial barriers: electron microscopist's view. Brain Res Brain Res Rev, 42: 221-242.

Vorbrodt AW, Li S, Brown WT, Ramakrishna N. (2008) Increased expression of beta-catenin in brain microvessels of a segmentally trisomic (Ts65Dn) mouse model of Down syndrome. Brain Cell Biol, 36: 203-211.

de Vries HE, Kooij G, Frenkel D, Georgopoulos S, Monsonego A, Janigro D. (2012) Inflammatory events at blood-brain barrier in neuroinflammatory and neurodegenerative disorders: implications for clinical disease. Epilepsia, 53:45–52.

Wachter B, Schürger S, Schmid A, Gröger A, Sadler R, Speidel A, Rolinger J, Pichler BJ, Berg D, Wagner HJ, von Ameln-Mayerhofer A, Küppers E. (2012) 6-Hydroxydopamine leads to T2 hyperintensity, decreased claudin-3 immunoreactivity and altered aquaporin 4 expression in the striatum. Behav Brain Res 232:148–158.

Wajant H, Pfizenmaier K, Scheurich P. (2003) Tumor necrosis factor signaling. Cell Death Differ, 10: 45-65.

Walcott BP, Kahle KT, Simard JM. (2012) Novel treatment targets for cerebral edema. Neurotherapeutics, 9: 65-72.

Wang BF, Cui ZW, Zhong ZH, Sun YH, Sun QF, Yang GY, Bian LG. (2015) Curcumin attenuates brain edema in mice with intracerebral hemorrhage through inhibition of AQP4 and AQP9 expression. Acta Pharmacol Sin, 36: 939-948.

Wang Q, Ishikawa T, Michiue T, Zhu BL, Guan DW, Maeda H. (2014) Molecular pathology of brain matrix metalloproteases, claudin5, and aquaporins in forensic autopsy cases with special regard to methamphetamine intoxication. Int J Legal Med, 128: 469-474.

Wang YF, Parpura V (2016) Central role of maladapted astrocytic plasticity in ischemic brain edema formation. Front Cell Neurosci 10:129.

Wang W, Lv S, Zhou Y, Fu J, Li C, Liu P. (2011) Tumor necrosis factor-α affects blood-brain barrier permeability in acetaminophen-induced acute liver failure. Eur J Gastroenterol Hepatol, 23: 552-558.

Warth A, Simon P, Capper D, Goeppert B, Tabatabai G, Herzog H, Dietz K, Stubenvoll F, Ajaaj R, Becker R, Weller M, Meyermann R, Wolburg H, Mittelbronn M. (2007) Expression pattern of the water channel aquaporin-4 in human gliomas is associated with blood-brain barrier disturbance but not with patient survival. J Neurosci Res, 85: 1336-1346.

Winslow BT, Voorhees KI, Pehl KA. (2007) Methamphetamine abuse. Am Fam Physician, 76: 1169-1174.

Wolburg H, Noell S, Mack A, Wolburg-Buchholz K, Fallier-Becker P. (2009) Brain endothelial cells and the glio-vascular complex. Cell Tissue Res, 335: 75-96.

Yamamoto BK, Moszczynska A, Gudelsky GA. (2010) Amphetamine Toxicities, Classical and emerging mechanisms. Ann N Y Acad Sci, 1187: 101-121.

Yamamoto BK, Raudensky J. (2008) The role of oxidative stress, metabolic compromise, and inflammation in neuronal injury produced by amphetamine-related drugs of abuse. J Neuroimmune Pharmacol, 3: 203-217.

Yamamoto BK, Zhu W. (1998) The effects of methamphetamine on the production of free radicals and oxidative stress. J Pharmacol Exp Ther, 287: 107-114.

Yan Y, Nitta A, Koseki T, Yamada K, Nabeshima T. (2012) Dissociable role of tumor necrosis factor alpha gene deletion in methamphetamine self-administration and cue-induced relapsing behavior in mice. Psychopharmacology (Berl), 221: 427-436.

Yang CM, Hsieh HL, Lin CC, Shih RH, Chi PL, Cheng SE, Hsiao LD. (2013) Multiple factors from bradykinin-challenged astrocytes contribute to the neuronal apoptosis: involvement of astroglial ROS, MMP-9, and HO-1/CO system. Mol Neurobiol, 47: 1020–1033.

Yang Q, Wang EY, Huang XJ, Qu WS, Zhang L, Xu JZ, Wang W, Tian DS (2011) Blocking epidermal growth factor receptor attenuates reactive astrogliosis through inhibiting cell cycle progression and protects against ischemic brain injury in rats. J Neurochem 119:644–653.

Yang Y, Estrada EY, Thompson JF, Liu W, Rosenberg GA. (2007) Matrix metalloproteinase-mediated disruption of tight junction proteins in cerebral vessels is reversed by synthetic matrix metalloproteinase inhibitor in focal ischemia in rat. J Cereb Blood Flow Metab, 27: 697-709.

Yang Y, Rosenberg GA. (2011) MMP-mediated disruption of claudin-5 in the blood-brain barrier of rat brain after cerebral ischemia. Methods Mol Biol, 762: 333-345.

Yao Y, Chen Z, Norris EH, Strickland S (2014) Astrocytic laminin regulates pericyte differentiation and maintains blood brain barrier integrity. Nat Commun 5:3413.

Yukutake Y, Tsuji S, Hirano Y, Adachi T, Takahashi T, Fujihara K, Agre P, Yasui M, Suematsu M. (2008) Mercury chloride decreases the water permeability of aquaporin-4-reconstituted proteoliposomes. Biol Cell, 100: 355-363.

Yukutake Y, Yasui M. (2010) Regulation of water permeability through aquaporin-4. Neuroscience, 168: 885-891

Zelenina M, Zelenin S, Bondar AA, Brismar H, Aperia A. (2002) Water permeability of aquaporin-4 is decreased by protein kinase C and dopamine. Am J Physiol Renal Physiol, 283: F309-318.

Zelenina M. (2010) Regulation of brain aquaporins. Neurochem Int, 57: 468-488.

Zhang S, Kan QC, Xu Y, Zhang GX, Zhu L. (2013) Inhibitory effect of matrine on blood-brain barrier disruption for the treatment of experimental autoimmune encephalomyelitis. Mediators Inflamm, 2013: 736085.

Zhang X, Banerjee A, Banks WA, Ercal N. (2009) N-Acetylcysteine amide protects against methamphetamine-induced oxidative stress and neurotoxicity in immortalized human brain endothelial cells. Brain Res, 1275: 87-95.

Zhong X, Li X, Liu F, Tan H, Shang D. (2012) Omentin inhibits TNF-alpha-induced expression of adhesion molecules in endothelial cells via ERK/NF-kappaB pathway. Biochem Biophys Res Commun, 425: 401–406.

Zhong Y, Smart EJ, Weksler B, Couraud PO, Hennig B, Toborek M. (2008) Caveolin-1 regulates human immunodeficiency virus-1 Tat-induced alterations of tight junction protein expression via modulation of the Ras signaling. J Neurosci, 28: 7788-7796.

Zhong Z, Wang B, Dai M, Sun Y, Sun Q, Yang G, Bian L (2013) Carvacrol alleviates cerebral edema by modulating AQP4 expression after intracerebral hemorrhage in mice. Neurosci Lett 555:24–29.

Zhu JP, Xu W, Angulo N, Angulo JÁ. (2006) Methamphetamine-induced striatal apoptosis in the mouse brain: comparison of a binge to an acute bolus drug administration. Neurotoxicology, 27: 131-136.

Zou J, Vetreno RP, Crews FT (2012) ATP-P2X7 receptor signaling controls basal and TNFα-stimulated glial cell proliferation. Glia 60:661–673. doi: 10.1002/glia.22302.